Interlayer Thermodynamics in Nanoscale Layered Structures for EUV Radiation

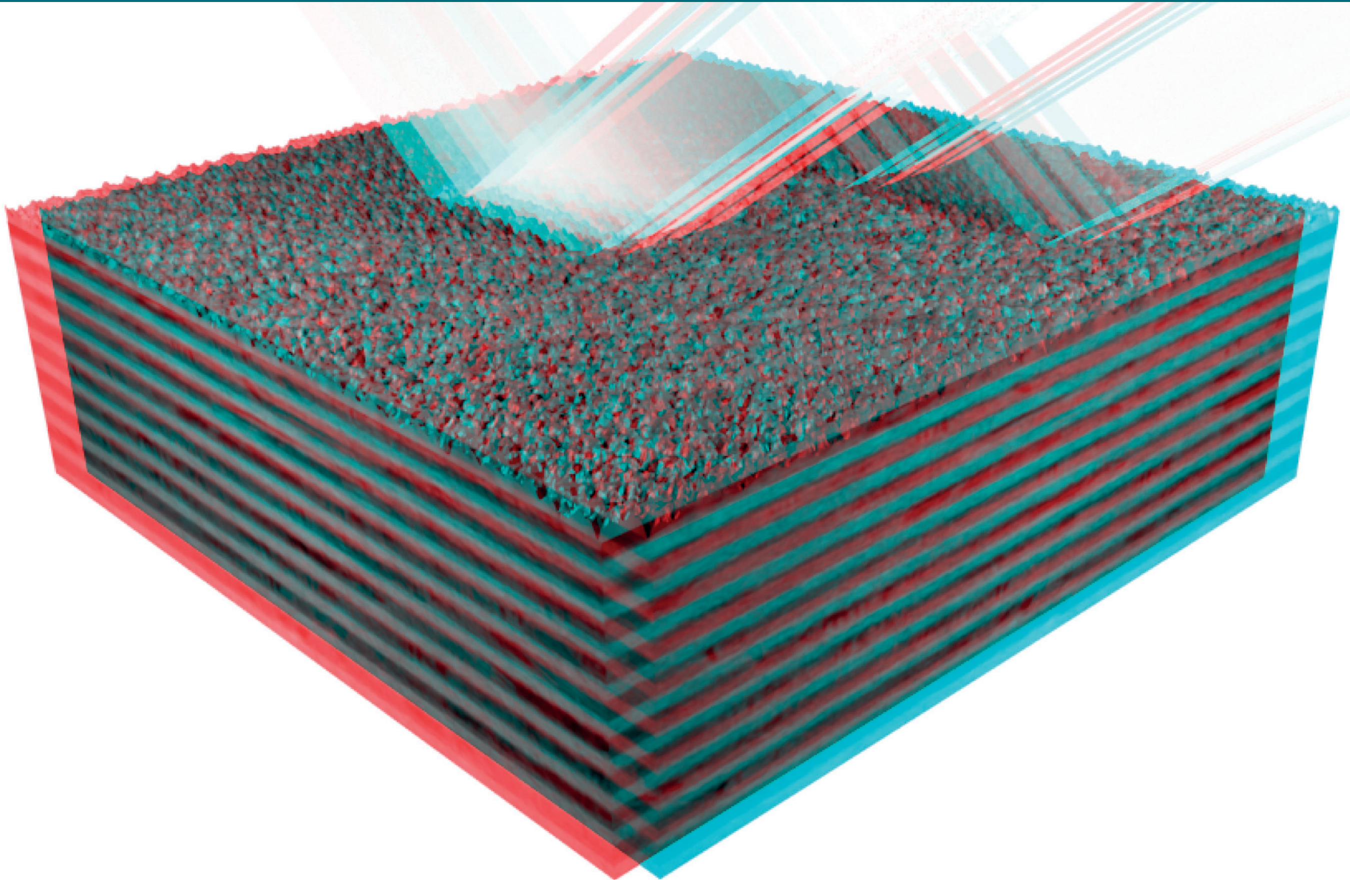

Jeroen Bosgra

Interlayer thermodynamics in nanoscale layered structures for reflection of EUV radiation

Jeroen Bosgra

"Those who do not know the torment of the unknown cannot have the joy of discovery."
– Claude Bernard

This thesis is based on the following publications:

- **Chapter 3:**
  J. Bosgra, J. Verhoeven, A.E. Yakshin, F. Bijkerk, Mo-Si interlayer growth during deposition, to be submitted
- **Chapter 4:**
  J. Bosgra, E. Zoethout, A.M.J. van der Eerden, J. Verhoeven, R.W.E. van De Kruijs, A.E. Yakshin, F. Bijkerk, Structural properties of subnanometer thick Y layers in extreme ultraviolet multilayer mirrors, Applied Optics 51 (2012), 8541
- **Chapter 5:**
  J. Bosgra, J. Verhoeven, R.W.E. van De Kruijs, A.E. Yakshin, F. Bijkerk, Non-constant diffusion characteristics of nanoscopic Mo-Si interlayer growth, Thin Solid Films 522 (2012), 228
- **Chapter 6:**
  J. Bosgra, L.W. Veldhuizen, E. Zoethout, J. Verhoeven, R.A. Loch, A.E. Yakshin, F. Bijkerk, Interactions of C in layered Mo-Si structures, submitted to Thin Solid Films
- **Chapter 7:**
  J. Bosgra, E. Zoethout, J. Verhoeven, F. Bijkerk, Improvement of Si/C interface correlation during annealing, to be submitted

Contribution to other publications:

- R.A. Loch, R. Sobierajski, E. Louis, J. Bosgra, F. Bijkerk, Modelling single shot damage thresholds of multilayer optics for high-intensity shortwavelength radiation sources, Optics Express 20 (2012), 28200
- S.L. Nyabero, R.W.E. van de Kruijs, A.E. Yakshin, E. Zoethout, G. von Blanckenhagen, J. Bosgra, R.A. Loch, F. Bijkerk, Interlayer growth in Mo/B_4C multilayered structures upon thermal annealing, J. Appl. Phys 113 (2013), 144310
- R.A. Loch, R. Sobierajski, J. Bosgra, E. Louis, F. Bijkerk, Li_2O-based multilayer optics for water-window wavelength radiation, submitted to Optics Express

Patent:

- J. Bosgra, J. Verhoeven, A.E. Yakshin, F. Bijkerk, Enhancement of thermal stability of Mo-Si based EUV multilayer mirrors by minimizing the chemical driving force for interdiffusion, (IDF) 2012

CONTENTS

1 Introduction **10**

1.1 Miniaturization of electronics 10
1.2 Multilayer reflective optics 12
1.3 Design to increase multilayer mirror reflection 14
1.4 Interlayer formation during depostion 17
1.5 Interdiffusion in layered structures 18
1.6 Outline 20

2 Experimental **24**

2.1 Deposition of layered structures 24
2.2 Hard X-ray reflection and diffraction 25
 2.2.1 Fourier analysis 25
 2.2.2 X-ray reflection during annealing 27
 2.2.3 Diffraction 29
2.3 X-ray photoelectron spectroscopy 30
2.4 Extended X-ray absorption fine structure 31
2.5 Ellipsometry 34

3 Mo-Si interlayer growth during deposition **36**

Abstract 36
3.1 Introduction 37
3.2 Experimental 38
3.3 Results and discussion 39
 3.3.1 Calculations of Mo on a Si (100) surface 39
 3.3.2 Calculations of Si on a Mo (100) surface 40
 3.3.3 Deposition of Mo on non-ordered Si surfaces 43
3.4 Conclusions 47

4 **Increasing EUV reflection of Mo/Si based multilayer structures** **50**
Abstract 50
4.1 Introduction 51
4.2 Experimental 52
4.3 Results and discussion 54
4.3.1 EUV reflection 54
4.3.2 Interface roughness 55
4.3.3 Interlayer structure 57
4.4 Conclusions 64

5 **Non-constant diffusion characteristics of Mo-Si interlayer growth** **68**
Abstract 68
5.1 Introduction 69
5.2 Experimental 69
5.3 Results and discussion 72
5.4 Conclusions 79

6 **Reducing driving force for interdiffusion in Mo/Si based multilayer structures** **82**
Abstract 82
6.1 Introduction 83
6.2 Experimental 84
6.3 Results and discussion 84
6.3.1 Diffusion of C in Mo and Si layered structures 84
6.3.2 Effect of C layers in a Si/Mo_2C/Si structure 88
6.3.3 Applicability as EUV multilayer mirrors 92
6.4 Conclusions 93

7 **Improvement of Si/C interface correlation during annealing** **96**
Abstract 96
7.1 Introduction 97
7.2 Experimental 97
7.3 Extension of Fourier analysis for X-ray reflectometry measurements 98
7.4 Results and Discussion 100
7.4.1 Interlayer formation during deposition 100
7.4.2 Interface dynamics during annealing 107
7.5 Conclusions 110

8 **Valorisation** **112**

9 **Summary** **116**

10 Samenvatting 118

Acknowledgements 122

CHAPTER 1

INTRODUCTION

1.1 Miniaturization of electronics

"There is plenty of room at the bottom". This was the title of a famous talk by Richard P. Feynman on December 26th in the year 1959, at the annual meeting of the American Physical Society at the California Institute of Technology. In this talk, Feynman discusses a few problems on manipulating and controlling things on a small scale. One example given by Feynman is the dimension of the computer and the question whether they cannot be made smaller[1], i.e. reducing the size of the building blocks:

> *"For instance, the wires should be 10 or 100 atoms in diameter, and the circuits should be a few thousand angstroms across."*

Feynman elaborates with an example on face recognition, something a human brain can do easily, however these huge computers cannot:

> *"The computers that we build are not able to do that. The number of elements in this bone box of mine are enormously greater than the number of elements in our 'wonderful' computers. But our mechanical computers are too big; the elements in this box are microscopic. I want to make some that are sub-microscopic."*

Ever since his talk in 1959, this vision has been constantly pursued. The elements in computers have continuously decreased in size. In miniaturisation of the electronic circuits, optics play an important role. The current

[1]Microchips were not available at the time of the talk, and personal computers would not appear before the 70's.

technique that is widely used to make the microelectronic devices is immersion photo lithography. In photo lithography, basically a light pattern from a mask is projected and demagnified by a system of lenses onto a wafer that is coated with a photoresist layer. This photoresist layer is etched at the illuminated areas to leave a height profile for further steps. In immersion lithography, a liquid film is present between the lens system and resist. This liquid film increases the depth of focus and improves the resolution (the smallest resolvable distance between two objects) of the lithography tools. The current resolution of the lithography tools which use light having a wavelength of 193 nm, is about 38 nm.

Diffraction of light places an intrinsic limit on the resolution. According to the Rayleigh criterion, the resolution is proportional to the wavelength. Therefore, to further improve the resolution, smaller wavelengths are required in photo lithography. In the next generation lithography tools, Extreme Ultraviolet Lithography (EUVL), a wavelength of 13.5 nm will be used. Using light with a wavelength of 13.5 nm, a resolution of 10 nm (half pitch) can currently be obtained [1]. However, taking into consideration different optical properties of materials at this short wavelength (i.e. refraction and absorption of light), the optical system to be applied in the projection of patterns requires reconsideration. To clarify this, we describe the relevant factors in scaling down the wavelength.

For all wavelengths, the refractive index of a material is given by

$$\tilde{n} = 1 - \delta + i\beta \ \ (= n + ik), \tag{1.1a}$$

$$\delta = \frac{2\pi\rho_a r_0}{k_0^2}(f^0(0) + f'), \tag{1.1b}$$

$$\beta = \frac{2\pi\rho_a r_0}{k_0^2} f'', \tag{1.1c}$$

where ρ_a is the atomic density, $r_0 = 2.82{\cdot}10^{-6}$ nm (classical electron radius), $k_0 = 2\pi/\lambda$ where λ is the wavelength of the radiation, and $f^0(0)$ (=Z, number of electrons in the atom), f' and f'' are anomalous scattering factors related to electronic excitation and absorption. The factors are tabulated by Henke [2]. For (soft) X-rays, the refractive index decrement δ (contrast) for solids is very small, and the absorption (related to β) cannot be neglected. Due to the high absorption at these wavelengths, lenses cannot be applied in EUVL [3].

For radiation incident perpendicular to an interface between 2 materials, the electric fields are given by

$$E_r = \frac{\tilde{n}_1 - \tilde{n}_2}{\tilde{n}_1 + \tilde{n}_2} E_i, \tag{1.2a}$$

$$E_t = \frac{2\tilde{n}_1}{\tilde{n}_1 + \tilde{n}_2} E_i, \tag{1.2b}$$

where E_i is the amplitude of the electric field of the incident wave, E_r of the reflected wave and E_t of the transmitted wave. The reflectance from the interface between the two materials at this angle is given by

$$R = \left| \frac{\tilde{n}_1 - \tilde{n}_2}{\tilde{n}_1 + \tilde{n}_2} \right|^2 . \tag{1.3}$$

Due to the small values of δ, single surfaces do not reflect much for a wide range of incidence angles. However, total reflection from a surface can be obtained for angles smaller than the critical angle. The critical angle is given by

$$\theta_c \approx \sqrt{2\delta}. \tag{1.4}$$

Given the small value of θ_c for (soft) X-rays, the numerical aperture ($NA = \tilde{n} \sin \omega$, with ω the acceptance angle) below this angle is very small. Therefore the resolution (which is proportional to 1/NA) is too large to be used in most applications.

1.2 Multilayer reflective optics

A solution to increase reflection of mirrors for EUV radiation at angles above θ_c, is to exploit interference of radiation reflected by a stack of nanometer thick layers like in figure 1.1. The relation between the period thickness Λ of the structure and the angles θ_m for which the reflected waves of the interfaces interfere constructively, is to good approximation given by the corrected Bragg equation

$$m\lambda = 2\Lambda \sin \theta_m \sqrt{1 - \frac{2\bar{\delta}}{\sin^2 \theta_m}}, \tag{1.5}$$

where $\bar{\delta}$ is the average δ of the period. At near normal incidence, $\Lambda \approx \lambda/2$. At boundaries were the refractive index of layer $i+1$ is larger than the refractive index of layer i, a phase shift of 180° occurs (negative E_r in equation 1.2a). Therefore, the optical thicknesses of the individual layers in the period have to be equal to $\lambda/4$ for constructive interference of all reflected waves to occur.

EUV multilayer mirrors designed for 13.5 nm radiation are usually constructed from alternating Mo and Si layers. When 50 periods are used, the theoretical reflection of such a structure is approximately 75% of the incoming radiation[2]. However, in the design of EUVL systems, up to 10 reflective optics may be necessary [4]. This means that only 5.6% of the power of the

[2] In the calculation of this value, no imperfections like surface roughness and intermixing of Mo and Si are assumed: in practice, the reflection is only about 70%.

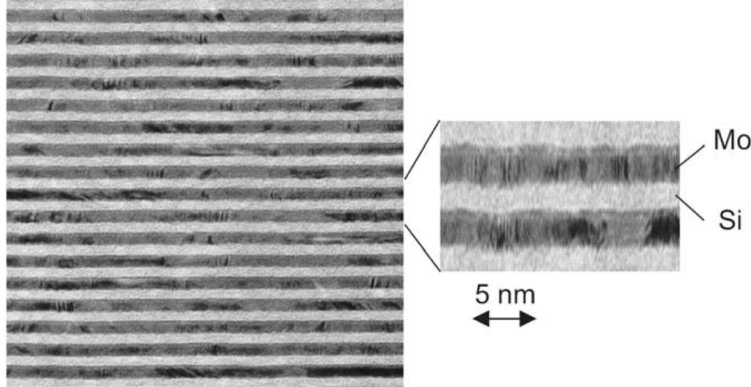

Figure 1.1: *Transmission electron microscopy image of the cross section of a Mo/Si multilayer mirror.*

source at the selected wavelength is available for the final step in the lithography process. If the total reflection of a single mirror would be increased by $\Delta\varepsilon$, the increase after p reflections would be

$$\Delta R = (R_0 + \Delta\varepsilon)^p - R_0^p = \sum_{k=0}^{p-1} R_0^k \Delta\varepsilon^{p-k} \approx pR_0^{p-1}\Delta\varepsilon \tag{1.6}$$

where the approximation is valid for small values of $\Delta\varepsilon$. When the reflection of a single mirror would be increased to 76%, the total throughput of the optical setup (10 reflections) increases to 6.4%. Consequently, for EUVL applications, it is very important to increase the reflection of the multilayer structures, even if it is only by a fraction of a percentage.

Theoretically, the Mo/Si multilayer mirror reflection can be increased by modifying the bilayer structure. One of the methods to increase the reflection by inserting additional layers into the structure will be introduced in section 1.3.

Up to now, only perfect multilayer structures were discussed. However, in practice the reflection will be lower than the maximum calculated reflection. For a Mo/Si multilayer structure designed for 13.5 nm near normal incidence radiation, the reflection will be approximately 70% instead of 75%. The reduction with respect to the theoretical maximum is mainly caused by interlayer formation between Mo and Si and interface roughness in the as deposited multilayer structures. The interlayer formation during deposition of metal/Si structures is discussed in section 1.4.

Another important design feature in multilayer mirror optics related to interlayer formation is thermal stability. When the multilayer structures are subjected to elevated temperatures, the as deposited interlayer structures can grow further. Usually, interdiffusion of material affects the period

thickness of the multilayer structure. Therefore, under a fixed angle of incidence for a fixed wavelength of radiation, reflected waves from the interfaces of the multilayer structure are no longer in phase with each other. This reduction of constructive interference causes a relative loss in reflection. In section 1.5, the basic concept of interdiffusion is introduced and some important observations for diffusion on the nanoscale are discussed.

To summarize, two important issues in multilayer optics for reflection of EUV radiation are: thermal stability and increasing the reflection. So far, no perfectly stable multilayer optics existed and reflection of the multilayer optics is still far below (about 5%) the theoretical maximum of a Mo/Si multilayer structure.

At the end of this chapter, it is outlined how these two topics ((1) increasing the reflection of multilayer mirrors by introducing additional interlayers into the period, and (2) interlayer growth during deposition or annealing), are related to research as presented in this thesis, aimed at improving the characteristics of the Mo/Si based multilayer structures.

1.3 Design to increase multilayer mirror reflection

For multilayer structures containing highly or moderately absorbing materials, the total reflection can be increased by introducing sub-quarter wavelength thick layers into the period structure [5, 6, 7]. Below, a brief summary of the selection rules for the materials is given.[3]

The amplitude reflectance of a bilayer is given by

$$r = \frac{r_{inc,1} + r_{1,2}\exp\left(\dfrac{4\pi i z_1 \tilde{n}_1 \sin\theta_1}{\lambda}\right)}{1 + r_{inc,1} r_{1,2}\exp\left(\dfrac{4\pi i z_1 \tilde{n}_1 \sin\theta_1}{\lambda}\right)} \tag{1.7}$$

where $r_{inc,1}$ is the Fresnel reflection coefficient between the incidence medium and layer 1, and $r_{1,2}$ is the Fresnel reflection coefficient between layer 1 and layer 2. At normal incidence, this latter coefficient is given by

$$r_{1,2} = \frac{\tilde{n}_1 - (\tilde{n}_1 + \Delta\tilde{n})}{\tilde{n}_1 + (\tilde{n}_1 + \Delta\tilde{n})} = -\frac{\Delta\tilde{n}}{2\tilde{n}_1} + O(\Delta\tilde{n}^2) \tag{1.8}$$

where $\Delta\tilde{n} = \tilde{n}_2 - \tilde{n}_1 \equiv \Delta n + i\Delta k$. This gives

$$R = rr^* = R_{inc,1} - \frac{4}{|\tilde{n}_{inc} + \tilde{n}_1|^4}\mathrm{Re}\left[\frac{\zeta}{\tilde{n}_1}\Delta\tilde{n}\exp\left(\frac{4\pi i \tilde{n}_1 z_1}{\lambda}\right)\right], \tag{1.9a}$$

$$\zeta = \tilde{n}_{inc}\tilde{n}_1\left(\tilde{n}_{inc}^{*2} - \tilde{n}_1^{*2}\right) \tag{1.9b}$$

[3]Note: to be consistent with previously used symbols, I changed some of the symbols compared to the papers by Larruquert.

The thickness z_1 for which maximum reflection occurs, can be found by setting the first derivative of R to 0 and the second derivative smaller than 0. After some mathematics, the requirement of the optical constants reduces to the solution

$$\Delta n A + \Delta k B > 0 \tag{1.10}$$

with

$$A = (n_{inc}^2 + k_{inc}^2 + n_1^2 + k_1^2)(n_{inc}k_1 - k_{inc}n_1) \tag{1.11a}$$
$$B = (n_{inc}^2 + k_{inc}^2 - n_1^2 - k_1^2)(n_{inc}n_1 + k_{inc}k_1) \tag{1.11b}$$

Generalization of this solution to more layers results in

$$\Delta n_1 A + \Delta k_1 B > 0 \tag{1.12a}$$
$$\Delta n_1 \Delta k_2 < \Delta n_2 \Delta k_1 \tag{1.12b}$$
$$\dots$$
$$\Delta n_{m-1} \Delta k_m < \Delta n_m \Delta k_{m-1} \tag{1.12c}$$

Basically, by taking into account absorption, and by making systematic steps in the refraction coefficient by the addition of thin layers, constructive interference of reflected waves from the interfaces results in a higher reflection than the two-layer system.

A graphical depiction of an example of the requirement on the optical constants is illustrated in figure 1.2. This figure illustrates one of the solutions which can be used to increase the reflection of Mo-Si based multilayer structures. The layers within the period, top to bottom, have to be selected with a rotation in the nk-plane (clockwise for this specific example, complying with eq. 1.12). However, the selected materials in figure 1.2 are for an unrealistic, idealized case.

In reality, interlayers between 2 materials will form upon deposition of the layers. In Mo/Si multilayer structures, the Mo-on-Si interlayer will have a thickness of approximately 1 nm and the Si-on-Mo interlayer thickness will be approximately 0.5 nm [8, 9]. In total, both interlayers together are about one quarter of the entire period thickness. When taking this significant interlayer formation into account, the inevitability of silicide formation has to be used in the material selection for improvement of the design of a Mo-Si based multilayer structure (chapter 4).

In addition to the possible loss in reflection due to interlayer formation, interface roughness is another factor that affects the reflection of a multilayer structure. Whereas the interlayer formation usually reduces reflection at an interface due to a reduced optical contrast, the interface roughness affects the radiation reflected in the specular direction. A common method to take

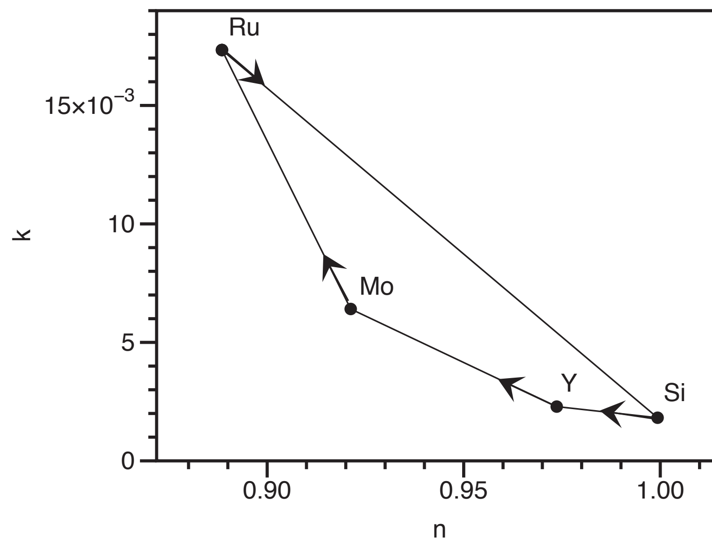

Figure 1.2: *Graphical depiction of the selection rule to increase the reflection of a multilayer structure by using sub-quarter wavelength layer thicknesses. The arrows illustrate the sequence of the layers to be placed in the period.*

into account the interface roughness on the reflection, is to use the Debye-Waller factor. The attenuation of the reflection of a Bragg order m is given by

$$R = R_0 \exp\left(-\frac{4\pi^2 m^2 \sigma^2}{\Lambda^2}\right) \tag{1.13}$$

From this equation, it can be seen that as the period thickness Λ decreases, the roughness σ becomes more dominant in attenuating the specular reflection of the multilayer structure.

For multilayer structures, it is also important to take into account the extent of correlation between the interfaces. Figure 1.3 gives some examples for different situations of interface roughness distributions in a multilayer structure. When there is no correlation between the interfaces, the diffuse scattering component is featureless. However, as the interface correlation increases, broad peaks appear at the Bragg condition. As the correlation approaches unity, the diffuse scattering component starts to sharpen again [10]. This means, that for an X-ray reflection measurement of the multilayer structure in the $\theta{-}2\theta$ setup[4], the reflection in the specular direction increases when the correlation between the interfaces increases. During annealing of multilayer structures, the correlation between the interfaces can change. This effect is observed in Si/C multilayer structures (chapter 7).

[4]See experimental section on X-ray reflection

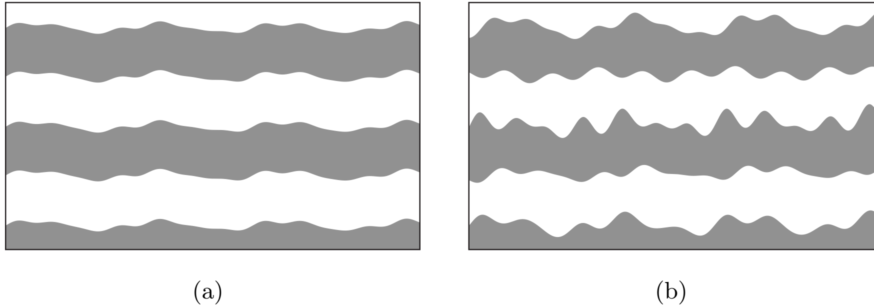

(a) (b)

Figure 1.3: *Illustration of different situations of roughness distributions in a multilayer structure: (a) perfect correlation; (b) partly correlated.*

1.4 Interlayer formation during depostion

Considering the previous section, it cannot be postulated that intermixed layers in general will decrease the reflection of multilayer structures. However, control of interlayer thickness is required to use the intermixing to increase the reflection. In the Mo-Si case, the naturally formed interlayers are too thick to be used to increase the reflection. Given that Mo-silicides have a negative formation enthalpy, formation of these interlayers cannot be prevented if the local temperature (or energy) is high enough during deposition to overcome the local potential barrier for interdiffusion.

For reduction of interlayer formation, knowledge on interlayer growth during deposition at room temperature is required. Formation of metal-silicide interlayers during deposition has been studied widely. However, these studies are almost always for elevated substrate temperatures (several hundred degrees Celsius) and mostly about which silicide phase grows on the Si crystalline template. Nevertheless, from a few studies on metal silicide formation at room temperature, a general process can be extracted to explain interlayer formation in Mo-Si structures.

Based on ion scattering, TEM and Auger measurements, van Loenen *et al* proposed a mechanism for Ni-Si [11] and Ti-Si interlayer formation at room temperature [12]. As Ni (or Ti) is deposited on a clean Si (111) surface, Ni atoms will form small clusters. They propose that the cluster energy is equal to a significant fraction of the cohesive energy of Ni (4.3 eV). This energy would then be enough to overcome the energy barrier for silicide formation (1.5 eV for Ni_2Si). In addition, the exothermic reaction energy would allow Si to diffuse over the islands. The available Si atoms are used for further reaction. After coalescence of the islands, when a continuous layer is formed, the interlayer formation stops, and a pure layer starts to grow.

Recently, an STM study for Mo growth on Si (111)-(7x7) was performed at room temperature which confirms this process [13]. During slow deposi-

tion of Mo on the Si surface, small clusters appear with a relative height of 0.1 nm to the original surface. Additionally, the weakly bound Si adatoms of this 7x7 reconstructed surface appear to be removed. The author suggests, using a simple model, that 2 to 3 Mo atoms need to cluster before a silicide nucleus can form.

A common explanation for the asymmetry in interlayer growth in the Mo-Si system is related to the difference in embedding atoms in the open, amorphous Si layer versus the closely packed, crystalline Mo layer [9, 14]. However, clustering energies may be another important factor for interlayer formation. The melting temperature (related to cohesive energy) of crystalline Mo is higher than of crystalline Si (2896 vs 1687 K). Therefore, a larger local energy release can be expected for the Mo-on-Si than the Si-on-Mo interface. However, this disregards the Mo-Si bonds, present in both situations. The Mo-Si bonds could reduce the large asymmetry in clustering energy. In chapter 3 the energetics related to the deposition of Mo-Si structures are further investigated.

To reduce interlayer formation at the Mo-on-Si interface, a possible approach is to increase the cohesive energy of the Si surface. That is, either a Si based compound with a higher melt temperature should be formed at the Mo-on-Si interface, or a thin layer of a material having a higher cohesive energy should be introduced between Si and Mo. Several solutions have been used in literature, for example Si_3N_4, Mo_2C and B_4C [15, 16, 17]. Although in theory, all layers should reduce reflection of the multilayer structure at 13.5 nm due to the reduced optical contrast and too large thickness, structures containing B_4C (or C) at the Mo-Si interfaces slightly increase the reflection with respect to standard Mo/Si multilayers [18]. The reason for this slight increase is suppression or reduction of Mo-Si interlayer formation in these enhanced structures. The B_4C barrier layers are studied more than C barrier layers in Mo-Si based multilayer structures. However, C appears to be more logical to use, considering that the melt temperature for C is much higher than B or B_4C. B is mentioned here specifically, because it is unlikely that deposition of B and C atoms from a B_4C target will result in (re)construction of a perfect B_4C compound in the multilayer structure. The effect of a C layer in the Mo-Si multilayer structure is discussed in chapter 6.

1.5 Interdiffusion in layered structures

During irradiation of the multilayer, the temperature inside the structure increases. When the structures are subjected to elevated temperatures, the interlayers can grow further due to interdiffusion of the materials. Equations to describe diffusion were derived in 1855 by Fick. Fick postulated that the flux goes from regions having a high concentration to regions with a low

concentration. The magnitude of the flux J is given by

$$J = -D\frac{\partial C}{\partial z} \tag{1.14}$$

where for simplicity we used only one spatial dimension. In this equation, D is the diffusion rate and C is the concentration. This equation is usually known as Fick's first law.[5] The diffusion rate is related to the activation energy for interdiffusion E_a and to the temperature T by the empirical Arrhenius relation

$$D = D_0 \exp\left(-\frac{E_a}{kT}\right) \tag{1.15}$$

where k is the Boltzmann constant.

Fick's first law is only valid when the concentration gradient is time independent. In the non steady state with the requirement of conservation of matter, the concentration profile is given by the non linear partial differential equation

$$\frac{\partial C}{\partial t} = \frac{\partial}{\partial z}\left(D\frac{\partial C}{\partial z}\right) \tag{1.16}$$

which is also known as Fick's second law. In this general form, where D may depend on the concentration, usually numerical computations are required to solve the equation. When using the Boltzmann transformation $\xi = z/\sqrt{4t}$ the equation reduces to an ordinary differential equation

$$-2\xi\frac{dC}{d\xi} = \frac{d}{d\xi}\left(D(C)\frac{dC}{d\xi}\right). \tag{1.17}$$

The trivial solution to this equation is given for the motion of the plane with constant composition ($dC/d\xi = 0$): $z \propto \sqrt{t}$. This relation is usually called the parabolic growth law. However, this simple relation is not always valid for diffusion on the nanoscale. For example, as time goes to 0, the plane of constant composition goes with an infinite shift velocity.

Another important example that diffusion on the nanoscale can be quite different from the quite commonly assumed Fick's first law, and that nanoscale diffusion effects can be useful for multilayer applications, results from the concentration dependence of the diffusion rate. The interplay between diffusion asymmetry (i.e. a composition dependence of the diffusion coefficient: $D(C) = D(0)\exp(mC)$ as used by Erdélyi [21]) and phase-separation tendency on the movement of the interface between two materials have been studied by computer simulations. When the asymmetry is large, a transient interface sharpening takes place [22]. This interface sharpening has also been observed experimentally in Mo/V multilayer systems [23]. Using computer simulations, they also observe that a chemically sharp interface does

[5] For chemical systems, this equation can also be written in terms of the gradient of the chemical potential: the basic structure of the equation is exactly the same.

not shift according to the simple solution from the Fick equation: depending on the mixing energy (related to the factor m), kinetic exponents can be found between 0.25 and 1 (0.5 corresponds to the parabolic growth) [22]. Consequently, for diffusion on the nanoscale, the simple parabolic growth is not always a valid description of the interface motion (chapter 5).

An extension and slight modification to the work of Erdélyi and coworkers was given by Roussel and Bellon [24]. They performed computer simulations on Cu-Ni layered structures. When the interfaces are sharp, it was concluded that for large diffusion asymmetries the tendency towards phase separation broadens and increases the roughness of the interfaces. The layer-by-layer growth of the interfaces is suppressed by the short range order. For diffuse and flat interfaces they find the same results as Erdelyi, namely transient interface sharpening. However, for sharp and rough interfaces two different results are possible: below a threshold wavelength for the roughness an apparent transient sharpening of the interface takes place, whereas above the threshold wavelength no sharpening occurs. In chapter 7 another effect related to roughness and interdiffusion is described.

1.6 Outline

Requirements and limitations of the structures for EUV multilayer mirrors have been introduced. Two important topics in research of multilayer mirror structures are: increasing the reflection and increasing thermal stability. Although much research has already been done for these topics on Mo-Si based multilayer structures, this thesis will present new experimental results which are important to gain further insight into diffusion phenomena on the nanoscale and to further improve the reflection and thermal stability of Mo-Si based multilayer mirror optics for EUV radiation. In chapter 2, the experimental techniques used for this thesis will be discussed in their relation to the research topics.

Reflection of Mo/Si multilayer structures is limited due to formation of silicide interlayers. To improve the reflectivity, either the silicide interlayer thickness has to be reduced, or a different silicide layer with better optical properties has to be included in the multilayer structure. In chapter 3, using density functional theory calculations, the mechanism responsible for the (asymmetry in) Mo-Si interlayer growth is discussed. In relation to the calculations, using ellipsometry, the influence of Ar ion sputtering of Si on the reduction of Mo-on-Si interlayer growth during deposition is discussed. In chapter 4, a structure is discussed which makes use of the theory to increase multilayer mirror reflectance by introducing sub-quarter wavelength thick layers into the periodical structure. An improved design (for total reflection) of the Mo-Si based multilayer structure is discussed by taking into account that silicide interlayers will form upon deposition. In addition,

this chapter contains a new method to characterize sub nanometer thick (inter)layers using extended X-ray absorption fine structure (EXAFS).

Apart from interlayer formation during growth of the multilayer structures, interlayers also grow under thermal treatment. In chapter 5, in situ X-ray reflection measurements during annealing of Mo-Si based multilayer structures are described. The Si-on-Mo and Mo-on-Si interlayer growth and the evolution of the activation energy for interdiffusion at both interfaces are discussed for conditions where no constant diffusion rate can be assumed. Whereas interdiffusion during deposition and annealing in Mo-Si based multilayer structures is inevitable, in chapter 6 an improved design for thermally stable Mo-Si mutilayer structures is discussed. In this chapter, X-ray photoelectron spectroscopy (XPS) is used to study thermal stability of Mo-Si based layered structures with the inclusion of C interlayers. One of the outcomes of that research was a strong indication of thermal stability of Si-C interfaces up to 600°C, which is discussed in chapter 7.

References

[1] J.V. Hermans, H. Dai, A. Niroomand, D. Laidler, M. Mao, Y. Chen, P. Leray, C. Ngai, S. Cheng, Proc. of SPIE, 8679 (2013), 86791K

[2] B.L. Henke, E.M. Gullikson, J.C. Davis, Atomic data and nuclear data tables, 54 (1993), 181

[3] E. Spiller, Soft X-ray optics (SPIE, Bellingham, 1994)

[4] E. Louis, A.E. Yakshin, T. Tsarfati, F. Bijkerk, Progress in Surface Science, 86 (2011), 255

[5] J.L. Larruquert, J. Opt. Soc. Am. A, 18 (2001), 1406

[6] J.L. Larruquert, J. Opt. Soc. Am. A, 18 (2001), 2617

[7] J.L. Larruquert, J. Opt. Soc. Am. A, 21 (2004), 1750

[8] R.S. Rosen, D.S.P. Vernon, G. Stearns, M.A. Viliardos, M.E. Kassner, Y. Cheng, Appl. Opt., 32 (1993), 6975

[9] S. Yulin, T. Feigl, T. Kuhlmann, N. Kaiser, A.I. Fedorenko, V.V. Kondratenko, O.V. Poltseva, V.A. Sevryukova, A.Yu. Zolotaryov, E.N. Zubarev, J. Appl. Phys., 92 (2002), 1216

[10] A.P. Payne, B.M. Clemens, Phys. Rev. B, 47 (1993), 2289

[11] E.J. van Loenen, J.F. van der Veen, F.K. LeGoues, Surf. Sci., 157 (1985), 1

[12] E.J. van Loenen, A.E.M.J. Fischer, J.F. van der Veen, Surf. Sci., 155 (1985), 65

[13] V. Fokkema, thesis: Real-time scanning tunneling microscopy studies of thin film deposition and ion erosion (2011)

[14] D.G. Stearns, M.B. Stearns, Y. Chang, J.H. Stith, N.M. Ceglio, J. Appl. Phys., 67 (1990), 2415

[15] I. Nedelcu, R.W.E. van de Kruijs, A.E. Yakshin, F. Bijkerk, J. Appl. Phys., 103 (2008), 083549

[16] S. Bajt, J.B. Alameda, T.W. Barbee, W.M. Clift, J.A. Folta, B. Kaufmann, E.A. Spiller, Opt. Eng., 41 (2002), 1797

[17] T. Feigl, S. Yulin, N. Kaiser, R. Thielsch, Emerging Lithographic Technologies IV (SPIE, Santa Clara),3997 (2000), 420

[18] S. Braun, H. Mai, M. Moss, R. Scholz, A. Leson, Jpn. J. Appl. Phys., 41 (2002), 4074

[19] Hu Xu, X.B. Yang, C.S. Guo, R.Q. Zhang, Appl. Phys. Lett., 95 (2009), 253106

[20] R. Schlattman, A. Keppel, Y. Xue, J. Verhoeven, C.H.M. Marée, F.H.P.M. Habraken, J. Appl. Phys., 80 (1996), 2121

[21] Z. Erdélyi, D.L. Beke, P. Nemes, and G.A. Langer, Philos. Mag. A, 79 (1999), 1757

[22] Z. Erdélyi, D.L. Beke, J. Mater. Sci., 46 (2011), 6465

[23] Z. Erdélyi, M. Sladecek, L.M. Stadler, I. Zizak, G.A. Langer, M. Kis-Varga, D.L. Beke, B. Sepiol, Science, 306 (2004), 1913

[24] J.M. Roussel, P. Bellon, Phys. Rev. B, 73 (2006), 085403

CHAPTER 2

EXPERIMENTAL

2.1 Deposition of layered structures

All layered structures described in this thesis were deposited using physical vapour deposition techniques: electron beam evaporation and magnetron sputter deposition. In both methods, material is vaporized from the target material and condenses at the surface of the substrate. In e-beam evaporation, the target material is melted by an electron beam. The evaporated material particles arrive at the substrate with a kinetic energy of about 0.1 eV [1]. Magnetron sputter deposition is based on a gas discharge combining an electric and magnetic field. Noble gas ions (Ar or Kr) sputter the target material. In contrast to thermal evaporation, the sputtered particle energy distribution peaks around 1 to 2 eV. A small percentage of the particles are ionized. These particles, together with reflected neutral gas atoms have a kinetic energy peaking around 5 to 10 eV [1, 2, 3]. This may induce intermixing effects at shallow interfaces with layers underneath the surface of the substrate. The total impact of energy of the particles arriving at the substrate is demonstrated to cause smooth layer growth in Mo/Si multilayer structures [4]. To reduce the roughness in e-beam deposited samples, ion beam treatment of surfaces can be used. Post-deposition treatment of the Si layer by 300 eV Kr ion bombardment smoothens the surface [5]. Treatment of the Mo layer by 300 eV Kr or Ar ions can lead to smoothening if the Mo layer is still amorphous or if the crystallites are not too large. When the crystallites are too large, preferential sputtering increases the roughness of the layer [5, 6].

In the work presented in this thesis, only Si layers in multilayer mirror structures are treated by around 100 eV Kr ions, after growth of a full layer. Using Kr ions with this energy, the build-up of roughness is prevented. It is

assumed that the Si-on-Mo interfaces are not affected by the ion treatment.

Various techniques were applied to study the interlayer structures and nanoscale diffusion effects in the multilayer structures: hard x-ray reflectometry and diffraction, x-ray photoelectron spectroscopy, Auger electron spectroscopy, ellipsometry and extended x-ray absorption fine structure. A brief description of the techniques and how they were applied is given in the remainder of this chapter.

2.2 Hard X-ray reflection and diffraction

X-ray reflection and diffraction are non-destructive measurement techniques. Therefore, these techniques are suitable to be used during annealing experiments of the multilayer structures. The diffractometer that was used for these measurements is a Philips X'pert diffractometer, with a four bounce asymmetrically cut Ge (220) monochromator and Cu K_α ($\lambda = 0.154$ nm) radiation (see figure 2.1). The instrumental broadening of the measurement configuration is 0.005°.

2.2.1 Fourier analysis

Reconstruction of the multilayer structure from a $\theta - 2\theta$ X-ray reflectivity scan is no trivial task. Lack of phase information from the X-ray reflectivity measurements results in non-unique solutions. Therefore, assumptions have to be made to find a solution.

This so called inverse problem can be solved by using a Fourier transform of the Bragg peaks in a $\theta - 2\theta$ scan to express the reflectivity as a function of the electron density distribution $\rho(z)$

$$R(q_z) \propto \left| \int \frac{d\rho(z)}{dz} \exp(iq_z z) dz \right|^2, \tag{2.1}$$

where q is the out-of plane momentum transfer vector.

For small interface roughness values and neglecting layer thickness errors, the Fourier transform of the reflectivity of the Bragg orders is given by [7]

$$I_{re,m}(0) \approx \frac{2k_0^2 a_m^2 \pi L}{q_m^2} \tag{2.2}$$

where L is the total thickness of the multilayer structure, $k_0 = 2\pi/\lambda$, and a_m correspond to the amplitudes of the Fourier series (only the even terms) to describe the dielectric distribution.

Although this results in a unique reconstruction of the multilayer structure, there is one problem: as we know from the previous chapter, interlayers do not tend to be the same. In Mo/Si multilayer structures, the Mo-on-Si

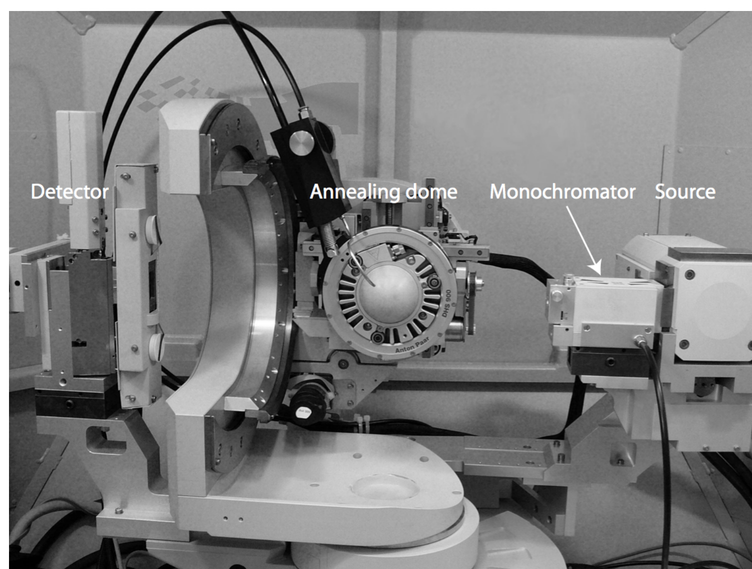

(a)

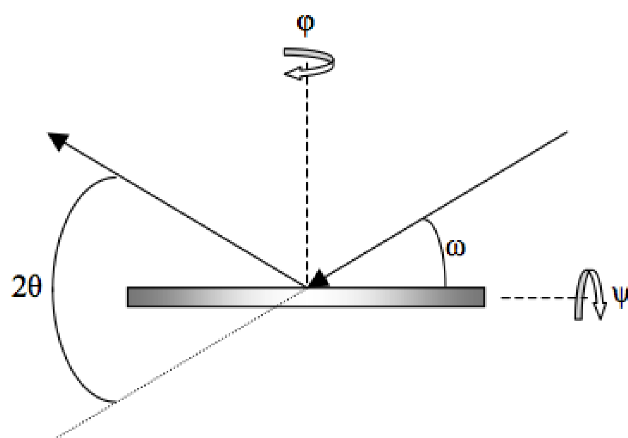

(b)

Figure 2.1: *(a) Cu K_α diffractometer: a dome covers the sample for the in situ diffusion studies (see section 2.2.2); (b) definition of the angles used throughout the text.*

interlayer is observed to be thicker than the Si-on-Mo interlayer [8]. Therefore, nanoscopic structures where interlayers are a significant part of the period and where the asymmetry in interlayer width is significant (in this case 1 nm versus 0.5 nm), the dielectric distribution of the multilayer period cannot always be approximated by only the cosine or sine part of the Fourier series.

Including asymmetric dielectric distributions into the analysis, changes equation 2.2 into

$$I_{re,m}(0) \approx \frac{2k_0^2(a_m^2 + b_m^2)\pi L}{q_m^2} \tag{2.3}$$

However, equation 2.3 has an infinite number of solutions. Therefore, a function needs to be assumed to describe the periodic dielectric profile, such that the relation between a_m and b_m is known. A reasonable description of the dielectric profile would be one with error functions at the interfaces to effectively describe intermixing.

In chapter 7 we apply this model to describe the Si/C multilayer structure. By taking the ratio of the Fourier transform of the reflectivity of different Bragg orders, we additionally eliminate the permittivities of the Si and C layer. Therefore, without assuming the densities of the individual layers, the best fit of the thicknesses of the Si, C, Si-on-C and C-on-Si (inter)layers is obtained. Elimination of densities in this case is quite relevant, given the large spread in possible C densities, namely 2.2 g/cm^3 for graphite to 3.5 g/cm^3 for diamond.

2.2.2 X-ray reflection during annealing

To measure diffusion phenomena in multilayer structures during annealing, an annealing stage with dome is mounted in the diffractometer. Before annealing, the system is aligned and a reference scan of the multilayer structure is made using the Bragg-Brentano setup (source at an angle $\omega = \theta$ and detector at an angle 2θ) for $\theta \in [0, 10°]$.

When increasing the temperature of the multilayer structure, the sample will become misaligned due to thermal expansion of the sample and sample holder. Therefore, the initial measurement cycles also include a sample realignment procedure. After a while, the system has stabilized, and realignment is not necessary anymore and is omitted from the measurement process.

During annealing, interdiffusion of the layers causes further growth of the interlayers in the multilayer structures. This results in a change of period thickness (Λ) if the atomic density (in the growth direction) of the interlayer is different than the combined atomic density (in the same direction) of the individual constituents. Hence, a change in period thickness contains information of the diffusion process. In order to accurately determine $\Lambda(t)$, $d\Lambda(t)/dt$ must be kept as low as possible. Therefore, instead of continuously

measuring from 0 to 10°, only angular regions around a few selected Bragg peaks are measured. Using a relation, derived from the corrected Bragg equation 1.5, the change in average period thickness can be calculated with picometer accuracy.

With an angular resolution of 0.005°, a total angular region of 1.3° and a measurement time of 1s per angular step, this method results in a time resolution of 260 s. An additional advantage of this measurement method is that misalignment errors in θ have limited influence on the change in the determined period thickness. In chapter 5, this measurement analysis is used to describe the initial stages of Mo-on-Si and Si-on-Mo interlayer growth.

Apart from a change in period thickness, also the change in Bragg peak intensity can be used to describe diffusion in a multilayer structure. To explain, we start from the simplified form of Fick's second equation, assuming a constant diffusion rate

$$\frac{\partial C}{\partial t} = D \frac{\partial^2 C}{\partial z^2} \tag{2.4}$$

We introduce the following periodic boundary conditions

$$\frac{\partial C(-L,t)}{\partial z} = \frac{\partial C(+L,t)}{\partial z} \tag{2.5a}$$

$$C(-L,t) = C(L,t) \tag{2.5b}$$

$$C(z,0) = f(z) \tag{2.5c}$$

where $2L = \Lambda$, and we have assumed that Λ is constant during diffusion. Using separation of variables and superposition of the solutions, we get

$$\begin{aligned} C(z,t) = &\sum_{n=0}^{\infty} A_n \cos\left(\frac{n\pi z}{L}\right) \exp\left(-D\left(\frac{n\pi}{L}\right)^2 t\right) \\ &+ \sum_{n=1}^{\infty} B_n \sin\left(\frac{n\pi z}{L}\right) \exp\left(-D\left(\frac{n\pi}{L}\right)^2 t\right) \end{aligned} \tag{2.6}$$

with coefficients

$$A_0 = \frac{1}{2L}\int_{-L}^{+L} f(z)\mathrm{dz} \tag{2.7a}$$

$$A_n = \frac{1}{L}\int_{-L}^{+L} f(z)\cos\left(\frac{n\pi z}{L}\right)\mathrm{dz} \quad n = 1,2,3,\ldots \tag{2.7b}$$

$$B_n = \frac{1}{L}\int_{-L}^{+L} f(z)\sin\left(\frac{n\pi z}{L}\right)\mathrm{dz} \quad n = 1,2,3,\ldots \tag{2.7c}$$

For hard X-rays, the concentration profile is easily converted into a dielectric profile when the atomic densities (as a function of the concentration) are known.[1] Hence, a_m in equation 2.3 is related to A_m by

$$a_m \propto A_m \exp\left(-D\left(\frac{m\pi}{L}\right)^2 t\right) \tag{2.8}$$

[1] At this moment it is not important which assumptions can be used for the densities.

where A_m is a constant, depending only on the initial concentration distribution. The relation between b_m and B_m is the same. Substituting equation 2.8 into equation 2.3, we see that $\ln(I_n(t)/I_n(0)) \propto -Dn^2t$.

However, in general the diffusion rate depends on the local concentration. In nanoscopic systems, this concentration dependence cannot be neglected. This is illustrated by diffusion in Cu/Au multilayer films ($\Lambda = 3.31$ nm) [9]. Upon annealing of the multilayer structures, the Fourier harmonics (or $I_n(t)/I_n(0)$) did not decrease exponentially. Instead, the nth order amplitude changes it's sign (n-1) times before decaying asymptotically to zero. Using numerical calculations, this effect was explained by using a concentration dependent diffusion rate: $D(u) = D_0 + D_1u + D_2u^2$, $u = c - c_0$, with c_0 being the atomic fraction of Au. The constants can be related to thermodynamic values, described in Cahn's theory of spinodal decomposition in cubic crystals [10] (see [9] for details). According to the authors, the behaviour of the oscillations appeared to be very robust. Even for $D_2 = 0$, i.e. a linear concentration dependence of the diffusion rate, the oscillations persist.

In chapter 7 we use the information of the intensity of the Bragg peaks during annealing to study interdiffusion in Si/C multilayer structures.

2.2.3 Diffraction

The Mo layers in the multilayer structures used in the in situ X-ray reflection measurements have a poly-crystalline structure, whereas the Si layers are amorphous. During annealing of the Mo-Si multilayer structures, interdiffusion will result in the reduction of the Mo layer thickness. Consequently, the Mo crystallites will gradually reduce in size. Therefore, the interlayer width and the Mo crystallite size are intrinsically coupled. Using some assumptions, discussed in chapter 5, the ratio between the crystallite size and interlayer width values can give an estimation of the stoichiometry of the growing interlayer. The ratio can more reliably be used to show whether the same phase is growing at the Si-on-Mo and Mo-on-Si interlayer.

For the measurements of diffraction peaks of the lattice plains in the Mo crystallites, the sample was positioned at $\omega = 1°$ to obtain a large illumination area. This is required, because the intensity of the diffracted peaks is quite small. The azimuthal angle ϕ was set to 20° to suppress the diffraction peak of the Si substrate. A 2θ detector scan is performed to measure the diffraction spectrum.

The crystallite size $L_{crystal}$ can be calculated using the Scherrer equation

$$L_{crystal} = \frac{K\lambda}{\beta\cos\theta}. \tag{2.9}$$

The constant $K = 0.94$ for lattices having a cubic symmetry [11], while β is the full width half maximum of the diffraction peak.

2.3 X-ray photoelectron spectroscopy

In X-ray photoelectron spectroscopy, soft X-rays (commonly Mg Kα (1253.6 eV) or Al Kα (1486.7 eV)) irradiate a sample. Due to the photoelectric effect, electrons are emitted from the sample. Due to the small inelastic mean free path of the photoelectrons, emission of electrons is only up to a few nanometers below the sample surface. The emitted electrons have a kinetic energy given by

$$E_k = h\nu - E_b - \phi_s \tag{2.10}$$

where $h\nu$ is the energy of the photon, E_b is the binding energy of the photoelectron coming from a specific atomic orbital, and ϕ_s is the work function of the spectrometer. Given that each element has a unique set of binding energies, XPS can be used to determine the elements and their concentration in the probed region. In addition, the environment of the specific elements can lead to variations in the binding energies of the atomic levels. The chemical shift can be used to identify the chemical state of the elements.

To obtain more information on the location of atomic species in depth, the emission of electrons is measured at different angles. The fractional resolution ($\Delta z/z$) is usually between 0.8 and 1.3 [12]. Therefore, the data cannot be described by a unique model on a detailed level. However, ARXPS can be used as a qualitative analysis method to describe the relative location of elements (including chemical shifts).

Sputter erosion of the sample by a noble gas, like Ar or Kr, is used to obtain information on the composition of structures in depth. Calibration of the sputter rate for different materials can be used to convert the sputter time to depth of the sample. This basically assumes that the sputter rate is constant throughout the layer of a fixed composition. Calibration of layer thicknesses was related to thicknesses deduced from quartz crystal microbalances during deposition. Therefore, the depth scale is only accurate for the film thickness. Variations of the individual layer composition can introduce large sputter rate differences. For example, C has an approximately 2.5 higher atomic density compared to Mo, but a more than 4 times lower sputter yield for the 500 eV Ar used [13]. The sputtering may cause differences in the sample composition and chemical state near the surface. Consequently, it difficult to use this technique to probe the composition of a structure with sub nanometer accuracy. However, when the technique is used to look at relative changes between almost similar samples, qualitative answers on a change of structure can be obtained.

Due to the complexity of the C/Mo_2C/C/Si structure (chapter 6), and the large number of possibilities for interdiffusion during annealing of these structures, sputter-depth profiling was preferred over X-ray reflection to look at in depth compositional changes.

2.4 Extended X-ray absorption fine structure

Similar to XPS, extended X-ray absorption fine structure (EXAFS) is a technique where X-rays are absorbed to produce photoelectrons. In EXAFS, measurement of the absorption of light around the absorption edge of an element is used to determine the local atomic structure of that element. This technique can provide detailed information about the layered structure. Below, a short derivation of the EXAFS fine-structure function $\chi(k)$ is given.[2]

The absorption coefficient μ in the X-ray absorption process is proportional to the transition probability of the photoelectron, given by Fermi's golden rule

$$\mu(E) \propto |\langle i|H|f\rangle|^2 \tag{2.11}$$

where $\Delta\langle i|$ is the initial state (X-ray, atom in normal state), and $|f\rangle$ is the final state (photoelectron, excited atom). The final state can also be written like

$$|f\rangle = |f_0\rangle + |\Delta f\rangle \tag{2.12}$$

where $|f\rangle$ is related to the effect of the neighbouring atom. This gives

$$\mu(E) \propto |\langle i|H|f_0\rangle|^2 \left[1 + \langle i|H|\Delta f\rangle \frac{\langle f_0|H|i\rangle^*}{|\langle i|H|f_0\rangle|^2} + C.C.\right] \tag{2.13}$$

where the first term on the right hand side is related to the absorption of an isolated atom, and the information of the fine structure comes from $\chi(E) \propto \langle i|H|\Delta f\rangle$. The relevant part of the interaction term H for absorption is proportional to $\exp(ikr)$, where k is the wave number of the photoelectron. The tightly bound core-level of the initial state is approximated by a delta function. The final state is represented by the wave function of the scattered photo-electron. This gives

$$\chi(E) \propto \int \delta(r) \mathrm{e}^{ikr} \psi_{scatt}(r) dr = \psi_{scatt}(0) \tag{2.14}$$

The outgoing photoelectron travels as a spherical wave towards a neighbouring atom at distance R, and travels back to the absorbing atom as a sperical wave. The fine-structure function $\chi(k)$ is now given by

$$\begin{aligned}\chi(k) \propto \psi_{scatt}(k, r=0) &= \frac{\mathrm{e}^{ikR}}{kR} \left[2kf(k)\mathrm{e}^{i\delta(k)}\right] \frac{\mathrm{e}^{ikR}}{kR} + C.C. \\ &= \frac{f(k)}{kR^2} \sin(2kR + \delta(k))\end{aligned} \tag{2.15}$$

where $f(k)$ and $\delta(k)$ are scattering properties of the neighbouring atom, which are unique for every atomic species. Taking into account different

[2]Brief summary of "Fundamentals of XAFS" by M. Newville.

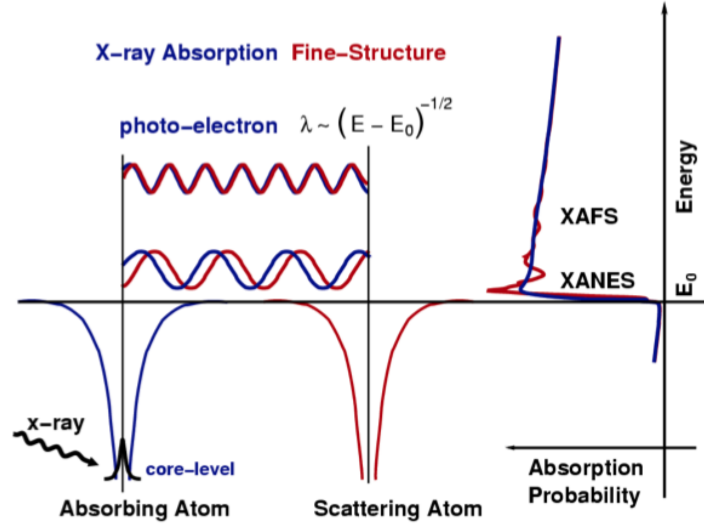

Figure 2.2: *Graphical description of the EXAFS measurement. Illustration taken from "Fundamentals of XAFS" by M. Newville.*

types of atoms can be at neighbouring sites, thermal and static disorder in the structure, a finite core-hole lifetime and inelastic scattering of the photoelectron, the EXAFS function becomes

$$\chi(k) = \sum_j \frac{N_j \mathrm{e}^{-2k^2\sigma^2} \mathrm{e}^{-2R_j/\lambda(k)} f_j(k)}{kR_j^2} \sin(2kR_j + \delta_j(k)) \tag{2.16}$$

A graphical depiction of the EXAFS measurement is given in figure 2.2. By scanning the energy over the absorption edge, the changes in the interference of the waves gives rise to a fine structure on the absorption signal.

Although EXAFS measurements probe the local atomic structure of a specific atomic species, this information is averaged over the entire illuminated area. If the environment of the element under study is not homogeneous throughout the sample, this may limit the accuracy: if only a small part of a layer is of interest (for example an interlayer), the EXAFS signal is 'polluted' by information from the rest of the layer.

One solution is to use standing waves in combination with EXAFS. Two different approaches have been used: (1) a multilayer structure is probed around a Bragg peak [14]; (2) generation of a standing wave by total external reflection from a high Z element layer [15]. By using a wedge in the structure, several locations of the layer are probed (see figure 2.3). Although both approaches indeed make the EXAFS measurements more sensitive to certain regions, the resolution of both approaches is limited by the thickness of the structure. In the multilayer structure, the wavelength of the standing

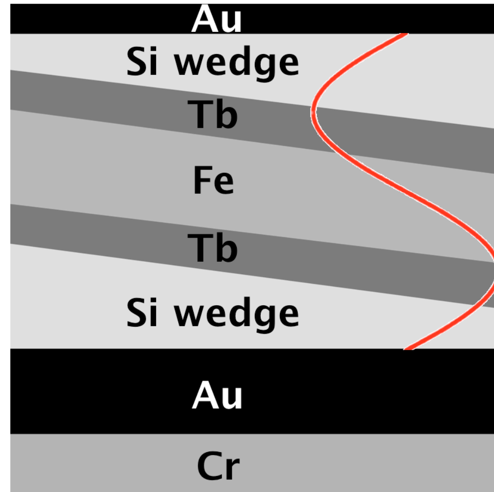

Figure 2.3: *Waveguide setup for the use of standing wave in EXAFS measurements; graph based on setup from Gupta et al. to study the interfaces in a Tb/Fe/Tb structure [15].*

wave should be equal to the period thickness, otherwise multiple regions in one period are probed. In the waveguide structure, the wavelength of the standing wave should be limited to at least the thickness of the middle layer and both interlayers. Otherwise, when measuring one interface, a significant signal of the other interface will be measured.

To overcome this limitation, we used a different approach to increase the EXAFS sensitivity to the interface region. Instead of using a complete layer of material A (where A is the material we want to study), all of the layer with material A is replaced by material $\tilde{A}$, except the specific region of interest. It is required that material $\tilde{A}$ has the same lattice as material A, and that the absorption edge of $\tilde{A}$ is sufficiently far removed from the absorption edge of A.

To study the Mo layer at the Y interface in a B_4C/Mo/Y/Si multilayer structure, we substituted a part of the Mo layer by Nb. Like Mo, the crystallographic structure of Nb is BCC. The lattice parameter of Mo and Nb are given by 315 and 330 pm, respectively. They both have a similar distribution of surface free energies (based on ab-initio calculations [16]). Therefore, we expect a similar kind of polycrystalline growth. An additional suggestion that Mo and Nb will grow similar in this kind of system, is that Nb/Si multilayer structures also exhibit asymmetric interlayer widths. The interlayer thicknesses are in very good agreement with the Mo-Si interlayer thicknesses [17]. The results of this method are described in chapter 4.

2.5 Ellipsometry

To study growth of layers during deposition, ellipsometry is another useful technique. In ellipsometry the change in polarization of the reflected light of a structure is measured. The complex reflectance ratio ρ is usually parametrized into an amplitude component and a phase component

$$\rho = \tan \Psi e^{i\Delta} = \frac{r_s}{r_p} \tag{2.17}$$

where r_s and r_p are the complex reflection coefficients for the perpendicular and parallel field, respectively. For a structure with N layers on a substrate, they are given by the recursive Rouard equation

$$r_j^{p,s} = \frac{r_{j-1,j}^{p,s} + r_{j+1}^{p,s} \exp(-2i\phi_j)}{1 + r_{j-1,j}^{p,s} r_{j+1}^{p,s} \exp(-2i\phi_j)} \qquad j = 1, 2, \ldots, N \tag{2.18a}$$

$$\phi_j = \frac{2\pi}{\lambda} n_j d_j \cos\theta_j \tag{2.18b}$$

$$r_{i,i+1}^{s} = \frac{n_i \cos\theta_i - n_{i+1} \cos\theta_{i+1}}{n_i \cos\theta_i + n_{i+1} \cos\theta_{i+1}} \tag{2.18c}$$

$$r_{i,i+1}^{p} = \frac{n_i \cos\theta_{i+1} - n_{i+1} \cos\theta_i}{n_i \cos\theta_i + n_{i+1} \cos\theta_{i+1}} \tag{2.18d}$$

When either the optical constants, or the exact thicknesses of the layers are known, this can be solved easily. However, for in situ study of layer deposition at a (sub) nanometer scale, in general both the refractive indices and the exact thicknesses are not known.

The so-called virtual substrate analysis for monitoring layer growth during deposition was developed by Aspnes [18]. The method can be used to calculate the refractive index of the growing layer, without accurate knowledge of the underlying "virtual" substrate. However, this method is not applicable when the underlying layer changes it's properties continuously. This is the case when there is interdiffusion during layer growth. Therefore, ellipsometry cannot be used directly, using such models, to study interlayer growth. However, ellipsometry can be used as an indirect measurement technique to look at relative interlayer growth in Mo-on-Si structures with different treatments of the Si surface. This will be discussed in chapter 3.

References

[1] P.J. Martin, Journal of Materials Science, 21 (1986), 1

[2] W. Eckstein, Journal of Nuclear Materials, 248 (1997), 1

[3] T. Mousel, W. Eckstein, H. Gnaser, Nuclear Instruments and Methods in Physics Research B, 152 (1999), 36

[4] E. Spiller, Appl. Phys. Lett., 54 (1989), 2293

[5] R. Schlatmann, C. Lu, J. Verhoeven, E.J. Puik, M.J. van der Wiel, Appl. Surf. Sci., 78 (1994), 147

[6] J. Verhoeven, Lu Chunguang, E.J. Puik, M.J. van der Wiel, T.P. Huijgen, Appl. Surf. Sci., 55 (1992), 97

[7] A.D. Akhsakhalyan, A.A. Fraerman, N.I. Polushkin, Yu.Ya. Platonov, N.N. Salashchenko, Thin Solid Films, 203 (1991), 317

[8] R.S. Rosen, D.S.P. Vernon, G. Stearns, M.A. Viliardos, M.E. Kassner, Y. Cheng, Appl. Opt., 32 (1993), 6975

[9] E.S.K. Menon, P. Huang, M. Kraitchman, J.J. Hoyt, P. Chow, D. de Fontaine, J. Appl. Phys., 73 (1993), 142

[10] J.W. Cahn, Acta.Metall., 10 (1962), 179

[11] A.L. Patterson, Phys. Rev., 56 (1939), 978

[12] P.J. Cumpson, Journal of Electron Spectroscopy and Related Phenomena, 73 (1995), 25

[13] Y. Yamamura, H. Tawara, Atomic Data and Nuclear Data Tables, 62 (1996), 149

[14] D.C. Meyer, K. Richter, P. Paufler, P. Gawlitza, T. Holz, J. Appl. Phys., 87 (2000), 7218

[15] A. Gupta, D. Kumar, C. Meneghini, J. Zegenhagen, J. Appl. Phys., 101 (2007), 09D117

[16] L. Vitos, A.V. Ruban, H.L. Skiver, J. Kollár, Surf. Sci., 411 (1998), 186

[17] E.E. Fullerton, J. Pearson, C.H. Sowers, S.D. Bader, Phys. Rev. B, 48 (1993), 17432

[18] D.E. Aspnes, J. Opt. Soc. Am. A, 10 (1993), 974

CHAPTER 3

MO-SI INTERLAYER GROWTH DURING DEPOSITION

Abstract

To study the mechanism behind the asymmetry in interlayer growth in Mo-Si multilayer structures, we performed density functional theory calculations. We calculated the adsorption energy of Mo atoms and the energy related to formation of a Mo cluster on a Si (100) surface as well as the case of Si atoms on a Mo (100) surface. Furthermore, the energy related to diffusion of a Si substrate atom towards the Mo cluster and of a Mo substrate atom towards the Si cluster was calculated. In relation to the calculations, ellipsometry measurements were performed to study the Mo-on-Si interlayer growth. To modify the morphology of the Si surface, Ar ion sputtering of the Si layer was used in the energy range of 300-1000 eV. The influence of the different surface morphologies on the Mo-on-Si interlayer growth is discussed.

3.1 Introduction

The Si-on-Mo and Mo-on-Si interlayers in Mo-Si multliayer structures are known to have different composition and thickness. Various interlayer widths are reported. However, as can be seen from the overview reported by Yulin [1], both in magnetron sputtering and e-beam evaporation, the Mo-on-Si interlayer is larger than the Si-on-Mo. Based on the reported interlayer thickness values, it may even be suggested that the possible difference in kinetic energy of deposited atoms between e-beam and magnetron deposition has no influence on the Mo-Si interlayer formation. Several explanations for the difference in Mo-on-Si and Si-on-Mo interlayer widths are given in literature, however they are non conclusive.

According to both Yulin [1] and Stearns [2], the structure of the surface is the explnation for the asymmetry in interlayer thickness. According to Stearns, the amorphous Si layer has an open and disordered structure. Consequently, Mo atoms can easily be embedded in the Si layer. A modified explanation is provided by Bedrossian [3]. Using tunneling microscopy, Bedrossian showed that the Si (100) surface can be penetrated by Mo atoms at certain crystallographic locations. Consequently, the Mo atoms assist in breaking the strong Si covalent bonds. This mechanism of weakening some Si surface bonds due to metal implantation was also proposed by Tu [4]. The low activation energy of Si surface diffusion is the reason that the Si atoms can sustain the interlayer growth for a while.

Contrary to the amorphous Si layer, the Mo layer usually has a polycrystalline structure (above 2.3 nm Mo thickness [1]). Yulin argues that Si atoms arriving at the Mo surface penetrate into the Mo grains mainly due to bulk diffusion. The diffusion rate of Si in Mo is very low for the (low) temperatures during deposition. Therefore, small interlayers are formed.

A different explanation is given by van Loenen *et al.* [5, 6]. They suggest that clustering of metal atoms on a Si surface provide a fair amount of energy to the system. This energy could be used for interdiffusion of atoms at the interface. Fokkema [7] has shown using STM measurements during growth of Mo on a Si (111)-(7x7) reconstructed surface, that initially clusters of 2-4 Mo atoms grow on the Si surface. In the vicinity of these clusters, formation of shallow holes are observed (removal of Si adatoms).

If we consider only the cohesive energy of the material that is growing on the substrate, this explanation of clustering provides an additional explanation for the difference between Si-on-Mo and Mo-on-Si layer growth. Namely, the cohesive energy of Si is much lower than the cohesive energy of Mo. This can easily be seen from the difference in melt temperature: 1687 K for Si vs. 2896 K for Mo. However, also the Si-Mo bonds should be considered for the formation of clusters on the surface.

To take the Mo-Si bonds into account during cluster formation, we performed density functional theory calculations to gain more insight in the

energies that are related to thin film growth in Mo-Si structures and to understand the reason behind the asymmetry between both interlayer structures. We calculate the clustering energy for Si atoms on a Mo (100) surface and for Mo atoms on a Si (100) surface. In addition, the energies are calculated for the interaction of surface atoms of the substrate with the growing cluster. In relation to the DFT calculations, experimental results are included to study interlayer growth during deposition of Mo atoms on Ar ion beam sputtered Si surfaces.

3.2 Experimental

All DFT calculations were performed using the plane wave pseudo-potential code Abinit [8].[1] For the calculations, norm-conserved GGA pseudo-potentials from the FHI code were used.[2] In all calculations, a 4x4x1 k-grid was used. The cut-off energy was set to 25 Ha.

We performd two different kind of energy calculations: (1) adsorption and clustering of Mo atoms on a Si (100) surface and Si atoms on a Mo (100) surface; (2) diffusion of substrate atoms towards the cluster on the surface.

Calculation of ΔE (energy gain) for clustering of n atoms of type B on a surface of atoms of type A is defined as

$$\Delta E = E_{substrate+n\cdot atom_B} - E_{substrate} - nE_{atom_B}, \qquad (3.1)$$

where $E_{substrate}$ is the energy of the substrate consisting of atoms of type A, $E_{substrate+n\cdot atom_B}$ is the energy of the substrate plus n atoms of type B adsorbed on the surface, and E_{atom_B} is the energy of atom B in a vacuum box.

For the calculations of surface diffusion of a substrate atom towards the surface cluster, ΔE is defined as the difference in energy between the atom of type A at the surface at lateral distance r from the initial substrate position and at the initial position at the substrate. In this case, a positive value of ΔE means that it requires additional energy to move the atom to that position.

In the calculations, it was the aim to get an estimate of the immediate energy gain during clustering, not the gain of energy when also allowing full relaxation of all atomic positions. The substrate was relaxed before depositing additional atoms at the surface (discussed in detail in section 3.3.1). During the clustering, we only allowed the adsorbed atoms to move to their preferred locations. Therefore, the calculated energies during adsorption should be considered as approximations. Furthermore, during the diffusion of substrate atoms towards the cluster on the surface, we do not relax all surface atoms. We presume that movement of the atom towards the cluster

[1] http://www.abinit.org

[2] http://www.abinit.org/downloads/psp-links/psp-links/gga_fhi

is faster than a full relaxation of all nearby surface atoms. This presumption is validated by calculating surface diffusion of a Mo atom on a Mo surface and of a Si atom on a Si surface and comparing this to reported literature values for surface diffusion.

For the experimental study, Si was deposited on a Si (100) substrate (with native Si-oxide) using a-beam evaporation, in a chamber with a base pressure lower than $1 \cdot 10^{-9}$ mbar. A Kaufmann ion source was used for Ar ion treatment (300, 600 and 1000 eV) of the Si layer under an angle of 45°. Mo was deposited on the untreated or ion treated Si layer. The Mo layers were deposited with a rate of 5 pm/s. Deposition was monitored using a quartz crystal microbalance. Furthermore, during deposition and ion beam treatment of the sample, spectroscopic ellipsometry was used to monitor the sample: wavelength region 245.331–1689.411 nm, acquisition time 1 s. The angles Ψ and Δ in this text are defined as

$$\tan \Psi \exp(i\Delta) = \frac{r_s}{r_p}, \tag{3.2}$$

where r_s and r_p are the complex refraction coefficients for the perpendicular and parallel field, respectively.

3.3 Results and discussion

3.3.1 Calculations of Mo on a Si (100) surface

Si atoms at the Si (100) surface have two dangling bonds. To reduce the energy of the surface, atoms at the surface may relax to different locations. The dimer formation in the 2x1 reconstructed (100) surface results in a large open area in between the dimers. This open space can easily be occupied by deposited Mo atoms. This will result already in an interlayer. For practical purposes, the calculations presented here are for the unreconstructed (100) surface, such that we can grow Mo in the BCC configuration on the Si surface. In the discussion of the results, we will take the likely underestimation of the calculation for interlayer formation into account.

Fig.3.1 shows the type of structures that were calculated for (a) adsorption (b) for diffusion. To see the effect of the cohesive energy of a cluster at the surface with respect to the Mo-Si surface bond, the Mo atoms were "positioned" in a BCC configuration. The results of Mo clustering on the Si surface are illustrated in Fig.3.2. The energy gain of adsorption of a Mo atom on the Si surface is around 9 eV/atom. As the Mo cluster grows, this energy is reduced. When the fifth Mo atom is deposited at the center of the Mo cluster, the energy gain for this atom is "only" 5.3 eV. This gain is less than the calculated cohesive energy of 7.63 eV for Mo. The relatively small energy gain can be explained by the relatively large Mo-Mo bond distance in this cluster: $\epsilon_x = \epsilon_y = 10.3\%$, $\epsilon_z = 15.7\%$. However, the local energy gain

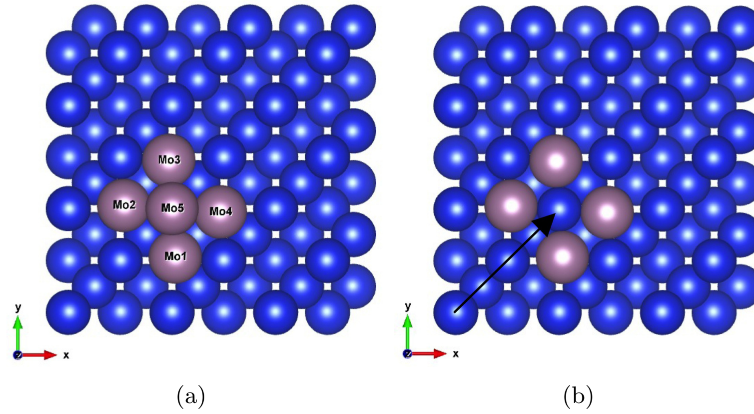

(a) (b)

Figure 3.1: *Top view Si slab with: (a) 5 Mo atoms at surface; (b) 4 Mo atoms at surface, Si atom at the surface of the substrate moving along the direction of the arrow.*

in all cases is higher than the cohesive energy of Si. Therefore, diffusion of Si surface atoms can be expected.

From Fig.3.2 we also see that the initial Mo atoms (1 to 4 in figure 3.1) are almost inside the Si surface. The center of the Mo atoms are only about 12 pm above the center of the Si surface atoms. When the fifth Mo atom is deposited in the center of the Mo cluster, the height of the first plain is increased to 34 pm. Concluding, it is not only true that amorphous Si has an open structure for Mo, it is also true for a crystalline Si surface (100).

The energy related to diffusion of a Si surface atom is illustrated in Fig.3.3. The first metastable point at a distance of approximately 0.15 nm is at the usual Si lattice position (if another layer of Si would grow on the surface). The required energy to diffuse to this position is 1.2 eV. To cross the second maximum, an energy of approximately 0.9 eV is required. This value is comparable to the Si (100) surface diffusion energy of 0.7 eV [9]. If either this Si atom, or another Si surface atom crosses this potential barrier, the Si atom effectively becomes trapped by the Mo cluster. Namely, the second minimum around 0.55 nm is at the bridge between the two Mo atoms. To diffuse back, outside the Mo cluster, an energy of more than 2 eV is required.

3.3.2 Calculations of Si on a Mo (100) surface

The type of structures that were calculated are illustrated in Fig.3.4. The results of the Si clustering at the Mo surface are illustrated in Fig.3.5. The energy gain per Si atom is about 7.5 eV. For the fifth Si atom deposited near the center of the Si cluster, the gained energy is still 5.1 eV. Even

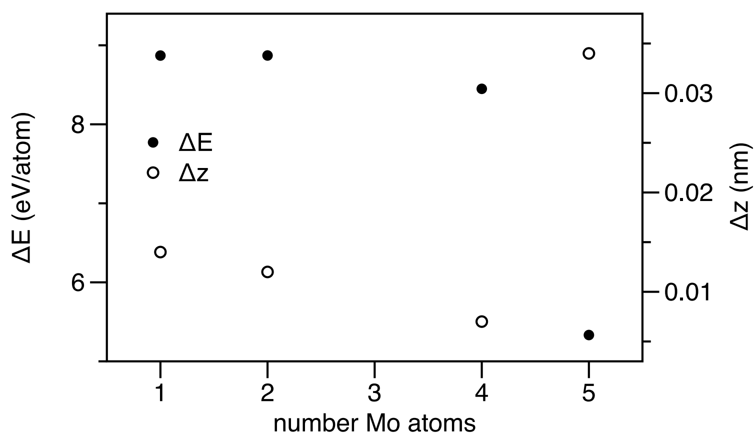

Figure 3.2: *Energy gain per additional atom in Mo cluster at the Si (100) surface and the distance of the first Mo layer (atoms 1 to 4 from figure 3.1) with respect to the Si surface atoms.*

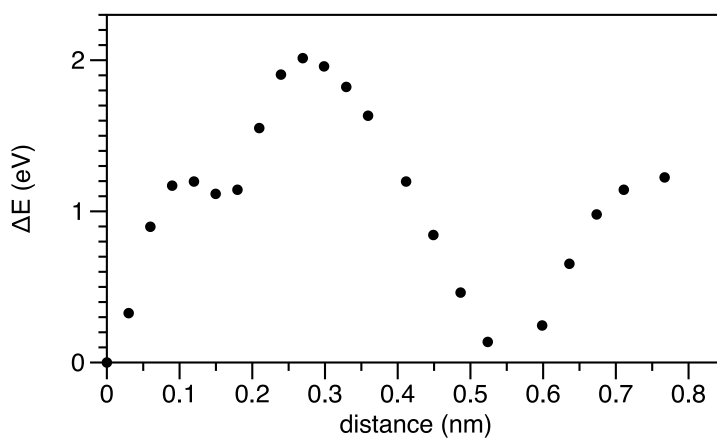

Figure 3.3: *Difference in total energy between the Si atom at the bottom left corner and at distance r from the initial position.*

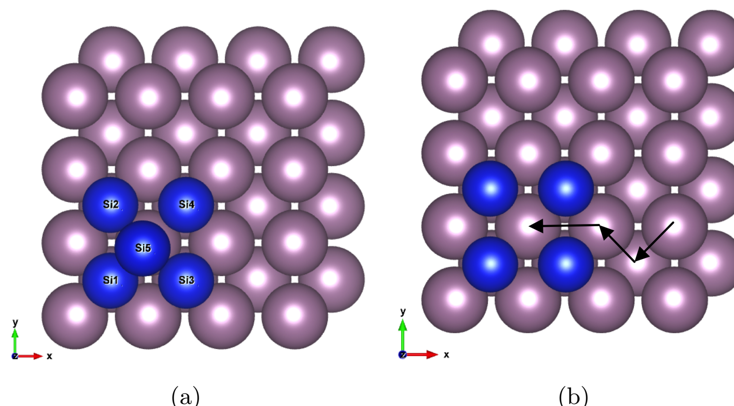

(a) (b)

Figure 3.4: *Top view Mo slab with: (a) 5 Si atoms at surface; (b) 4 Si atoms at surface, Mo atom moving along direction of the arrows.*

though the Si is not in the diamond configuration (and with the optimum Si-Si distances), this is still larger than the calculated cohesive energy of 4.5 eV.

Contrary to the Mo-on-Si situation, the first Si layer is still approximately 0.13 nm above the Mo surface and not, like the Mo-on-Si case, "inside" the surface plane. The energy required to move a Mo atom from the substrate to the surface is about 1.4 eV. Another 3.95 eV is required to move the Mo atom inside the Si cluster, along the path of the arrows in Fig.3.4. Therefore, the probability to move the Mo atom inside the Si cluster is lower than the probability to move the Si atom inside the Mo cluster.

Furthermore, the activation energy for Mo surface diffusion of 2.4 eV [10] or 1.8 eV in our calculations (energy for a surface Mo atom on a Mo slab) is rather high, compared to the low activation energy of 0.2 eV for the Mo atom to jump back to the initial position. Therefore, it is likely that the Mo atom will return to the initial Mo surface position.

Comparing the Si-on-Mo situation with the Mo-on-Si, we see that in both cases the local energy gain is comparable or higher than the cohesive energy of the substrate. More specifically, the Mo-on-Si adsorption energy is approximately 1.5 eV higher than the Si-on-Mo adsorption energy. This favors already Mo-on-Si interlayer growth over Si-on-Mo interlayer growth.

But more importantly, due to the very different height of the cluster of adatoms with respect to the substrate atoms (Mo grows "inside" the Si surface, whereas Si grows on top of the Mo surface), much less energy is required for Si substrate atoms to become trapped by the growing Mo cluster than for Mo substrate atoms to become trapped by the growing Si cluster. In addition, the asymmetry in energy for surface diffusion towards

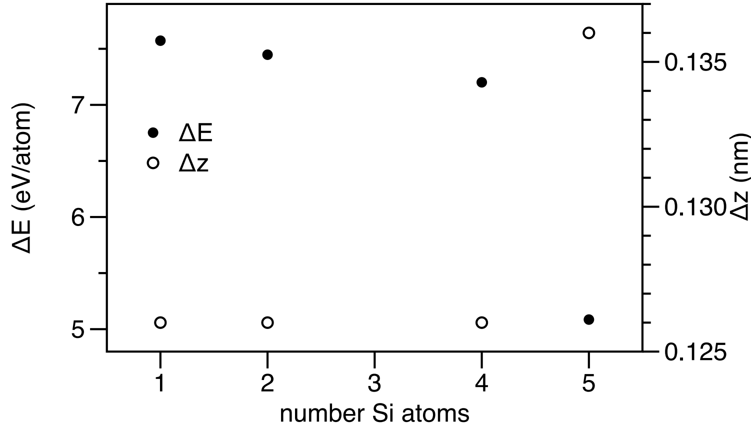

Figure 3.5: *Energy gain per additional atom in Si cluster at the Mo (100) surface and the relative distance of the first Si layer with respect to the Mo surface atoms.*

the inside of the cluster or to diffuse back towards the initial position is much smaller for Mo-on-Si than for Si-on-Mo layer growth.

Both effects should result in a larger probability for Mo-on-Si interdiffusion than for Si-on-Mo interdiffusion during deposition. Therefore, based on the asymmetry in trapping probability of substrate atoms by the growing clusters at the two interface types, the Mo-on-Si interlayer is expected to be larger (which is in agreement with the experimental observations).

Although the calculations are only for (100) surfaces, similar results should be expected for different orientations, based on the difference in atomic packing factor of body centered cubic structure (0.68) and diamond cubic structures (0.34): the atomic density at a Si surface is lower than at a Mo surface.

3.3.3 Deposition of Mo on non-ordered Si surfaces

In deposited structures, layers are not always crystalline. An amorphous layer has a lower atomic density than a (unstrained) crystalline layer. Therefore, the cohesive energy of atoms in an amorphous structure is lower than in the crystalline structure. In deposited multilayer structures, the Si layer has an amorphous structure whereas Mo has a polycrystalline structure. If the Mo crystallites are too large, ion bombardment cannot reduce the roughness of the Mo layer, but it can reduce the roughness of the amorphous Si layer [11, 12]. To study whether Ar ion bombardment of the Si surface increases the cohesive energy of the surface atoms and reduces Mo-on-Si interlayer growth, the Mo-on-Si interlayer growth was studied. The Mo-on-Si interlayer is also of particular interest since it is larger than the Si-on-Mo

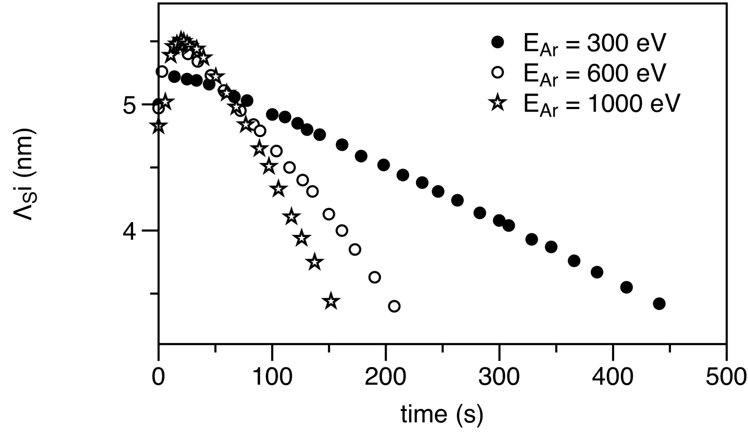

Figure 3.6: *Change of layer thickness and thickness of the roughness layer of a deposited Si layer (on a Si (100) substrate with native oxide) during Ar ion treatment with an energy of 300, 600 and 1000 eV.*

interlayer. Therefore, reduction of the Mo-on-Si interlayer width is most important for Mo-Si multilayer mirrors for EUV reflection.

To study Mo-on-Si interlayer growth, ellipsometry measurements were performed during deposition of Mo on Si. The surface of the Si layer was altered by Ar ion bombardment (300, 600 or 1000 eV). Mo was deposited on the ion treated Si surfaces. As a reference, Mo was also deposited on an untreated, amorphous Si surface.

In Fig.3.6 the evolution of the thicknesses of the treated Si layers is illustrated. For the Ar treated Si surfaces, we see initially an increase in Si layer thickness. This may be "swelling" of the Si layer due to implantation of Ar ions. The roughness of the Si layer decreased to a value of approximately 1 nm for all Ar ion treatments. The observation that the roughness layer thickness is independent of the used Ar ion energy, is in agreement with van den Boogaard [13]. They showed that the difference in energy (130 and 2000 eV) of Kr ion sputtering at 50° (normal angle of incidence) of e-beam deposited Si layers does not result in a difference of interface roughness.

The typical dependency of Ψ at 819.190 nm (selected due to high intensity of this wavelength, i.e. good signal to noise ratio) during growth of Mo on Si is included in Fig.3.7 a. Around 2.1 nm of deposited Mo, a discontinuity of the initial trend in Ψ is visible. To show the reproducibility of this feature, the measurement of two different samples is included. It is clear that the location of the feature is reproduced very accurately. Several authors reported that after approximately 2 nm of Mo is deposited on amorphous Si, the Mo layer starts to crystallize [14, 15]. For Mo layer thicknesses

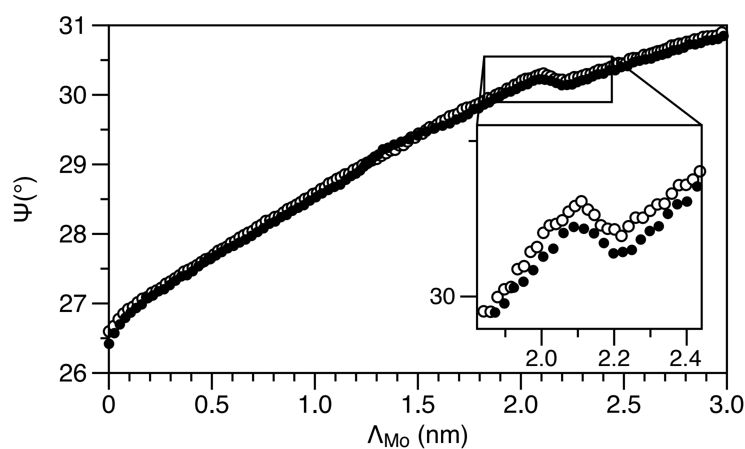

(a)

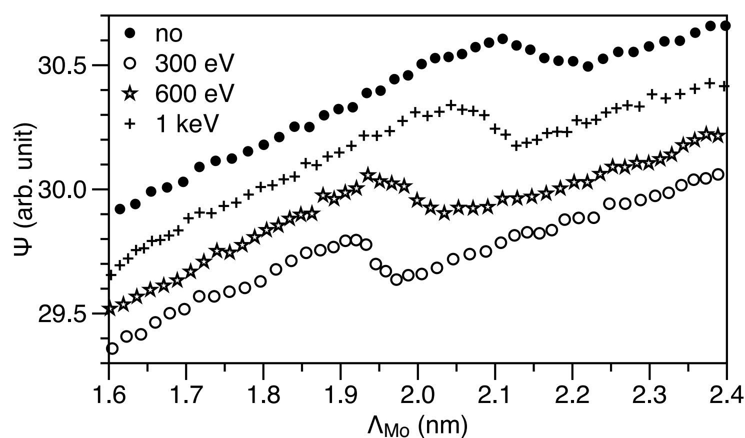

(b)

Figure 3.7: *Change of ellipsometric angle* Ψ *at 819.190 nm during: (a) Mo growth on 5 nm deposited Si; (b) Mo growth on 5 nm Si or on 6 nm deposited Si treated with energetic Ar ions. The curves in (b) are shifted in* Ψ *for viewing purposes.*

below this critical thickness, no crystallites are observed. However, for Mo layer thicknesses larger than the critical thickness, the Mo grain size in the growth direction is reported to be the same thickness as the Mo layer itself [16]. The authors show that when the Si concentration in Mo is below 7 at.%, Mo nano-crystals start to form. When crystallization occurs, the density of the Mo layer increases, and consequently the Mo layer reduces in thickness. Since Ψ at 819.190 nm increased during growth of Mo, crystallization results in a decrease of Ψ. Therefore, we presume that crystallization of the Mo layer is the reason for the feature around 2.1 nm of deposited Mo.

Instead of attempting to fit the ellipsometric data, we use this feature to indirectly resolve whether a certain treatment of the Si layer changes the Mo-on-Si interlayer growth. Namely, Mo crystallization is directly related to the Mo-Si interdiffusion: when the interlayer is thinner, i.e. when the threshold value of 7 at.% of Si in Mo is reached for a smaller amount of deposited Mo, the Mo layer will also start to crystallize at a smaller amount of deposited Mo.

In principle, X-ray diffraction also gives indirect information on whether a certain treatment results in different interlayer thicknesses. However, since the crystallite thickness is related to the full width half maximum of the diffraction peak, diffraction is highly sensitive to small errors. Furthermore, the shape of the diffraction peak may be influenced by the silicide interlayer. This introduces another inaccuracy and uncertainty.

In Fig.3.7, the results of the Mo growth on the treated Si surfaces are illustrated. For the lowest energy that was used for the Ar ions (300 eV), we observe the largest shift of the Mo crystallization threshold. The crystallization of the Mo layer occurs around 1.9 nm instead of the 2.1 nm. The crystallization of the Si surface treated by 1 keV Ar ions is around 2.05 nm. From the ellipsometric data, there was an indication that the roughness σ of the Si layer was the same for all the Ar treatments. The roughness was about 0.4 nm smaller than the untreated Si surface. Therefore, it appears that the surface roughness is not a dominant factor for the interlayer growth (or the crystallization threshold of the Mo layer). The difference between the Ar ion treatments is first of all in the interaction time of the Ar ions with the surface atoms. For a lower Ar ion energy, the interaction time with the surface is the largest. Therefore, more energy is released near the surface for lower energies of Ar ion bombardment. This results in a better relaxation of the surface atoms. Additionally, for higher energy of the ions, the probability is higher to create defects. Combining both effects, the cohesive energy of the Si surface atoms is expected to be higher for the sputtering with lowest energy of Ar ions. The increased Si cohesive energy at the surface in turn reduces the probability for Mo-Si interdiffusion during deposition.

3.4 Conclusions

Using DFT calculations, we determined the energies related to adsorption for two specific Mo-Si structures: Mo adsorption and cluster formation at a Si (100) surface and Si adsorption and cluster formation at a Mo (100) surface. It was calculated that in both cases, the local gain in energy is at least equal to the cohesive energy of the substrate atoms. For Mo-on-Si adsorption, the local energy gain is about 1.5 eV/atom higher than for Si-on-Mo adsorption. This supports the generally found phenomenon that the Mo-on-Si interlayer is thicker than the Si-on-Mo interlayer.

More importantly, based on the calculated energy for surface diffusion of substrate atoms towards the surface clusters, the probability for Si atoms to be trapped by deposited Mo clusters is expected to be higher than for Mo atoms to be trapped by deposited Si clusters. We propose that it is the difference in trapping probability that mainly explains the observed asymmetry in Mo-Si interlayer widths in Mo/Si multilayer structures.

In addition, using ellipsometry during deposition, we also studied the effect of Si surface treatment by Ar ions on the Mo-on-Si interlayer growth. The crystallization of the Mo layer occurs at 1.9 nm for the Si surface that was sputtered by 300 eV Ar ions, whereas for the untreated Si surface crystallization occurs at 2.1 nm. The ion treatment resulted in a better surface relaxation, thereby increasing the cohesive energy of the Si surface atoms. The increased cohesive energy reduced the probability for interdiffusion with Mo clusters. This resulted in a thinner Mo-silicide interlayer, and hence in crystallization of the Mo layer at a smaller amount of deposited material. This demonstrates that by modifying the Si surface morphology, Mo-on-Si interlayer formation can be reduced.

References

[1] S. Yulin, T. Feigl, T. Kuhlmann, N. Kaiser, A.I. Fedorenko, V.V. Kondratenko, O.V. Poltseva, V.A. Sevryukova, A.Yu. Zolotaryov, E.N. Zubarev, J. Appl. Phys., 92 (2002), 1216

[2] D.G. Stearns, M.B. Stearns, Y. Chang, J.H. Stith, N.M. Ceglio, J. Appl. Phys., 67 (1990), 2415

[3] P.J. Bedrossian, Surf. Sci. 320 (1994), 247

[4] K.N. Tu, Appl. Phys. Lett. 27 (1975), 221

[5] E.J. van Loenen, J.F. van der Veen, F.K. LeGoues, Surf. Sci., 157 (1985), 1

[6] E.J. van Loenen, A.E.M.J. Fischer, J.F. van der Veen, Surf. Sci., 155 (1985), 65

[7] V. Fokkema, thesis: Real-time scanning tunneling microscopy studies of thin film deposition and ion erosion (2011)

[8] X. Gonze, B. Amadon, P.-M. Anglade, J.-M. Beuken, F. Bottin, P. Boulanger, F. Bruneval, D. Caliste, R. Caracas, M. Cote, T. Deutsch, L. Genovese, Ph. Ghosez, M. Giantomassi, S. Goedecker, D.R. Hamann, P. Hermet, F. Jollet, G. Jomard, S. Leroux, M. Mancini, S. Mazevet, M.J.T. Oliveira, G. Onida, Y. Pouillon, T. Rangel, G.-M. Rignanese, D. Sangalli, R. Shaltaf, M. Torrent, M.J. Verstraete, G. Zerah, J.W. Zwanziger, Computer Phys. Commun. 180 (2009), 2582

[9] Y.W. Mo, J. Kleiner, M.B. Webb, M.G. Lagally, Phys. Rev. Lett. 66 (1991), 1998

[10] B.C. Allen, Metallurgical Transactions 3 (1972), 2544

[11] R. Schlatmann, C. Lu, J. Verhoeven, E.J. Puik, M.J. van der Wiel, Appl. Surf. Sci., 78 (1994), 147

[12] J. Verhoeven, Lu Chunguang, E.J. Puik, M.J. van der Wiel, T.P. Huijgen, Appl. Surf. Sci., 55 (1992), 97

[13] A.J.R. van den Boogaard, E. Louis, E. Zoethout, S. Müllender, F. Bijkerk, Journal of Vaccum Science and Technology A 28 (2010), 552

[14] I. Nedelcu, R.W.E. van de Kruijs, A.E. Yakshin, F. Bijkerk, Physical Review B 76, (2007) 245404

[15] S. Bajt, D.G. Stearns, P.A. Kearney, Journal of Applied Physics (90), 2001 1017

[16] A. Patelli, V. Rigato, G. Salmaso, N.J.M. Carvalho, J.Th.M. De Hosson, E. Bontempi, L.E. Depero, Surface & Coatings Technology 201 (2006), 143

CHAPTER 4

INCREASING EUV REFLECTION OF MO/SI BASED MULTILAYER STRUCTURES

Abstract

We studied the structure and optical properties of B_4C/Mo/Y/Si multilayer systems. Using Extended X-ray Absorption Fine Structure (EXAFS) measurements at the Y and Mo K-edge, the structure of the sub nanometer thick Y layer and the underlying Mo layer were analyzed. It was found that even a 0.2 nm thick Y layer significantly reduced silicon diffusion towards Mo thus reducing Mo-silicide formation. Hard X-ray reflectometry showed that the difference in average interface roughness of the B_4C/Mo/Y/Si multilayer structure compared to Mo/Si and B_4C/Mo/B_4C/Si multilayer structures was negligible. Soft X-ray reflectometry showed optical improvement of B_4C/Mo/Y/Si with respect to Mo/Si and B_4C/Mo/B_4C/Si multilayer structures.

4.1 Introduction

This chapter focuses on a modification of Mo/Si based Bragg reflectors, designed for 13.5 nm radiation, to be applied as optical components in Extreme Ultraviolet Lithography (EUVL). For this application a high reflectance is very important in order to gain a high transmission of the EUV optical system. As this full optical system can consist of up to 10 multilayer elements [1], even a gain in reflectance of a few tenths of a percentage can significantly improve transmission. For standard multilayer mirrors, consisting of alternating, quarter wavelength thick layers of Mo and Si [2], the reflectivity is theoretically limited to 75% at near-normal incidence.

A general mathematical analysis to further improve the reflection by adding subquarter wavelength thick layers to the multilayer period is given by Larruquert [3]. The principle is based on further improvement of the refractive index distribution in the period taking into account both reflectance of the individual layers and absorption of the radiation in the entire structure. Numerically based examples of this principle for EUV mirrors are given by Singh [4] and Larruquert [5]. However, the numerical examples concern perfect systems, as they do not take into account possible differences in roughness or intermixing of layers occuring during deposition of the structures. For example, in the case of Mo-Si multilayer systems, the interface of Mo-on-Si extends to an interlayer thickness of approximately 1.2 nm and the interface of Si-on-Mo extends to an interlayer of approximately 0.6 nm [6].

To reduce or prevent the formation of an intermixed layer of Mo and Si, chemically inert interlayer materials are selected as a diffusion barrier at the interfaces of Mo and Si. Although it has been demonstrated that a thin interlayer of B_4C improves the reflectance of a Mo/Si multilayer [7], adding a B_4C layer to a perfect Mo/Si system theoretically should not result in an optical improvement.

Fig. 4.1 shows some calculated reflectances for a few materials at the Si-on-Mo interface. The optical constants were taken from the library supplied with the IMD code developed by Windt [8]. The values of the optical constants are illustrated in Fig. 4.2. To improve the reflection, materials have to be selected based on a rotation in the n-k plane [9]. For a perfect system without intermixing, by adding a 0.7 or 0.8 nm thick Y layer, the reflection at 13.5 nm improves by 0.64% compared to the Mo/Si multilayer structure. However, in view of the chemical affinity between Y and Si, silicide formation for such tri-layer periodic systems also has to be taken into account. Even though an YSi_2 layer on top of Mo results in a lower reflectance than a perfect Mo/Si multilayer system, its reflectance can be significantly larger than that of a realistic Mo/Si structure when taking into account intermixing. Here we have taken from literature that the intermixed layer has a $MoSi_2$ structure [10]. Other similar solutions than Y exist, for example Zr or Nb.

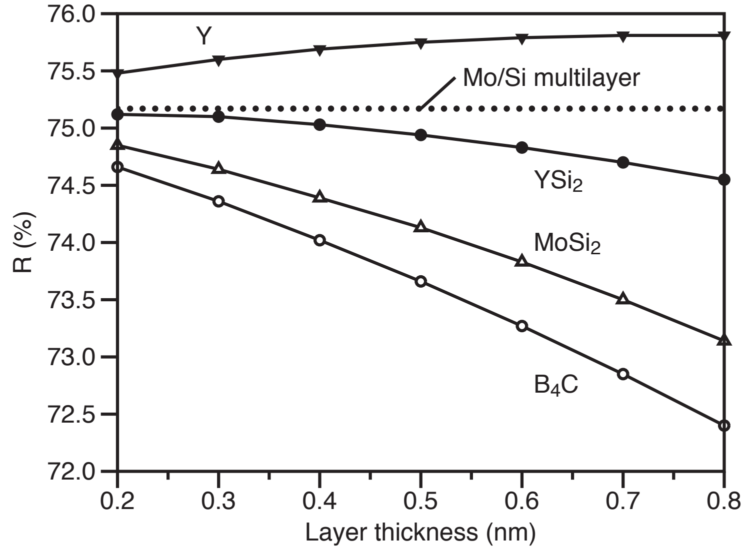

Figure 4.1: *Numerically calculated peak reflectances for 13.5 nm radiation at near normal incidence of the model systems: (Mo/barrier/Si)x50 with "barrier" being either Y, YSi_2, $MoSi_2$, or B_4C. The straight line is the peak reflectance of the Mo/Si multilayer system with 50 periods. No roughness is included in the calculations.*

However, both as a pure layer or as a silicide, the calculated reflectances are lower than Y or Y-silicide. Additionally, also the B_4C layer below Mo could be replaced by for example Ru. However, a Ru-silicide has a negative effect on the reflectance compared to B_4C. Therefore, in this paper we only focus on introducing an Y layer on top of Mo. We will describe the effects of the thin Y layer on the structure and reflection of the multilayer structure.

4.2 Experimental

Multilayers were deposited on Si (100) substrates by DC magnetron sputtering in a chamber with a base pressure lower than $1 \cdot 10^{-8}$ mbar. Quartz crystal microbalances were used to calculate the layer thickness from the monitored amount of deposited material. A Mo/Si multilayer structure, optimized for near normal incidence reflection of 13.5 nm radiation, was deposited as a reference system. The other samples for EUV reflection contained either a thin Y or B_4C layer on top of Mo. It should be noted that for a thin, sputtered B_4C layer of only 0.2-0.3 nm, we do not expect a stoichiometric compound. Below we will use B_4C designation only as a label to refer to the boron-carbide layer.

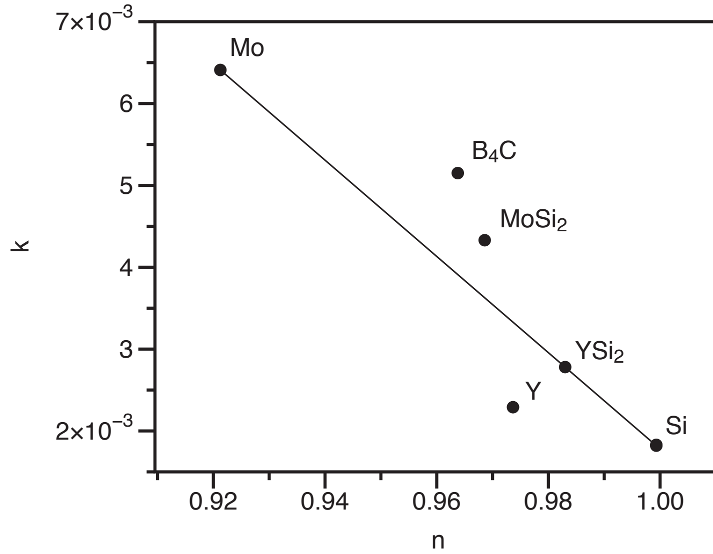

Figure 4.2: *Optical constants n and k of materials used for the calculations.*

Deposition of each Si layer was followed by a treatment with 100 eV Kr ions to control roughness development of the multilayer structures. To compare the development of the interface roughness within the periods of the multilayer structures, Cu K_α reflectometry was applied. A grazing incidence $\theta - 2\theta$ scan gave information about the average value of the interface roughness. Rocking curves provided more accurate information about the relative interface roughness development between all multilayer systems.

Layer growth and interlayer formation of Si on Y bi-layer systems, were studied using Angular Resolved XPS (ARXPS) as a non-destructive depth profiling technique. Since tri-layer systems like Mo/Y/Si would be too complex for a depth profiling using ARXPS, Extended X-ray Absorption Fine Structure (EXAFS) at the Mo K-edge in fluorescence setup was used as an additional technique to study interlayer formation. The EXAFS measurements were performed at the DUBBLE beam line at the ESRF synchrotron facility. The beam line is equiped with a Si(111) double-crystal monochromator and has an energy resolution dE/E of $5 \cdot 10^{-4}$.

Since we are interested in possibly formed Mo-silicides at the interface region with the Y layer, we improved the EXAFS sensitivity to this region. To achieve this, we reduced the Mo layer thickness by replacing the bottom part of the Mo layer by Nb. In the results section we explain this in more detail. Fluorescence EXAFS at the Y K-edge was applied to resolve the Y (-silicide) structure.

To determine the optical response of the multilayer mirrors, reflectivity

Table 4.1: *Overview samples including measurement technique they were used for; N is number of periods in the multilayer structure, Λ is the layer thickness, and RC means rocking curve. The layers for all structures are listed from bottom to top per period.*

Structure	Specific details	Analysis technique
Mo/Si	N=50	EUVR, RC
B_4C/Mo/B_4C/Si	N=50	EUVR, RC
B_4C/Mo/Y/Si	N=50, Λ_Y = 0.2-0.6 nm	EUVR, RC, EXAFS Y_K
B_4C/Nb/Mo/Si	N=50, $\Lambda_{Mo;Y}$ = 0.5; 0.2-0.6 nm	EXAFS Mo_K
Mo/Nb	N=50, $\Lambda_{Nb;Mo}$ = 0.5; 0.5 nm	EXAFS Mo_K
Y/Si	Λ_{Si} = 0.5-3.0 nm	ARXPS
Mo film	Λ_{Mo} = 200 nm	EXAFS Mo_K
Y film	Λ_Y = 200 nm	EXAFS Y_K

for 13.5 nm radiation was measured at near normal incidence at PTB at the BESSY II storage ring.

An overview of all the relevant structures, including the measurement technique they were used for, is given in table 4.1.

4.3 Results and discussion

4.3.1 EUV reflection

Reflectivity measurements for 13.5 nm at near normal incidence revealed for the 50 period Mo/Si multilayer a peak reflectance of 69.1% and 70.0% for the B_4C/Mo/B_4C/Si system, with a relative accuracy of 0.1%. Based on the refractive index, a B_4C interlayer is not expected to improve the reflectance of the multilayer structure compared to the perfect Mo/Si system. Since it is known that Mo-silicide interlayers are formed in the Mo/Si system, improvement of the reflection by 0.9% upon introduction of thin B_4C layers is likely to be ascribed to the reduction of Mo-silicide formation.

As shown in Fig. 4.1, a good choice to achieve an improved reflectance is to replace the B_4C layer on top of Mo by Y. EUV reflection measurements at 13.5 nm for 0.2 and 0.4 nm of Y on top of Mo give a peak reflection value of 70.3 ± 0.1% and 70.1 ± 0.1%, respectively (Fig. 4.3). Although we do see a gain in reflectance, the gain is slightly lower than the expected 0.5%.

In order to find out which effects -roughness and Y and/or Mo silicide formation- caused the limited increase in reflectance due to deposition of extremely thin interlayers, we will first discuss the difference in average interface roughness of all systems.

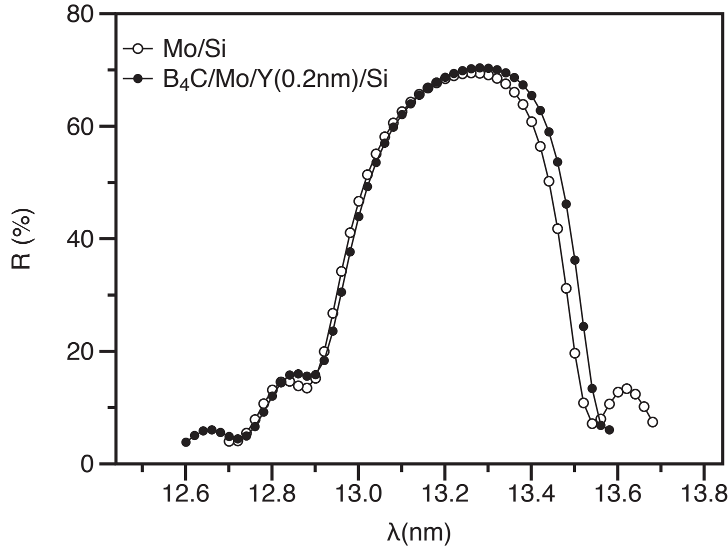

Figure 4.3: *EUV reflection curves of a Mo/Si and B_4C/Mo/Y(0.2nm)/Si multilayer structure with 50 periods.*

4.3.2 Interface roughness

The average interface roughness of the multilayer systems with a thin Y or B_4C layer on top of Mo and the Mo/Si reference system were compared to each other. From a grazing incidence $\theta - 2\theta$ scan the average interface roughness can be estimated from the relative decrease of the high order Bragg peaks. For the Mo/Si system an average interface roughness of roughly 0.2 nm was determined.

To obtain more accurate information on relative differences in roughness, rocking curves around the third order Bragg maximum was measured for all structures (Fig. 4.4). This Bragg order was selected to cover the largest possible frequency range of the roughness. From the rocking curves, we can determine the amplitude and the lateral correlation length of the roughness. The lateral correlation length of the roughness is inversely proportional to the width of the diffuse scattering peak [11]. The amplitude of the roughness can be determined from the off-specular intensities. If the amplitude of the roughness is sufficiently small, the diffuse scattering intensity for a single rough surface is approximately equal to the power spectral density [12]. For a simple exponential form of the correlation function, given by

$$C(R) = \sigma^2 \exp\left(-\frac{R}{\xi}\right) \tag{4.1}$$

where σ is the amplitude of the roughness, ξ is the in-plane radial correlation length, and R is the radial distance, the resulting power spectral density is

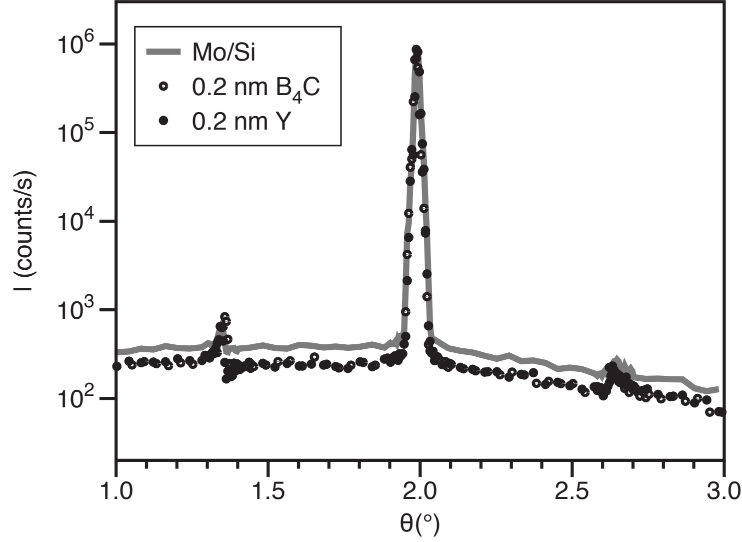

Figure 4.4: *Rocking curves around the third Bragg order for the multilayer systems with B4C below and either Y or B_4C on top of Mo compared to the Mo/Si reference system. The rocking curve for the 0.2 nm thick Y sample has been slightly translated, and the rocking curve for the Mo/Si sample has been normalized to the peak intensity of the other curves. The Mo/Si system has a slightly higher amplitude of the average roughness.*

given by

$$PSD = \frac{2\pi\sigma^2\xi^2}{(1+q_r^2\xi^2)^{3/2}} \tag{4.2}$$

When the roughness in the multilayer systems is conformal, the diffuse scattering distribution is given by the same equation as for a single surface. When the roughness is not conformal, the PSD is attenuated by a constant factor. We are not able to claim that the roughness in the multilayer systems grows conformal. However, it is reasonable to assume that the conformality is not significantly affected by the growth of a 0.2-0.4 nm thick layer of B_4C or Y in each period of the multilayer structure of 6.7 nm. As a consequence, the PSD obtained from diffuse scattering can be used as a relative measure of the average interface roughness for all the structures.

From the measured rocking curves, we find that the radial correlation length is the same for all samples. Consequently, the difference in power spectral densities (or off-specular intensities) is described by a difference in amplitude of the roughness. We find that the relative intensity difference between the Mo/Si reference system and the other multilayer structures is a factor of 1.4. Hence, the estimated average amplitude of the roughness for

the Y and B_4C multilayer systems is about 0.17 nm.

We made a first order approximation on the effect of the difference in roughness for the reflection between the Mo/Si reference system and the other multilayer structures. For this we calculated numerically the reflection of a Mo/Si multilayer system using the two experimentally determined values for the interface roughness. For the perfect Mo/Si multilayer system (no silicides) with an average interface roughness of 0.17 or 0.20 nm, we calculate an absolute difference of 0.13% in peak reflection. Consequently, approximately 0.13% of the 0.9% gain in reflectance between the B_4C and the Mo/Si structures can be ascribed to a difference in average interface roughness.

Between the B_4C and Y structures there appears to be no difference in average interface roughness. Therefore, the difference in reflection between the two structures must be determined by the refractive indices of the two sub nanometer thick layers. In the remainder of this paper we will discuss the structure of the Y layer and how the presence of the Y layer affects the underlying Mo layer.

4.3.3 Interlayer structure

As silicide formation due to intermixing in Mo/Y/Si systems of Y and possibly also of Mo cannot be excluded, we investigated layer growth of Si on Y using angular resolved XPS. We covered a thick Y layer by a Si layer having a thickness ranging from 0.5 to 3.0 nm. Inelastic mean free paths of the X-ray induced photoelectrons were calculated using Cumpson and Seah [13]. For fitting the ARXPS data the number of degrees of freedom available for modeling usually do not exceed 3 [14]. In reality more parameters are needed to describe the system. Since we will not be able to find a unique solution to describe the ARXPS data, we used two simple models: (1) single overlayer model, (2) linear gradient model. Both models have a specific purpose in the study of the Si on Y growth.

In the single overlayer model we have two layers of different material, namely Y and Si. The two layers are separated by a sharp interface, i.e. the normalized concentration of one material discontinuously jumps from 1 to 0, and vice versa for the other material. This model is used to investigate whether Si grows on top of Y without intermixing. In the linear gradient model, we assume a linear decrease of Si concentration within the Y layer. The integrated area of the Si concentration in this model should be equal to the calculated layer thickness estimated from the deposited amount of material. If there is an interlayer formed between Y and Si, the oversimplified linear gradient model gives a very rough estimate for the Y-Si interlayer thickness.

We will start with the single overlayer model. The inelastic mean free path of the photoelectrons in this model is fully determined by the over-

layer. Consequently, we have to model the data using inelastic mean free paths of photoelectrons traveling through a Si layer. Calculated overlayer thicknesses resulting from the fit appear to be 20-30% too thick. When we reduce the inelastic mean free paths for example to that of photoelectrons traveling through an Y layer (having a lower inelastic mean free path than Si), the overlayer thicknesses are within 5% of deposited thickness. From this observation, we have to conclude that Si does not only grow on top of Y, but also forms an intermixed layer with Y.

Using the linear gradient model we estimate that only after a 2 nm thick Si layer has been deposited on Y, a pure Si overlayer starts to grow, see Fig. 4.5 a and b. According to this model the Y-Si interlayer has an approximate thickness of 4 nm. In line with our findings, intermizing zones of at least a few nanometers are also observed in Y/Si multilayer structures [15]. From this result we can at least expect that in the multilayer structures with sub nanometer thick Y layers on top of Mo, Y-silicides will be formed and that also the formation of Mo-silicides cannot be excluded.

To confirm the hypotheses of Mo-silicide formation in a Mo/Y/Si structure, we performed fluorescence EXAFS measurements at the Mo K-edge. For this experiment we are mainly interested in the structure of the Mo layer near and at the Y interface. Since the EXAFS signal comes from a thick Mo layer the information from the interface is outweighed by the signal from the bulk. To filter the interface signal from the EXAFS measurement, we reduced the thickness of the Mo layer such that it would not affect the amount of possible silicide formation and at the same time allow to detect interaction between Mo and Si significantly.

It is obviously very important that the reduction of the Mo layer thickness must not affect the polycrystalline structure of the Mo layer at the interface with Y as well as the other layers in the periodical stack. Since the template on which Mo grows, greatly affects the Mo structure, we cannot choose just any material for Mo to grow on. For example, Patelli [16] has shown that a very thin layer of B_4C at the interfaces of a Mo/Si multilayer affects both the crystal nano-structure and the interface morphology of Mo. We chose Nb as a suitable material to largely replace Mo. Nb has the same crystalline structure as Mo (BCC) with approximately the same lattice parameter (0.315 vs. 0.330 nm for Mo and Nb, respectively). Both Mo and Nb prefer growing in the (110) direction, followed by the (211) direction [17]. Therefore, we may expect that Mo grows coherently on a Nb template (heteroepitaxy) forming a similar structure to that in the polycrystalline Mo layer of the regular thickness. Hence if this assumption is valid, a thin Nb layer should not drastically alter the nearest neighbor distance and structure of a thin Mo layer and vice versa.

To plausibly confirm that the growth characteristics and structure of Mo, and consequently Y, indeed have not changed significantly when a 2.5 nm thick Mo layer is substituted for by a 2.0 nm thick Nb layer underneath

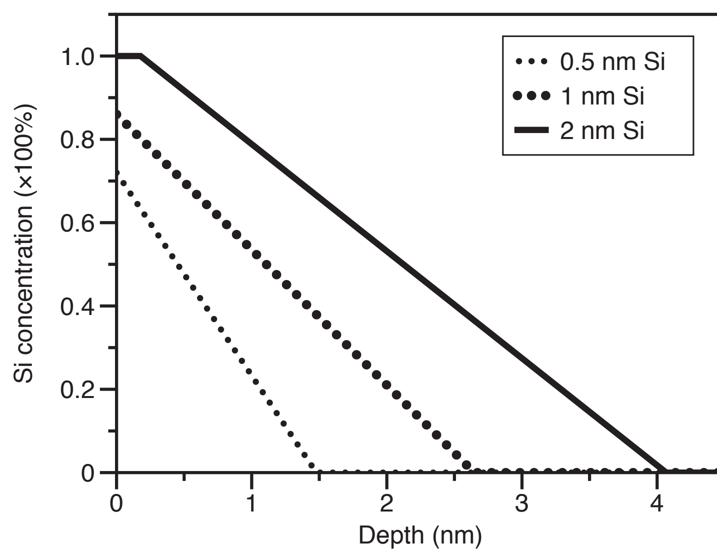

(a)

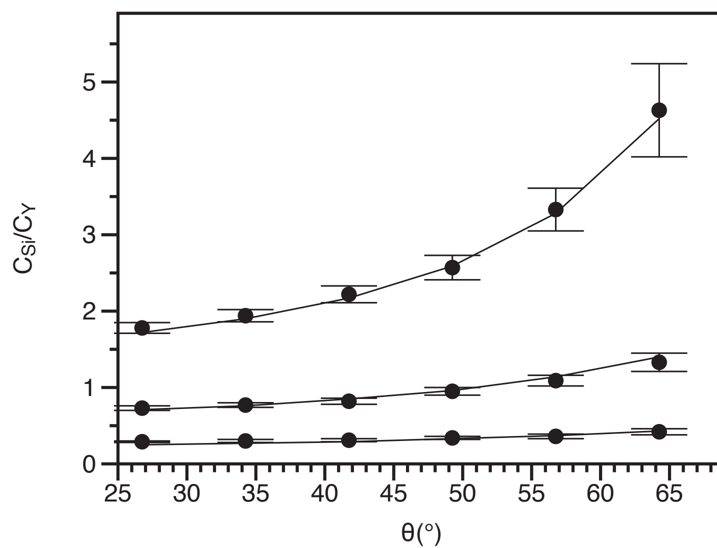

(b)

Figure 4.5: *(a) Si concentration profile for 0.5, 1.0 and 2.0 nm Si deposited on a thick Y layer obtained using a linear gradient model for ARXPS measurements (b) ARXPS data and the corresponding fits (linear gradient model) through the data.*

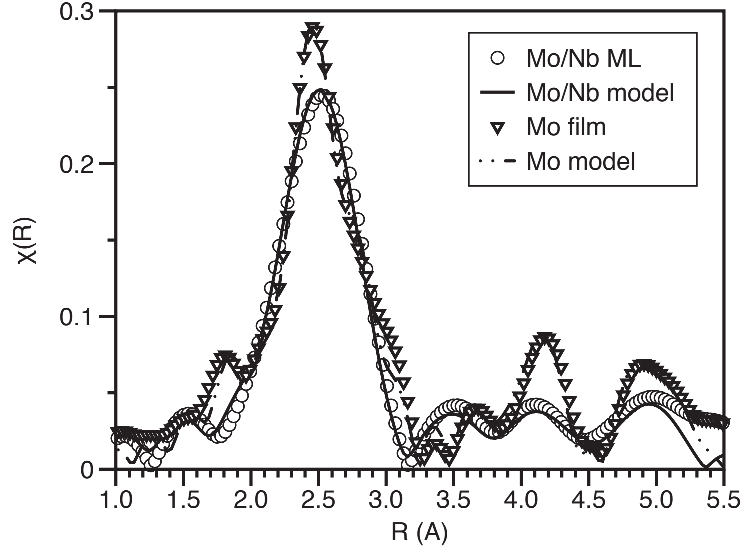

Figure 4.6: *Measured and calculated chi(R) distributions for the Mo K-edge for a 200 nm thick Mo layer and a Mo(0.5nm)/Nb(0.5nm) multilayer structure. The interatomic distance of the Mo BCC lattice of the multilayer structure is only 3 pm larger than that of the thick Mo layer.*

a 0.5 nm thick Mo layer, we deposited a 200 nm thick Mo film and a Mo(0.5 nm)/Nb(0.5 nm) multilayer structure. From the EXAFS measurements of these two structures we calculated the $\chi(R)$ [18], illustrated in Fig. 4.6. Such thin layers were chosen (4-5 monolayers per material) in order to show that Mo and Nb form a layered structure, and do not intermix significantly. We confirmed that we indeed have a Mo/Nb multilayer structure using a small angle $\theta - 2\theta$ X-ray reflectometry scan. The observed first order Bragg peak corresponded to the aimed period thickness.

For the analysis of the EXAFS spectra, FEFF6 has been used [19]. For both samples we used as input model a Mo BCC lattice. For the thick Mo layer we find a lattice parameter of 0.316 nm, whereas for the Mo/Nb multilayer we find a lattice parameter for Mo of 0.319 nm. Both calculated lattice parameters are very similar, with the lattice spacing of Mo being increased by only 3 pm. The mean square displacement in half-path length (σ^2) was smaller than 0.5 pm^2 –this is also the case for all other mentioned models/fits in this paper.

However, to accurately fit the EXAFS spectrum of the Mo/Nb sample, we had to slightly adjust some of the amplitudes of a few scattering paths. This is quite reasonable, considering that the Mo layers are extremely thin. Under these circumstances non-homogeneous conditions (for example crystal

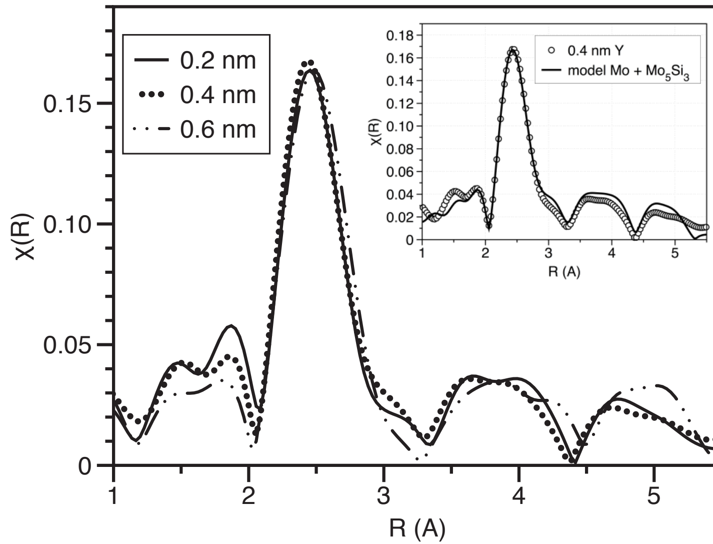

Figure 4.7: *Calculated $\chi(R)$ distributions for the Mo K-edge for the Mo/Y/Si structures with varying thickness of the Y layer. The inset shows a fit to the measured points for the structure with a 0.4 nm thick Y layer. All datasets were fitted using a modified Mo model obtained from the Mo/Nb multilayer structure and a Mo_5Si_3 structure.*

boundaries and Mo-Nb interfaces) and crystal orientations become important. As a consequence, the resulting model should be considered as an effective description of the Mo layer.

Analysis of the $\chi(R)$ spectra also plausibly confirms that Mo and Nb nanocrystals grow heteroepitaxially, since we managed to fit the EXAFS data using a single crystalline structure. Note that this does not imply that we have only one crystallographic orientation of Mo and Nb. However, it does follow that the crystallites are large enough in the lateral direction, such that inhomogeneities at the crystal boundaries have a negligible influence on the EXAFS signal.

The obtained model for Mo in the Mo/Nb multilayer structure was used as input for the more complex Nb/Mo/Y/Si systems as a first order approximation of the Mo structure. These complex structures were fitted up to 0.4 nm in R-space for the Mo K-edge EXAFS spectrum. The spectra are included in Fig. 4.7. We found that the only model system that adequately fits the data, is the (refined) Mo model from the Mo/Nb multilayer structure, combined with a Mo Si structure. As we increase the Y layer thickness from 0.2 to 0.6 nm, the relative amplitude of the Mo-silicide and the scaling amplitude for the scattering factors in the refined Mo model decreases. For

simplicity we will assume that a homogeneous Mo-silicide layer is formed. From the relative amplitudes, assuming bulk coordination numbers, we estimate that the Mo-silicide layer decreases in thickness from 0.15 to 0.10 nm.

One could argue that a continuously formed Mo Si layer of maximally 0.15 nm thickness, cannot be considered as a silicide layer. It is more likely that Mo-silicide clusters are formed. Remarkably, the estimated amount of formed Mo-silicide is significantly less than the $MoSi_2$ formed in conventional Mo/Si systems. Though from XPS we know that Si easily penetrates the Y layer, it is still to be explained why our ultra-thin Y layer reduced Mo-Si intermixing.

Additionally, we observed a change in interatomic distance of the Mo matrix in the Nb/Mo/Y/Si multilayer structure with respect to the interatomic distance of the Mo matrix in the Nb/Mo multilayer structure. Assuming we have a homogeneous film, strained homogeneously in the x and y direction (surface directions), we calculated the change of stress in the Mo layer. As the Y layer thickness increases and the Mo-silicide fraction decreases, the stress changes from 1.3 GPa to -0.3 GPa. The absolute values of the stress may be wrong, since we have assumed that the Mo matrix in the complex multilayer structure should be the same as that of the Mo/Nb multilayer structure. However, the trend of a decreasing value for the stress is true. The result of a decreasing stress appears to be in line with stress evolution of Mo/Si multilayer systems as mentioned by Freitag [20]. In that paper it is determined that initially, when Si is being deposited on Mo (and likely forming a Mo-silicide), the stress in the multilayer system increases. After a certain thickness of deposited Si, the stress starts to decrease again. Hence, it could be concluded that an increasing thickness of Mo-silicide causes an increase of the stress in Mo.

It should be emphasized that some difficulties in the fitting procedure of the EXAFS signal should be taken into consideration. In the fitting procedure we have disregarded the fact that for a layer with a thickness of only 0.5 nm, having different materials at the interfaces, the non-homogeneous conditions are important. More specific, in our case a changing structure of the Y layer may affect the Mo EXAFS signal significantly. To clarify this, we give the calculated $\chi(R)$ of the Y K-edge EXAFS signal in Fig. 4.8 for the samples with an Y layer thickness of 0.2-0.6 nm. Fitting this data accurately, appeared to be impossible due to the non-homogeneous condition within and around the Y layer. However, we do observe that the interatomic distance corresponding to the major peak in the $\chi(R)$ spectra corresponds very well to that of an YSi_2 structure. The difference in interatomic distance between the model and crystallographic data is less than 8 pm. We also see that the $\chi(R)$ spectra change slightly as we change the thickness of the Y layer. So, indeed as one would expect, the local environment of the Mo layer has changed.

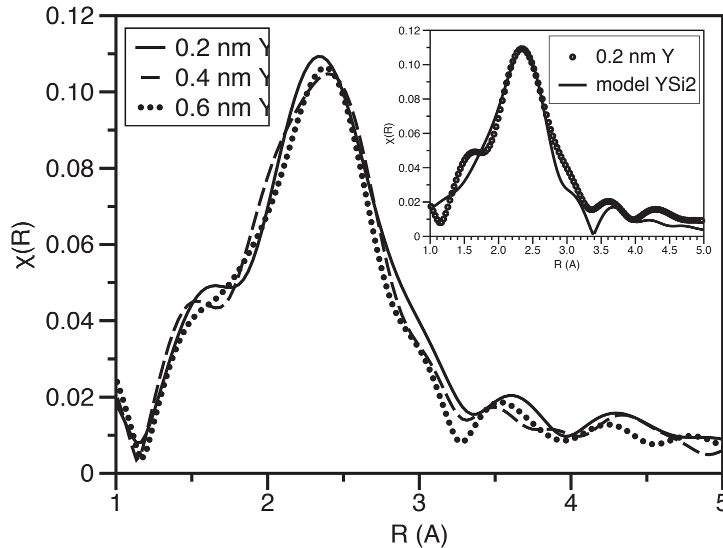

Figure 4.8: *Calculated distributions for the Y K-edge for the Mo/Y/Si structures with varying thickness of the Y layer. The inset shows a fit to the dataset with 0.2 nm Y layer using the YSi_2 model.*

Even if we were able to fit the Y spectra accurately, including the Y layer structure in the fitting procedure is practically an impossible task considering the amount of parameters one has to introduce. The main parameters are: (1) effective interatomic distance between (a) Nb and Mo layer (b) Mo and Y-silicide layer; (2) crystallographic orientations of (a) Nb structure at the Mo interface (b) assumed Y-silicide structures at the other Mo interface; (3) inhomogeneity at crystal boundaries (4) relative lateral shifts of all structures to be included.

However, the limitations mentioned above cannot rule out the main conclusion we should draw from the EXAFS measurements about the presense of intermixing of Y and Si which was also observed by ARXPS. Additionally from EXAFS we know that it is very likely that the Y-silicide is a Si-rich structure, most likely YSi_2. And finally we have found that even a 0.2 nm thick layer of Y reduces Mo-silicide formation significantly, compared to intermixed layer thicknesses at the Si-on-Mo interface reported in literature. The formed Mo_5Si_3 fraction was estimated to be approximately 20% of the 0.5 nm thick Mo layer, and has a refractive index that is less detrimental for 13.5 nm reflection than the reported MoSi layer at the Si-on-Mo interface.

4.4 Conclusions

We studied the structural and optical effects of sub nanomeer thick Y layers in B_4C/Mo/Y/Si multilayer systems applied as a substitution to the conventional B_4C layers in B_4C/Mo/B_4C/Si. The application of Y layers proved to give a gain in EUV reflectance of the structures although the gain was smaller than theoretically expected. The systems with Y or B_4C layers show slightly reduced average interface roughness of the period relative to that of a reference Mo/Si structure. Whereas the average roughness of both Y and B_4C samples was the same. Therefore, the increase of the EUV reflectance of the multilayer structure with Y instead of B_4C on top of Mo is concluded to be caused by the improved refractive index distribution within the period of the multilayer structure.

Using our method to increase interface sensitivity of the EXAFS measurements, we have shown that even a 0.2 nm thick layer of Y on top of Mo in a Mo/Si multilayer structure can significantly reduce Mo-silicide formation at the interface between Mo and Y. The formed Mo-silicide is of a Mo-rich nature, contrary to the usually reported Si-rich stoichiometry in the case of conventional Mo/Si multilayers. The Y layer has formed a silicide. Within the multilayer structures designed for 13.5 nm radiation the optical contrast of an Y-silicide layer is better than $MoSi_2$ or B_4C layers, therefore the introduction of a thin Y layer increases the EUV reflectance.

References

[1] E.Louis, A.E.Yakshin, T.Tsarfati, F.Bijkerk, "Nanometer interface and materials control for multilayer EUV-optical applications", Progress in Surface Science 86, 255-294 (2011)

[2] E. Spiller, Soft x-ray optics, ISBN 0-8194-1655-X, SPIE

[3] J.I.Larruquert, "General theory of sub-quarterwave multilayers with highly absorbing materials", J. Opt. Soc. Am. A 18, 2617-2627 (2001)

[4] M.Singh, J.J.M.Braat, "Design of multilayer extreme-ultraviolet mirrors for enhanced refelctivity", Appl.Opt. 39, 2189-2197 (2000)

[5] J.I.Larruquert, "Sub-quarterwave multilayers with enhanced reflectance at 13.4 and 11.3 nm", Opt. Communications 206, 259-273 (2002)

[6] S.Yulin, T.Feigl, T.Kuhlmann, N.Kaiser, A.I.Fedorenko, V.V.Kondratenko, O.V.Poltseva, V.A.Sevryukova, A.Yu. Zolotaryov, E.N. Zubarev, "Interlayer transition zones in Mo/Si superlattices", J. Appl. Phys. 92, 1216-1220 (2002)

[7] S.Bajt, J.Alameda, T.Barbee,Jr., W.M.Clift, J.A.Folta, B.Kaufmann, E.Spiller, "Improved reflectance and stability of Mo-Si multilayers", Opt.Eng. 41, 1797-1804 (2002)

[8] D.L. Windt, "IMD - software for modeling the optical properties of multilayer films", Computers in Physics 12, 360 (1998)

[9] J.I.Larruquert, Layer-by-layer design method for multilayers with barrier layers: application to Si/Mo multilayers for extreme-ultraviolet lithography, J.Opt.Soc.Am.A 21, 1750-1760 (2004)

[10] S.Bajt, D.G.Stearns, P.A.Kearney, "Incestigation of the amorphous-to-crystalline transition in Mo/Si multilayers", J. Appl. Phys 90, 1017-1025 (2001)

[11] J.M.Freitag, B.M.Clemens, "Nonspecular x-ray reflectivity study of roughness scaling in Si/Mo multilayers", J. Appl. Phys. 89, 1101 (2001)

[12] E.M.Gullikson, D.G.Stearns, D.P.Gaines, J.H.Underwood, "Nonspecular scattering from multilayer mirrors at normal incidence", in Grazing incidence and multilayer x-ray optical systems, Proc.SPIE 3113, 412-419 (1997)

[13] P.J.Cumpson, M.P.Seah, "Elastic scattering corrections in AES and XPS. II. Estimating attenuation lengths and conditions required for

their valid use in overlayer/substrate experiments", Surface and Interface Analysis 25, 430-446 (1997)

[14] P.J.Cumpson, "Angle-resolved XPS and AES: depth resolution limits and a general comparison of properties of depth-profile reconstruction methods", J. of Electron Spectroscopy and Related Phenomena 73, 25-52 (1995)

[15] T.L.Lee, L.J.Chen, Interfacial reactions in ultrahigh vacuum deposited Y-Si multilayer films, J.Appl.Phys. 75, 2007-2014 (1994)

[16] A.Patelli, V.Rigato, G.Salmaso, N.J.M.Carvalho, J.Th.M. De Hosson, E.Bontempi, L.E.Depero, "Ion bombardment effects on nucleation of sputtered Mo nano-crystals in Mo/B4C/Si multilayers", Surface & Coatings Technology 201, 143-147 (2006)

[17] L.Vitos, A.V.Ruban, H.L.Skriver, J.Kollar, "The surface energy of metals", Surface Science 411, 186-202 (1998)

[18] B.K.Teo, EXAFS: basic principles and data analysis, Springer-Verlag (1986)

[19] S.I.Zabinsky, J.J.Rehr, A.Ankudinov, R.C. Albers, M.J. Eller, "Multiple-scattering calculations of x-ray absorption spectra", Phys. Rev. B 52, 2992-3009 (1995)

[20] J.M.Freitag, B.M.Clemens, "Stress evolution in Mo/Si multilayers for high-reflectivity extreme ultraviolet mirrors", Appl. Phys. Lett. 73, 43-45 (1998)

CHAPTER 5

NON-CONSTANT DIFFUSION CHARACTERISTICS OF MO-SI INTERLAYER GROWTH

Abstract

In situ small-angle X-ray reflection and wide angle X-ray diffraction of synthetic, Mo-Si based multilayer structures were used to study layer interdiffusion dynamics at temperatures between 250 and 300 °C. The in situ reflection measurements revealed information on non-constant interdiffusion characteristics during the interlayer growth. The activation energy for interdiffusion was found to gradually increase with growing Si-on-Mo interlayer thickness, towards a saturation level of approximately 2.5 eV. Contrary, the activation energy for interdiffusion at the Mo-on-Si interlayer was almost constant at a value around 2.6 eV. Wide angle X-ray diffraction at different stages in the annealing cycle further showed the evolution of Mo crystallites. Evolution of these crystallites was found to be strongly correlated to the change in period thickness of the multilayer structures.

5.1 Introduction

Several studies have reported on silicide formation as a result of Mo-Si interdiffusion with the value of the activation energies for interdiffusion ranging from 0.5 to 2.4 eV [1, 2, 3, 4, 5, 6]. Especially the difference in results from Bruijn et al. [5] (0.5 eV), Nakajima et al. [3] (1.1 eV) and Rosen et al. [4] (2.4 eV) is remarkable, given the similarity of the experimental conditions, like bilayer thickness of the Mo/Si multilayer structure and annealing temperatures.

It has been reported that the diffusion rate in Mo/Si multilayer structures, having a bilayer thickness of only 0.8 nm, is time dependent [2]. The authors attributed this time dependence to structural relaxations. However, using high resolution electron microscopy, Rosen et al. observed a rapid initial growth of the Mo-Si interlayers, before the interlayer grew parabolically in time. Therefore, structural relaxation cannot explain the anomalous growth in the thicker multilayer structures.

To resolve the above discrepancies in the observed values of the activation energies, and to be able to follow the diffusion dynamics during all stages of the interlayer growth, analysis with an improved spatial resolution is required. In this chapter, we study the diffusion dynamics at a picometer scale for the Si-on-Mo and Mo-on-Si interlayer. We use in situ small angle X-ray reflection during annealing in the temperature range of 250-300°C to monitor changes in the period thickness, especially during the rapid initial interlayer growth.

5.2 Experimental

Multilayer structures consisting of 50 periods were deposited on Si (100) substrates by DC magnetron sputtering in a chamber with a base pressure lower than 1e-6 Pa. The periodical structure of the multilayer systems are given by [B_4C (1.5 nm)/Mo (3 nm)/Si (4 nm)] and [Mo (3 nm)/B_4C (1.5 nm)/Si (4 nm)]. The relatively thick B_4C layer at one of the two interfaces significantly reduces interdiffusion, even up to 400°C [7], so that any total multilayer phenomenon, like period thickness change, can easily be ascribed to a (diffusion) process at the opposite interface. The evolution of the period thickness of the multilayer structures during annealing was studied using hard X-ray reflectometry. Some specific details of the diffractometer are: Cu-K_α (0.154 nm) radiation, four bounce asymmetrically cut Ge (220) monochromator, and instrumental broadening of 0.005°.

The method we use to monitor the periodical thickness of multilayer structures during annealing using hard X-ray reflectometry has been discussed by Bruijn et al.[5]. For convenience we will summarize the most important parts here.

The periodical structure of a Bragg mirror consists of two or more layers of different optical materials. For certain angles θ, waves reflected at the interfaces interfere constructively. The n*th* Bragg angle for constructive interference is given by the corrected Bragg equation

$$n\lambda = 2\Lambda \sin\theta_n \sqrt{1 - \frac{2\bar{\delta}}{\sin^2\theta_n}}, \tag{5.1}$$

where λ is the wavelength of the radiation, Λ is the thickness of the period, and $\bar{\delta}$ is the average refractive index decrement. During annealing, it is required that the change in period thickness is measured with a high time resolution. Therefore, only a limited number of Bragg peaks are measured to reduce the measurement time of a single scan. To improve accuracy and remove possible misalignment in θ of the sample in the Bragg-Brentano setup, we derive an equation to determine the change in period thickness from the change in relative distance between two Bragg orders at two consecutive times. First we subtract the position of two Bragg orders at time t_j

$$\begin{aligned}\frac{(m-n)\lambda}{2\Lambda(t_j)} &= \sin\theta_m(t_j)\left(1 - \frac{\bar{\delta}}{\sin^2\theta_m(t_j)}\right) - \sin\theta_n(t_j)\left(1 - \frac{\bar{\delta}}{\sin^2\theta_n(t_j)}\right) \\ &\approx \theta_m(t_j) - \theta_n(t_j).\end{aligned} \tag{5.2}$$

The approximation is valid for small angles and $\bar{\delta} \ll \theta$, which is usually satisfied for hard X-rays. After subtracting the previous equation for two different times we obtain

$$\Lambda(t_2) = \frac{(m-n)\lambda\Lambda(t_1)}{(m-n)\lambda + 2(\Delta\theta_m - \Delta\theta_n)\Lambda(t_1)}, \tag{5.3}$$

where $\Delta\theta_i$ is the shift in Bragg angle between times t_1 and t_2 for Bragg order $i = (m, n)$. During annealing we measured two pairs of Bragg angles, for example orders $(m, n) = (2, 7)$ and $(m, n) = (2, 8)$ and averaged over the results. With a total scan range of 1.3° with steps of 0.005° and a count time of 1 second per angle, the scan time of the three Bragg peaks is 260 s. This time is the time resolution of our method to determine the change in period thickness. The error in change of period thickness is approximately 1 pm.

In a Bragg mirror consisting of two materials, interdiffusion occurs at the two different interfaces, namely A-on-B and B-on-A. The interdiffusion effects at both interfaces/interlayers can be different. For example, Erdélyi et al.[8] showed that the diffusion coefficient can depend quite strongly on local composition. Consequently, the change in period thickness is related to the amount and stoichiometry of interlayer formed upon interdiffusion at both interfaces. The change in period thickness is given by

$$\begin{aligned}\Delta\Lambda(t) = &[x_{A-B}(t) - x_{A-B}(t=0)]\Delta z_{A-B} \\ &+ [x_{B-A}(t) - x_{B-A}(t=0)]\Delta z_{B-A},\end{aligned} \tag{5.4}$$

where $x(t=0)$ is the initial width of the silicide interlayer formed after deposition of the multilayer structures, $x(t)$ is the total interlayer width at time t, and Δz is a dimensionless thickness change parameter due to interdiffusion of A and B. The labels $A-B$ and $B-A$ refer to the A-on-B or the B-on-A interface, respectively. In this study, the B-A term in eq.5.4 is removed by introducing B_4C at this particular interface, where A-B is then the alternating interface, without barrier, either Mo-on-Si or Si-on-Mo.

For the calculation of a change in period thickness, we still have to provide a value for the thickness change parameter. For this we consider the following reaction: *x mole of A + y mole of B → 1 mole of* A_xB_y. Transforming this to molar volumes using bulk denisty values and neglecting strain effects, we get an estimation for $\Delta z_{A_xB_y}$ by taking the cube root of the normalized change in volume.

From the measurements, the change in period thickness is given by

$$\Delta\Lambda(t) = \Lambda(t) - \Lambda_0 - \Delta\Lambda_T, \tag{5.5}$$

where Λ_0 is the initial period thickness at room temperature, $\Lambda(t)$ using eq.5.3 is the period thickness at time t at the annealing temperature T, and $\Delta\Lambda_T$ is the thermal expansion of a single period. The thermal expansion was estimated from the difference between the derived period thickness at the end of the annealing cycle at temperature T and the period thickness derived after cooling the structure down to room temperature. The added interlayer thickness during the interdiffusion process is very small compared to the total period thickness, therefore the difference in thermal expansion of the structure during annealing can be neglected.

Apart from a rapid initial interlayer growth [4], Mo-Si interlayer growth is reported to be diffusion limited [1, 3, 4, 5]. In this case, a parabolic relation exists between the interlayer width and the diffusion rate D,

$$x^2 \propto Dt. \tag{5.6}$$

From eq.5.4 under the simplified condition that we can neglect period contraction effects at one interface type, we obtain for the interlayer width squared

$$x^2(t) = \frac{1}{\Delta z_{A-B}^2}(\Delta\Lambda^2(t) + x_0^2\Delta z_{A-B}^2 + 2\Delta\Lambda(t)x_0\Delta z_{A-B}), \tag{5.7}$$

where $x(t)$ and $x_0(=x(t=0))$ both refer to the A-on-B interlayer.

In addition to measurement of the change in period thickness, we determined the change in size of the Mo crystallites using wide angle X-ray diffraction after several times of annealing at a few selected temperatures. To suppress the diffraction peak of the monocrystalline Si substrate, the sample was rotated by $\phi = 20°$. To maximize the illuminated area, the sample was positioned at an angle of $\theta = 1°$ with respect to the incident beam.

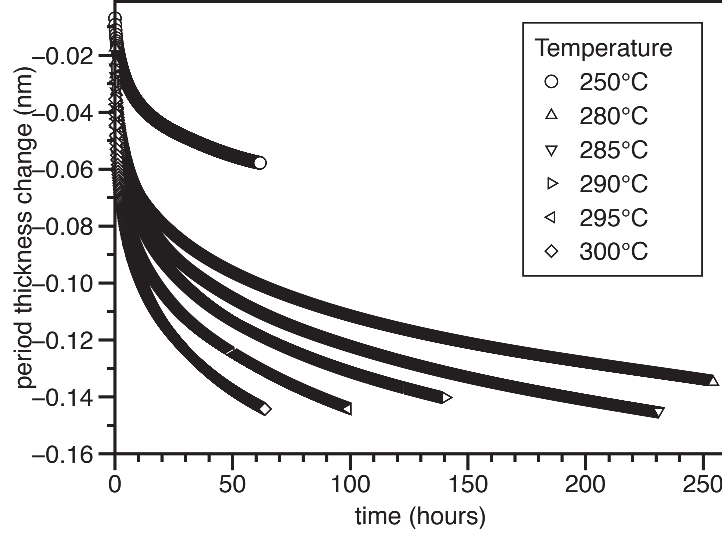

Figure 5.1: *Period thickness change evolution of the B_4C/Mo/Si structure at annealing temperatures of 250-300° C.*

5.3 Results and discussion

We subjected the B_4C/Mo/Si and Mo/B_4C/Si multilayer structures to temperature treatments between 250 and 300°C. The resulting change in period thicknesses of the B_4C/Mo/Si structures are illustrated in Fig. 5.1.

Using eq.5.7 we made a first approximation of the interlayer growth by transforming the change in period thickness data to an interlayer width as a function of time, illustrated in Fig. 5.2. In the calculation we used $x_0 = 0.5$ nm, a value corresponding to interlayer widths given in literature for the Si-on-Mo interlayer [4, 9]. For Δz we used a value corresponding to $MoSi_2$ formation from bulk Mo and Si. This particular compound was chosen, since for Mo-Si interdiffusion at temperatures below 800°C, (h-)$MoSi_2$ formation is usually reported as the phase of the growing layer [1, 6]. The h-$MoSi_2$ phase has the lowest heat of formation of Mo-silicide compounds [10]. The influence of the assumed parameter values on the results will be discussed later.

From Fig. 5.2 it is apparent that the interlayer width does not grow parabolically in time, confirming the rapid initial growth of the interlayer observed by Rosen. As a consequence, the diffusion rate cannot be constant in time or be independent of interlayer thickness. Therefore, during the rapid initial interlayer growth, either the assumption of diffusion limited interlayer growth or the assumption of a concentration independent diffusion rate appear to be invalid. Note that the concentration dependence implies

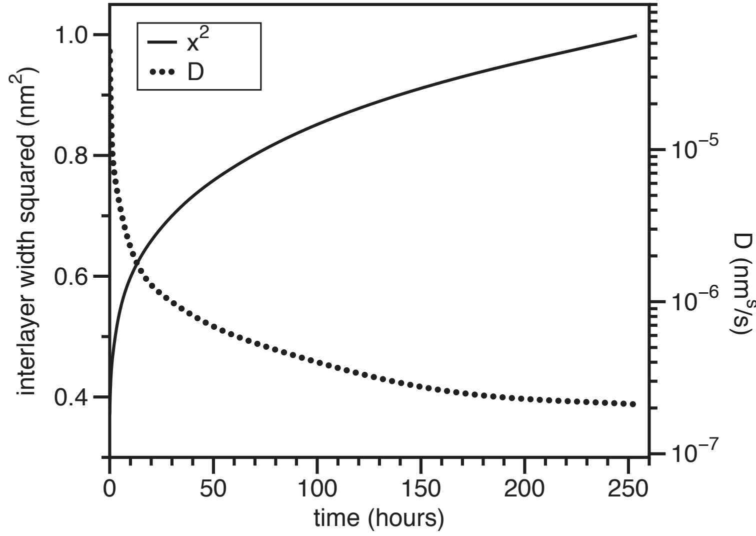

Figure 5.2: *Squared $MoSi_2$ interlayer width of the B_4C/Mo/Si structure annealed at 280 °C as a function of time, and the corresponding diffusion rate. For the calculation an initial interlayer width of 0.5 nm was assumed.*

that the structure/stoichiometry of both the 'bulk' of the interlayer and the moving boundary of the interlayer change during growth of the interlayer. As a result, Δz in eq.5.7 is not necessarily constant throughout the interdiffusion process.

In our analysis we have assumed that for every interlayer thickness value x_i, the structure and composition of the interlayer are identical for all selected temperature treatments as long as the range of annealing temperatures does not contain any (difference in) phase transitions of the material. If the growth of the interlayer is still diffusion limited, the diffusion rates determined using eq.5.6 combined with eq.5.7 at fixed interlayer widths are related to the temperature T and activation energy E_a by a single Arrhenius equation, given by

$$D = D_0 \exp\left(-\frac{E_a}{kT}\right). \tag{5.8}$$

The pre-exponential factor D_0 is related to the jump rate and jump distance of the diffusing atom. The parameters D, D_0 and E_a have become functions of x_i in our case.

Note that the assumption of a diffusion limited interlayer growth does not have to be valid. For now we only use it as our best estimate of the local (in time), effective diffusion rate. However, we always relate effective diffusion rates at fixed interlayer widths. Therefore, if we need to scale the

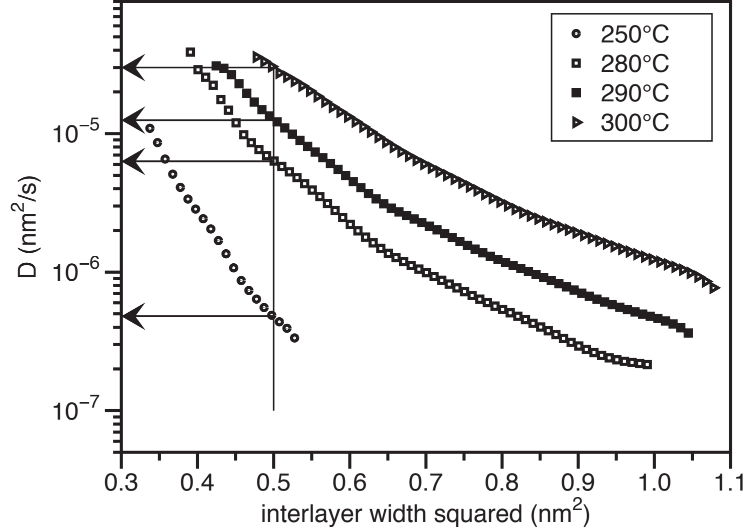

Figure 5.3: *Diffusion rate as a function of the interlayer width squared of the $B_4C/Mo/Si$ structure for a few selected temperatures: for selected values of the interlayer width squared the corresponding set of diffusion rates is determined.*

diffusion rate for example as D^α, this factor α can effectively be removed from the analysis when we are only interested in the activation energy. If we indeed find that the data scale nicely by the Arrhenius equation over an interval of interlayer thicknesses, we have found a way to describe the data in terms of a changing activation energy for interlayer growth, even though we have a non-constant diffusion rate.

The procedure is illustrated in Fig. 5.3 for the B_4C/Mo/Si system. In this Fig. we show the transformed data using a constant Δz corresponding to $MoSi_2$ formation from bulk Mo and Si. In Fig. 5.3 we selected a discrete set of values for the interlayer width squared x_i^2. For every temperature T for the value x_i^2, the local diffusion rate $D(x_i^2, T)$ is determined. In Fig. 5.4 the Arrhenius relation is demonstrated for a few selected values of x_i^2. The left curve in Fig. 5.5, related to the Si-on-Mo interlayer, gives the calculated activation energy for a set of values of x_i^2 using the Arrhenius relation. In Fig. 5.5 we also included the activation energy for the growing Mo-on-Si interlayer (right curve). We used the same thickness change value as used for the Si-on-Mo interlayer and assumed an initial interlayer width (x_0) of 1 nm, corresponding to literature values [4, 9].

We observe that the activation energy for interdiffusion at the Si-on-Mo interlayer increases as the interlayer grows. The activation energy starts at approximately 1.7 eV and saturates towards 2.5 eV. The activation energy of

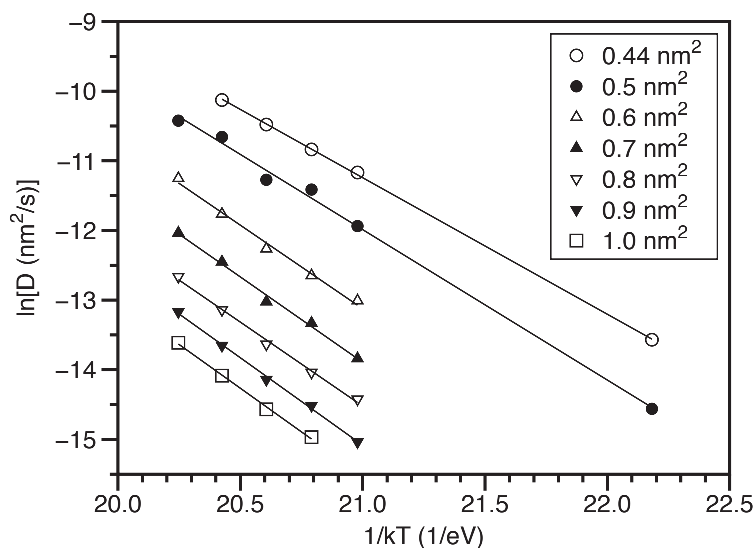

Figure 5.4: *Plot of the Arrhenius relation for a few selected interlayer widths of the B_4C/Mo/Si structure.*

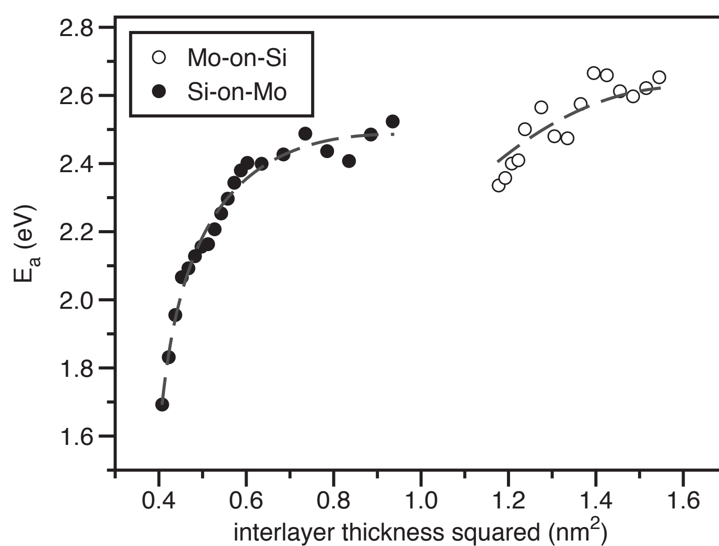

Figure 5.5: *Evolution of the activation energy for diffusion as the interlayer grows for the Si-on-Mo (left curve) and the Mo-on-Si interlayer (right curve).*

the thicker Mo-on-Si interlayer starts at approximately 2.4 eV and saturates around 2.6 eV. Although the error margin is about 0.2 eV, the activation energy at the Mo-on-Si may actually be considered constant. All activation energy values correspond reasonably well to the 1.9 or 2.3 eV activation energy reported for Si self diffusion in a $MoSi_2$ crystal, where the two values depend on the direction of diffusion in the lattice [11].

As for the assumptions used in our model, further calculations showed that the thickness change Δz and initial interlayer width x_0 only have a significant influence on the calculated interlayer thickness and pre-exponential factor. Concerning the thickness change parameter, we will explain the effect for a simplified condition. That is, we will treat it as though it remains constant throughout the diffusion process; an assumption that does not have to be true. If a larger thickness change upon interdiffusion should have been assumed, it means that we overestimated the interlayer width. However, the thickness change parameter is set constant for all temperature treatments applied. Therefore, the interlayer widths for different temperature treatments are still correctly coupled together. The resulting diffusion rates are scaled by a constant prefactor, which manifests itself only in the pre-exponential factor of the Arrhenius relation. This is even the case when the thickness change is not constant throughout the diffusion process. This is an obvious consequence of the analysis procedure introduced earlier in this paper. The initial interlayer width x_0 in eq.5.7 has a quite similar scaling behaviour as Δz, and has an effect on the interlayer thickness and pre-exponential factor, but not on the general trend of the activation energy.

Up to now we have assumed that only one specific process, namely Mo-Si interdiffusion, is responsible for a change in period thickness during annealing. Furthermore, we also stated that a changing interlayer structure during the diffusion process results in a change of diffusion rate and activation energy. Finding an Arrhenius scaling behaviour does not provide a full proof of this hypothesis.

Structural relaxations like free volume annihilation of the Si and/or Mo layer may also result in a change of period thickness [12]. We can describe these structural relaxations as self-vacancy of self-interstitial diffusion. Since both processes are also described by the empirical Arrhenius relation, it is evident that we can not a priori discriminate this process from the previously assumed Mo-Si interdiffusion.

Therefore, X-ray diffraction scans of the B_4C/Mo/Si structure were performed to measure crystallite sizes at different time steps of the annealing cycle at 250 and 300 °C. Fig. 5.6 shows the wide angle X-ray diffraction scan of a B_4C/Mo/Si structure before annealing and after two annealing cycles at 300°C. From the diffraction peaks we conclude that the Mo layer has a poly-crystalline structure. The position of the diffraction peak changes only slightly during the annealing cycle. The calculated strain from the (110) diffraction peak has changed by only 0.001 over the entire annealing cycle.

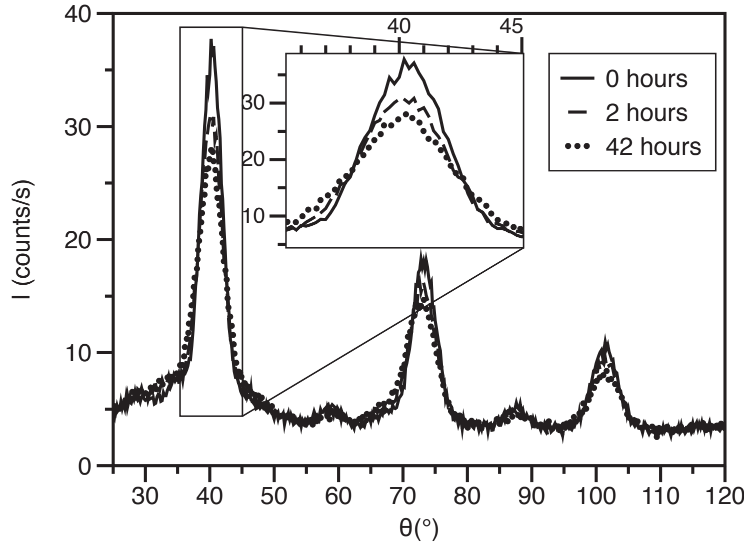

Figure 5.6: *X-ray diffraction scans of the $B_4C/Mo/Si$ structure treated at 300 °C after several annealing times; the inset shows a magnification of the Mo (110) diffraction peak.*

This results in a total change in period thickness of only 2-3 pm. Apart from a negligible change in strain, we do observe a reduction of the intensity and width of the diffraction peaks. Using the Scherrer equation we determined the evolution of the Mo crystallites. We selected the Mo (110) diffraction peak, since this plane is almost parallel (20 degrees) to the surface of the film. We observe that the crystallite size reduces from 1.94 nm to 1.45 nm in 60 hours of annealing at 300°C. This is illustrated in Fig. 5.7, where we divided the crystallite size by a constant factor of 3.5. The exact meaning of 3.5 will be adressed later. For now it is important to note that this factor is related to the structure of the interlayer that is being formed. Apart from the constant scaling factor, the trend of the change in period thickness and the reduction of the crystallites are identical. As we excluded straining of the crystallites to reduce the period thickness, it must be concluded that Si diffuses into the Mo crystallites, forming a silicide thereby reducing the size of the Mo crystallites. Additionally, since we used a constant scaling factor between change in crystallites and period thickness, we also conclude that the added interlayer structure is of a constant stoichiometry.

Combining the Mo crystallite size evolution and the change in period thickness of both the B_4C/Mo/Si and the Mo/B_4C/Si structures (Fig. 5.8), an additional, qualitative observation can be made about the stoichiometry of the growing interlayers. Relative to the change in period thickness, the Mo crystallite size decreases faster for the Mo/B_4C/Si structure compared to the

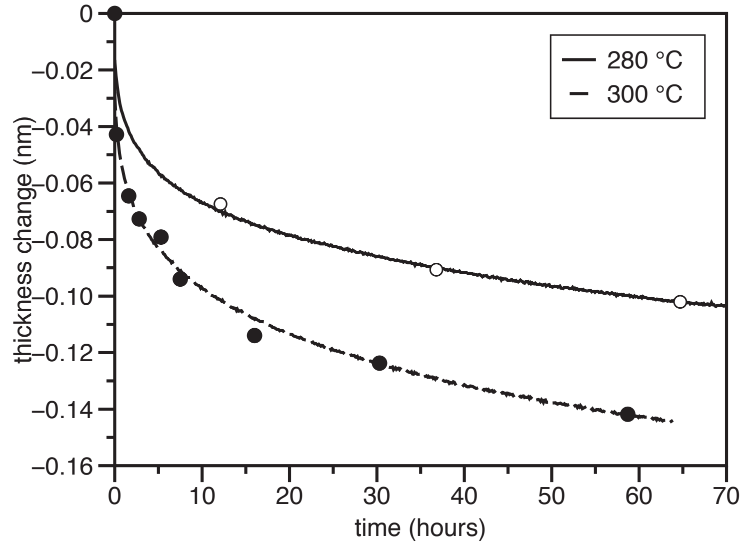

Figure 5.7: *Relative change of the Mo (110) crystallite size (open symbols) and change in period thickness (solid lines): the change in crystallite size is strongly correlated to the change in period thickness.*

B_4C/Mo/Si structure. The resulting scaling factor of 6 for the Mo/B_4C/Si sample, although constant, is significantly larger than before.

Calculations (as described in the experimental section) using bulk molar densities for Mo, Si and Mo-silicides gives us scaling factors γ of 1.6, 3.2 and 3.9 for $MoSi_2$, Mo_5Si_3 and Mo_3Si, respectively. The ratio $\gamma_{Mo_5Si_3}/\gamma_{MoSi_2}$ (=2.0) corresponds reasonably well to the measured ratio $\gamma_{Mo-on-Si}/\gamma_{Si-on-Mo}$ (=1.7). However, the absolute values for the γ's of the silicides are not in very good agreement with the measurements. The discrepancy is likely attributed to the assumption in the calculations that the Mo crystallites are reduced by continuously removing or affecting only the outer boundary atoms of the crystallites. Relaxing this restriction will increase the rate of crystallite reduction. Indeed, the depth concentration profile of diffused atoms is more likely to be gradual so that not only the boundary layer is affected but also the deeper layers in the crystallites. Assuming this gradual depth concentration profile the theoretical values for γ become in better agreement with the measured values.

As stated in the introduction, Rosen observed that the Mo-on-Si interlayer grows faster, in agreement with our measured crystallite size trend. Therefore, the initial assumption of a growing $MoSi_2$ phase for both interlayer structures was wrong. The thickness change parameter for the Mo-on-Si interlayer growth is smaller than that of the Si-on-Mo interlayer growth.

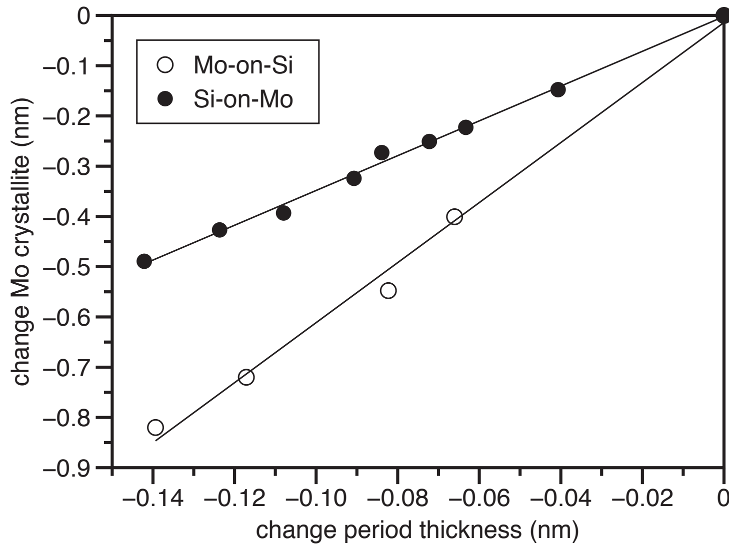

Figure 5.8: *Relation between the change in period thickness and the change in Mo crystallites for the B_4C/Mo/Si and the Mo/B_4C/Si structures.*

Hence, a different phase must be growing at the different interlayers. Although an exact value for the difference cannot be given based on this data, this difference does not affect the main conclusion on the change of diffusion rates in time and the determined activation energies.

5.4 Conclusions

In-situ X-ray reflection during annealing of Mo/Si based multilayer structures revealed that the interdiffusion layer initially grows non-parabolically with time. We found that the diffusion rate was not constant during the annealing cycle: as the interlayer grows, the diffusion rate gradually becomes smaller. Our analysis showed that during the interlayer growth, the activation energy for interdiffusion at the Si-on-Mo interlayer increases smoothly from 1.7 eV to 2.5 eV, whereas the activation energy at the Mo-on-Si interlayer is found to stay nearly constant (2.6 eV). In combination with wide angle X-ray diffraction, we observe that, although the final activation energies are quite similar, the stoichiometry of the growing Mo-on-Si and Si-on-Mo interlayers is different.

References

[1] E. Chi, J. Shim, J. Kwak, H. Baik, J. Mater. Sci. 31 (1996) 3567

[2] W.G. Sloof, O.B. Loopstra, Th.H. de Keijser, E.J. Mittemeijer, Scr. Metall. 20 (1986) 1683

[3] H. Nakajima, H. Fujimori, M. Koiwa, J. Appl. Phys. 63 (1988) 1046

[4] R.S. Rosen, D.S.P. Vernon, G. Stearns, M.A. Viliardos, M.E. Kassner, Y. Cheng, Appl. Opt. 32 (1993) 6975

[5] S. Bruijn, R.W.E. van de Kruijs, A.E. Yakshin, F. Bijkerk, Appl. Surf. Sci. 257 (2011) 2707

[6] K. Holloway, K. Do, R. Sinclair, J. Appl. Phys. 65 (1989) 474

[7] T. Böttger, D.C. Meyer, P. Paufler, S. Braun, M. Moss, H. Mai, E. Beyer, Thin Solid Films 444 (2003) 165

[8] Z. Erdélyi, D.L. Beke, J. Mater. Sci. 46 (2011) 6465

[9] S. Yulin, T. Feigl, T. Kuhlmann, N. Kaiser, A.I. Fedorenko, V.V. Kondratenko, O.V. Poltseva, V.A. Sevryukova, A.Yu. Zolotaryov, and E.N. Zubarev, J. Appl. Phys. 92 (2002) 1216

[10] F.R. de Boer, R. Boom, W.C.M. Mattens, A.R. Miedema, A.K. Niessen, Cohesion in metals. Transition metal alloys. North-Holland, 1988

[11] M. Salamon, A. Strohm, T. Voss, P. Laitinen, I. Riihimäki, S. Divinski, W. Frank, J. Räisänen, H. Mehrer, Philos. Mag. 84 (2004) 737

[12] O.B. Loopstra, E.R. van Snek, Th.H. de Keijser, E.J. Mittemeijer, Phys. Rev. B 44 (1991) 13519

CHAPTER 6

REDUCING DRIVING FORCE FOR INTERDIFFUSION IN MO/SI BASED MULTILAYER STRUCTURES

Abstract

Interdiffusion of a few nanometers thick C layer with Mo and Si under annealing at a temperature of 600°C was studied using XPS sputter depth profiling. A strong diffusion asymmetry of C in a Mo-Si layered structure is observed. C does interdiffuse with Mo, however, even at 600°C, no interdiffusion of Si and C was observed. Based on these results, the thermal stability of Mo/Si based layer structures was improved by depositing a Si/C/Mo_2C/C/Si layer structure. This structure shows superior thermal stability at 600°C compared to the Mo_2C/Si and Mo/Si layer structure.

6.1 Introduction

Mo/Si multilayer structures as Bragg reflectors for Extreme UltraViolet radiation (EUV) have been studied widely. However, two key issues in these multilayer structures still require further study: interlayer formation during deposition and interdiffusion of the materials under thermal load of for example 92 eV radiation for EUV lithography. Both effects reduce the optical contrast between the layers, and thereby reduce the peak reflectance. It has been observed that both the initial interlayer width and the interdiffusion rate are largest at the Mo-on-Si interface [1].

Additionally, the growth of the interlayers during annealing can not be described by the usually assumed parabolic growth (i.e. the squared interlayer width is proportional to time). There is a transition from anomalous to parabolic growth. During this transition, the diffusion rate reduces and the activation energy for interdiffusion at the Si-on-Mo interface increases from 1.7 to 2.5 eV, whereas at the Mo-on-Si interface the activation energy remains constant at 2.5 eV [2].

To reduce interdiffusion of Mo and Si it is common to put an additional barrier layer in between Mo and Si. This layer should have three properties: (1) chemically stable; (2) low interdiffusion rates with Mo and Si; (3) preferably a positive, otherwise a not too large negative effect on the reflection. The last requirement usually means that the additional layer should be very thin, usually a few tenths of a nanometer.

Reported compositions for this diffusion barrier layer are Si_3N_4, Mo_2C, and B_4C [3, 4, 5]. A thin B_4C layer significantly prevents interdiffusion up to 400°C [6]. For higher temperatures, the multilayer structures started to degrade. For annealing temperatures around 500°C, the B_4C layer decomposes and reacts with Mo and Si [7]. They speculate that a SiB_xC_y layer is formed, which is responsible for the thermal stability in Mo/Si multilayer structures containing B_4C barrier layers.

In this research we focus on the properties of a thin C layer in a Mo-Si layered structure, since: (1) for B and C there is a chemical driving force to intermix with Mo and Si (i.e. both have a negative enthalpy of formation with Mo and Si). However, the melt temperature for C is much higher than for B_4C, 3800 K vs 2445-3036 K. Therefore, a C layer might be more stable in this layer structure with Mo and Si; (2) like B_4C, a thin C layer slightly increases the reflectance of Mo/Si multilayer structures [8]. In both cases, this is likely due to the reduction of initial interdiffusion of Mo and Si. From optical point of view, this makes C, like B_4C, also a suitable candidate to be used in practice as a barrier layer between Mo and Si.

Furthermore, to passivate an entire layer in order to reduce interdiffusion, the Mo layer can be replaced by Mo_2C [9]. Although these multilayer structures were much more stable than the standard Mo/Si structures, the structure still degrades above 500°C. Based on our gained knowledge on

C interactions in a Mo-Si structure, described in this paper, we discuss a method to improve the Mo_2C/Si layer structure and to further reduce interdiffusion of Si into the Mo-carbide layer, especially during annealing.

6.2 Experimental

Samples containing C, Mo and Si were deposited onto super polished Si (100) wafers using electron beam evaporation. For electron beam evaporation, the arriving particles have a relatively low energy (0.1-0.2 eV). Therefor, intermixing at interfaces due to ballistical effects is minimized. To modify the density of the layers, after 1 nm of deposited material, a Kr ion beam was switched on (beam voltage 80 V, flux 7×10^{13} $cm^{-2}s^{-2}$, angle of incidence 45°) for the remainder of the layer. All samples were deposited at a base pressure lower than $2{\cdot}10^{-8}$ mbar. The film growth was monitored by quartz crystal microbalances.

All samples were analyzed using X-ray photoelectron spectroscopy: theta probe instrument, using monochromatic Al K_α radiation. To study interdiffusion of C, Mo and Si, XPS sputter depth profiling (0.5 keV Ar^+ at 45°) was used before and after annealing at 500 or 600°C. Four types of trilayer structures have been studied:

- substrate/Mo(10nm)/C(4nm)/Mo(10nm)
- substrate/Si(10nm)/C(4nm)/Si(10nm)
- substrate/Mo(10nm)/C(2nm)/Si(5nm)
- substrate/Si(10nm)/C(2nm)/Mo(5nm).

Based on the results of the previous series of samples, an additional series of samples was deposited and analyzed in the same manner:

- substrate/Si(10nm)/Mo_2C(5nm)/Si(10nm)
- substrate/Si(10nm)/C(2nm)/Mo_2C(5nm)/C(2nm)/Si(10nm)

To ensure the correct stoichiometry of the carbide layer, the Mo_2C layers were deposited using magnetron sputtering.

6.3 Results and discussion

6.3.1 Diffusion of C in Mo and Si layered structures

To study the effect of a thin C layer with Mo and Si, we first investigate the interaction of C with only Mo or Si. For this purpose, XPS sputter depth profiles of as deposited and annealed (1 hour) Si/C/Si and Mo/C/Mo

structures were measured. The XPS sputter depth profiles are illustrated in Fig.6.1(a) and 6.1(b). The depth scale (x-axis) is based on thicknesses determined by the quartz crystal microbalances and a constant sputter rate for every material. At 500°C, Mo and C interdiffuse, whereas even at 600°C we observe no interdiffusion of Si and C. Therefore, in the more complex structures where a C layer is in between Mo and Si, we can expect a strong diffusion asymmetry of the C.

In Fig.6.2(a) and 6.2(b) the XPS sputter depth profiles of Si(wafer)/Si/C-/Mo and Si(wafer)/Mo/C/Si layered structures are illustrated. For the as deposited structures it is clear that the carbon distribution for the Mo on C on Si is broader with a lower maximum than for the Si on C on Mo structure. This is usually interpreted as a more in depth localized carbon concentration, which suggests that the carbide interlayers are smaller for the second structure. This is in agreement with the usually observed asymmetry of interlayer widths in Mo/Si multilayer systems. In these structures, the Mo-on-Si interlayer is thicker than the Si-on-Mo interlayer [10].

The depth profile of the Si(wafer)/Si/C/Mo structure annealed at 600°C for 3 hours, shows that C has fully diffused into the Mo layer and on average has formed a homogeneous layer with Mo. The Mo/C ratio is approximately 2/1, suggesting that an amorphous or crystalline Mo_2C has formed. Nakanishi *et al* have shown that indeed annealing at 600°C for 1 hour of a Mo/C(diamond) layer structure leads to a 3-4 nm thick amorphous layer with crystalline Mo_2C and MoC particles, and a crystaline layer on top. The Mo_2C phase was identified as the dominant phase [11]. In agreement with our earlier observation described in this paper, C has not diffused into the Si layer. Additionally, with the experimental setup, predominantly the intermixed region due to sputter erosion is probed. Since the slope of the Si depth profile at the (Mo-)C interlayer has not changed, it is unlikely that Si has diffused into the Mo-carbide layer.

Annealing of the (wafer)/Mo/C/Si structure at 600°C for 3 hours results in a very different picture. First of all, the C is not homogeneously distributed into the Mo layer. The highest Mo/C ratio we observe is approximately 7/2. This does not necessarily mean that no Mo_2C has formed. Actually, we know that a Mo_2C should form. Therefore, it must be that laterally, no homogeneous Mo_2C layer is formed. Hence, there are Mo regions at the Si interface where a Mo-Si reaction can occur. Indeed, contrary to the previous system, the slope and maximum percentage of the Si has changed, and we do see additional content of Si in the Mo layer. It appears that without the formation of a sufficiently homogeneous Mo-carbide layer with an approximate stoichiometry of Mo_2C, Si will diffuse into the Mo layer. Given that Mo-silicides are always more favorable from enthalpy point of view than Mo-carbides (with the same ratio's of the elements) [12], Mo-silicides in the end will be the dominating phase.

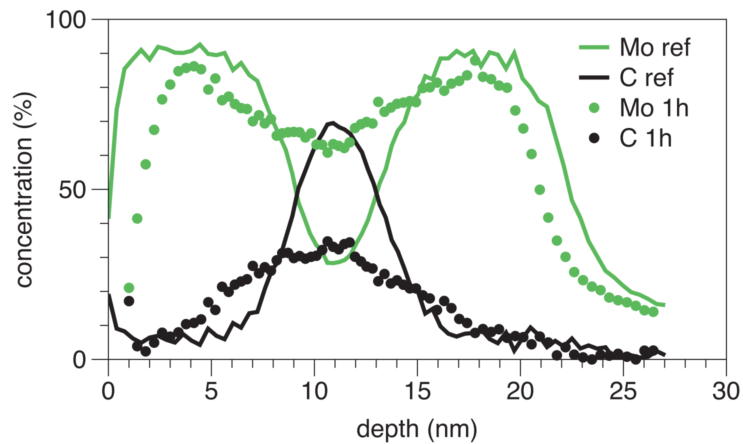

(a)

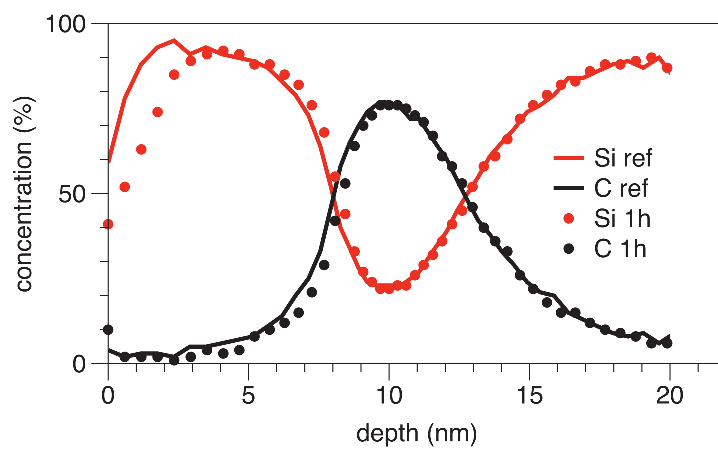

(b)

Figure 6.1: *XPS sputter depth profile of: (a) Mo/C/Mo before (solid line) and after (dotted line) annealing at 500° C for 1 hour; (b) Si/C/Si before (solid line) and after (dots) annealing at 600° C for 1 hour.*

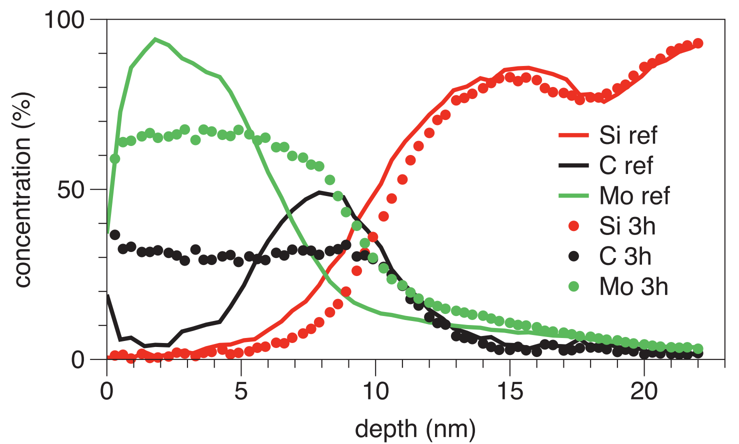

(a)

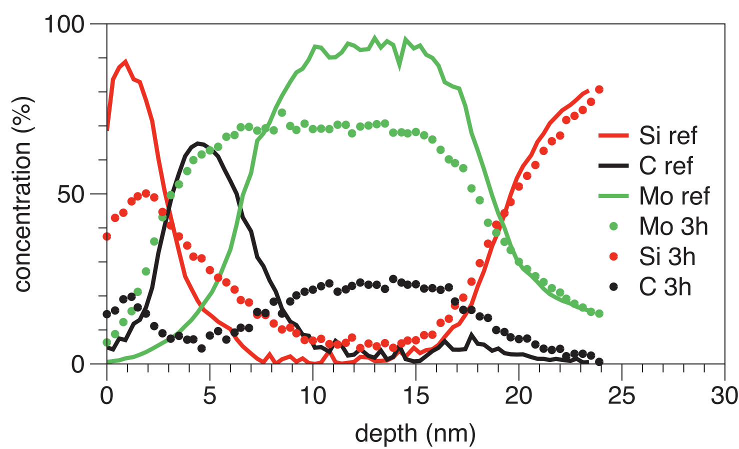

(b)

Figure 6.2: *XPS sputter depth profile of: (a) Si(wafer)/Si/C/Mo before (solid line) and after (dots) annealing at 600° C for 3 hours; (b) Si(wafer)/Mo/C/Si before (solid line) and after (dots) annealing at 600° C for 3 hours.*

6.3.2 Effect of C layers in a Si/Mo_2C/Si structure

As opposed to Mo/Si multilayer structures, Mo_2C/Si multilayer structures possess a superior thermal stability up to 500°C [9]. In the previous section we concluded that C diffuses into Mo, whereas no significant interdiffusion of Si and C is present at this temperature. Additonally, from the Si(substrate)/Mo/C/Si compared to the reverse system, we concluded that the Mo-C ratio may be very important with respect to Si diffusion towards Mo.

Based on these observations, we compare Si/Mo_2C/Si with and without additional C layers between Si and Mo_2C. The XPS depth profiles of the as-deposited and the annealed structures (1 hour at 600°C) are illustrated in Fig.6.3(a) and 6.3(b). In agreement with Feigl, we see that the Si/Mo_2C/Si layer structure deteriorates during annealing at 600°C. Si is diffusing into the Mo-carbide layer and is consequently reducing the C concentration in this layer. As mentioned before, the enthalpy of formation of Mo-silicides is always more negative than the formation enthalpy of the Mo-carbides (having the same ratio's of the elements). Therefore, the probability to have Mo-silicides in the structure is higher than that of Mo-carbides.

On the contrary, when we look at the system with 2 nm thick C layers around the Mo-carbide layer, there is little to no change in the concentration profile before and after annealing at 600°C for 1 hour. As expected, the Si and C layer show no interdiffusion. Inside the Mo-carbide layer there might be some redistribution of Mo and C. Activation energy values for C diffusion in Mo-carbide vary between 3.06 to 4.79 eV [13, 14, 15], whereas a value of only 1.89 eV is reported for C diffusion in Mo [14]. Therefore, compared to the Mo/C system, much less interdiffusion is to be expected. Apparently, the activation energy is high enough for the C layer to stay intact.

The XPS sputter depth profiles measured after 5 hours of annealing at 600°C are included in Fig. 6.4(a) and 6.4(b). In the Si/Mo_2C/Si system, we see a slight difference at the interface at 15 nm: Si is still diffusing into the Mo-carbide layer. Contrary, the concentration distribution with additional C layers between Si and Mo-carbide still shows no changes.

To further explain why the two systems with Mo_2C behave so differently, we made a graphical depiction of the expected layered structure after the deposition process and during annealing (Fig. 6.5(a) and 6.5(b)). During sputter depositing of a Mo_2C layer on Si, Mo and C atoms arrive separately. We have observed already that Mo-Si appears to be a more dominant reaction than Mo-C. Therefore, during deposition an interlayer consisting of Mo, C and Si will form. In addition to this interlayer, the Mo-C layer will not be in an ordered carbide phase. During annealing, Si is able to diffuse further into the amorphous Mo-carbide structure, before this layer can relax into an ordered, chemically stable state, as it appeared to be in the Si(wafer)/Si/C/Mo structure.

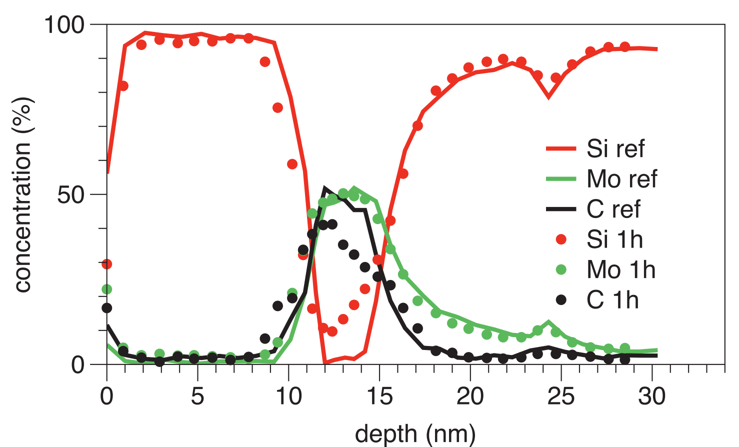

(a)

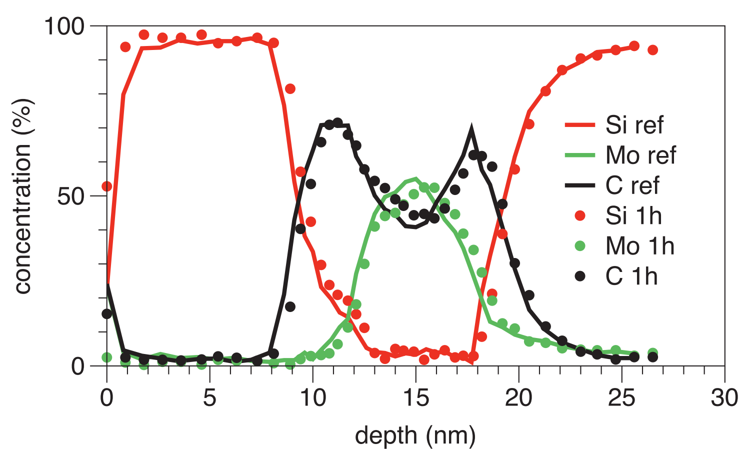

(b)

Figure 6.3: *XPS sputter depth profile of: (a) Si/Mo_2C/Si before (solid line) and after (dots) annealing at 600° C for 1 hour; (b) Si/C/Mo_2C/C/Si before (solid line) and after (dots) annealing at 600° C for 1 hour.*

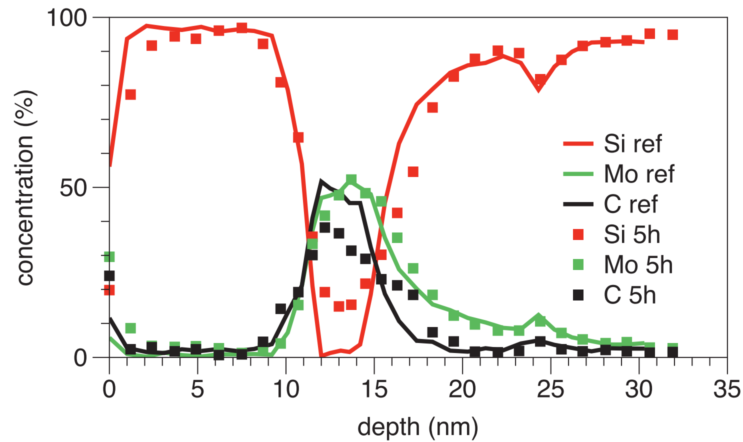

(a)

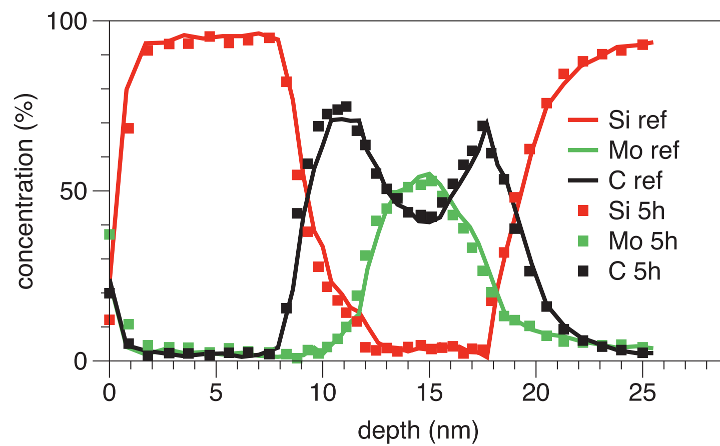

(b)

Figure 6.4: *XPS sputter depth profile of: (a) Si/Mo_2C/Si before (solid line) and after (dots) annealing at 600° C for 5 hours; (b) Si/C/Mo_2C/C/Si before (solid line) and after (dots) annealing at 600° C for 5 hours.*

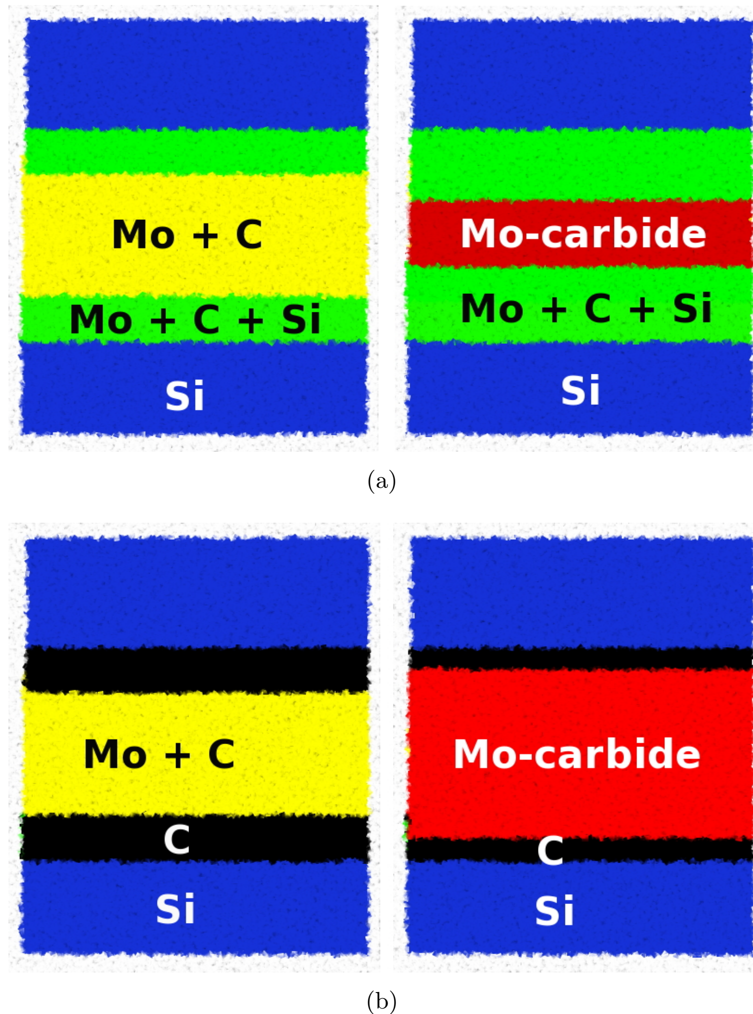

Figure 6.5: *Schematic depiction of deposition and annealing of (a) Si/Mo_2C/Si structure and (b) Si/C/Mo_2C/C/Si structure. The '+' in the illustrations means that all kind of bonds can be present between the mentioned elements.*

For the structures where a C layer is deposited on top of Si and also on top of the sputtered Mo-carbide layer, the situation is different. The arriving Mo and C atoms will not intermix with Si during deposition, but with the C layer (provided this layer is closed). Since C and Si do not or barely interdiffuse at 600°C, the Mo-carbide layer has time to relax into a more stable and ordered state. Given the high activation energy for C diffusion into a Mo-carbide layer, the C layer will largely remain intact, and Si will not be able to diffuse through the C layer, towards the Mo-carbide layer.

6.3.3 Applicability as EUV multilayer mirrors

For applications like EUV lithography, it is very important that multilayer structures have a good reflection and thermal stability. Mo/Si and Mo_2C/Si multilayer structures have been demonstrated to reflect 67.5% and 66.3% at a wavelength of 12.8 nm, respectively [9]. This means that replacing a Mo layer by Mo-carbide will result in a loss of about 1.2%. When looking at the theoretical difference in reflection between these two multilayer mirror structures (50 periods, no roughness, 13.5 nm wavelength radiation (used in EUVL), near normal incidence), we get a difference of 2.4% (75.2% and 72.8%, respectively). By simulating the small angle reflection spectra, Feigl *et al* found that the interlayers are 0.2 and 0.6 nm thick for the carbide system, whereas the interlayers have a thickness of 0.6 and 1.0 nm in the Mo/Si system. This large reduction in interlayer width may explain that in reality the loss in reflection is less than in theory.

Based on a trend in the (110) Mo diffraction peak with different C layer thicknesses, Braun *et al* [8] speculated that a continuous C layer forms after a layer thickness of 0.2 nm. When calculating the reflectance of a C/Mo_2C/C/Si multilayer structure (50 periods, no roughness, 13.5 nm wavelength radiation, near normal incidence) with C layer thicknesses of 0.2 or 0.5 nm, we get a reflection of 71.7 and 69.7%, respectively. Compared to the theoretical value of the Mo_2C/Si system, this is a loss of 1.1 or 3.1%. Since C layers will further reduce or prevent Mo-Si interlayers between the Si and Mo_2C layer, we would assume that these losses are an overestimation. Therefore, we would expect that the loss compared to standard Mo/Si multilayer structures will be less than 2.3% for 0.2 nm thick C layers between Si and Mo_2C (i.e. addition of the experimental loss of 1.2% between Mo/Si and Mo_2C/Si and the theoretical loss of 1.1% between the C/Mo_2C/C/Si and Mo_2C/Si multilayer structures). Based on this estimation, the improved multilayer structure (C/Mo_2C/C/Si) might be a viable candidate to be used as thermally stable Bragg mirrors for EUV reflection around 13.5 nm.

6.4 Conclusions

Using XPS sputter depth profiling, we found that there is a strong diffusion asymmetry for C in a Mo-Si layered structure at an annealing temperature of 600°C. Si and C do not tend to intermix, whereas Mo and C do intermix. When annealing Mo_2C/Si multilayer structures at 600°C, Si is able to diffuse into the carbide layer. This is also expected, based on the difference in Mo-carbide and Mo-silicide enthalpies of formation. Upon introducing C layers in between the Si and Mo_2C layer, the structure shows no changes under annealing at 600°C. The C/Mo_2C/C/Si structure shows a superior thermal stability over existing Mo-Si based multilayer structures.

References

[1] R.S. Rosen, D.S.P. Vernon, G. Stearns, M.A. Viliardos, M.E. Kassner, Y. Cheng, Appl. Opt. 32 (1993) 6975

[2] J. Bosgra, J. Verhoeven, R.W.E. van de Kruijs, A.E. Yakshin, F. Bijkerk, Thin Solid Films 522 (2012) 228

[3] I. Nedelcu, R.W.E. van de Kruijs, A.E. Yakshin, F. Bijkerk, J. Appl. Phys. 103 (2008) 083549

[4] S. Bajt, J.B. Alameda, T.W. Barbee, W.M. Clift, J.A. Folta, B. Kaufmann, E.A. Spiller, Opt. Eng. 41 (2002) 1797

[5] T. Feigl, S. Yulin, N. Kaiser, R. Thielsch, Emerging Lithographic Technologies IV (SPIE) 3997 (2000) 420

[6] T. Böttger, D.C. Meyer, P. Paufler, S. Braun, M. Moss, H. Mai, E. Beyer, Thin Solid Films 444 (2003) 165

[7] V.I.T.A. de Rooij-Lohmann, L.W. Veldhuizen, E. Zoethout, A.E. Yakshin, R.W.E. van de Kruijs, B.J. Thijsse, M. Gorgoi, F. Schaefers, F. Bijkerk, J. Appl. Phys. 108 (2010) 094314

[8] S. Braun, H. Mai, M. Moss, R. Scholz, A. Leson, Jpn. J. Appl. Phys 41 (2002) 4074

[9] T. Feigl, H. Lauth, S. Yulin, N. Kaiser, Microelectronic Engineering 57-58 (2001) 3

[10] S. Yulin, T. Feigl, T. Kuhlmann, N. Kaiser, A.I. Fedorenko, V.V. Kondratenko, O.V. Poltseva, V.A. Sevryukova, A.Yu. Zolotaryov, and E.N. Zubarev, J. Appl. Phys. 92 (2002) 1216

[11] J. Nakanishi, A. Otsuki, T. Oku, O. Ishiwata, M. Murakami, J. Appl. Phys. 76 (1994) 2293

[12] F.R. de Boer, R. Boom, W.C.M. Mattens, A.R. Miedema, A.K. Niessen, Cohesion in metals. Transition metal alloys. North-Holland, 1988

[13] C.J. Rosa, Metall. Trans. A 14 (1983) 199

[14] W.P. Leroy, C. Detavernier, R.L. Meirhaeghe, A.J. Kellock, C. Lavoie, J. Appl. Phys. 99 (2006) 063704

[15] B.M. Warnes, G. Simkovich, J.Less-Common Met. 106 (1985) 241

CHAPTER 7

IMPROVEMENT OF SI/C INTERFACE CORRELATION DURING ANNEALING

Abstract

We studied the asymmetry in interlayer growth at Si on C and C on Si interfaces using X-ray reflectometry and angular resolved X-ray photoelectron spectroscopy after deposition. In addition, we studied the diffusion effects at the Si-C interfaces during annealing of Si/C multilayer structures at 250°C. We observed no significant change in period thickness, suggesting limited to no interlayer growth. Additionally, we observed an increase in reflection of the first order Bragg peak during annealing of the Si/C multilayer structure. We show that the increase in first order Bragg peak intensity is related to an improved correlation of the roughness between interfaces.

7.1 Introduction

Multilayer structures are widely used as Bragg reflectors for soft X-ray and EUV radiation. One specific example is a Mo/Si multilayer structure, which is used for EUV lithography. Two specific problems related to EUV lithography and Mo/Si multilayers are suppression of IR radiation coming from the EUV source and multilayer thermal stability.

IR radiation coming from the source is reflected from the multilayer structures throughout all the optics in EUVL machines. Reflection of the IR radiation in Mo/Si multilayer structures is mainly due to the Mo layers. Other high electron density materials, which can be used instead of Mo in EUV multilayer mirrors, are generally metals [1], which will also reflect the IR radiation.

A solution to suppress IR radiation without a significant loss of EUV reflection, is to use Si/C multilayer structures as a integral part of an anti reflection coating. Using this structure, Soer *et al* achieved values of 42.5% and 4.4% for EUV and IR reflection, respectively [1].

Thermal stability of the Mo/Si multilayer structures can be significantly improved by fabricating C/Mo_2C/C/Si layered structures. Even though there is a chemical driving force for Si and C to intermix (formation enthalpy $\Delta_f H_{298}\langle\alpha\text{-SiC}\rangle$ = -74.4 kJ/mol [2]), the structure did not show any significant intermixing of the materials under annealing at 600°C [3]. It was not investigated in that study whether a SiC layer had formed during deposition to act as a diffusion barrier or how thick the Si-C interlayers are after deposition. The latter is important both to optimize the C layer thickness for the C/Mo_2C/C/Si multilayer structures and to investigate the possibility to improve the Si/C layered structure.

In this chapter the interlayer formation in Si/C layered structures after depostion, and the dynamics at the Si-C interfaces during annealing are described.

7.2 Experimental

Si(5.5 nm)/C(1 nm) multilayer structures composed of 50 periods were deposited on Si (100) substrates by DC magnetron sputtering in a chamber with a base pressure lower than 1e-6 Pa. The film growth was monitored by quartz crystal microbalances. The multilayer structure was measured using hard X-ray reflectometry in the Bragg-Brentano setup. Some specific details of the diffractometer are: Cu K_α radiation, four bounce asymmetrically cut Ge (220) monochromator, and instrumental broadening of 0.005°.

To determine the initial layer structure, we extended the Fourier analysis of X-ray reflectometry measurements. To validate the obtained value for the interface roughness σ_r from our model, we performed an AFM scan

of the surface of the multilayer structure. Furthermore, to complement the fit of the initial Si/C layer structure with chemical information on the interlayer structures, Si(10 nm)/C(1 nm) and C(7.5 nm)/Si(1 nm) bilayer structures were deposited using electron beam evaporation. The bilayer structures were measured using angular resolved X-ray photoelectron spectroscopy (ARXPS): theta probe instrument, monochromatic Al K_α radiation. Thick C and co-deposited SiC layers were used as reference structures to interpret the measurements of the bilayer structures. All samples were transported in vauum from the deposition chamber to the XPS chamber, i.e. the samples were never exposed to ambient conditions before the measurements.

Changes of the Si/C multilayer structure during annealing were measured using hard X-ray reflectometry during annealing. The method to measure changes in the period thickness with picometer accuracy with a time resolution of a few minutes is described by Bosgra *et al* [6]. The annealing temperature was set to 250°C, such that the dymanics at the interfaces are not too fast,

7.3 Extension of Fourier analysis for X-ray reflectometry measurements

For hard X-rays, reflection from a structure is related to the Fourier transform of the electron density distribution. The Fourier transformation of the mth order Bragg peak is related to the mth order Fourier harmonic of the dielectric distribution in depth [4]

$$I_{re,m}(0) \approx \frac{2\pi L a_m^2 k^4}{q_m^2} \tag{7.1}$$

where L is the thickness of the total multilayer stack, wavenumber $k = 2\pi/\lambda$ with λ the wavelength of the radiation, $q_m = 2\pi m/\Lambda$, Λ is the period thickness, and a_m are the renormalized Fourier harmonic amplitudes of an even or odd dielectric distribution. The Fourier harmonic amplitudes, including roughness effects, are given by

$$a_m = a_{m,id} \exp\left(-\frac{q_m^2 \sigma_r^2}{2}\right), \quad m = 1, 2, \ldots \tag{7.2}$$

where $a_{m,id}$ is the amplitude of the mth harmonic of an ideal structure and σ_r in the Debye-Waller factor is the interface roughness.

However, the limitation of even or odd distributions in equation 7.1 is not always correct for nanoscopic multilayer structures. For example, in Mo-Si multilayer systems, the Mo-on-Si interlayer is larger than the Si-on-Mo interlayer [5]. To extend the previous analysis, such that it also includes

asymmetric dielectric distributions, we get by superposition of the even and odd solutions

$$I_{re,m}(0) \approx \frac{8\pi L c_m c_{-m} k^4}{q_m^2} \tag{7.3}$$

where we used the complex Fourier series. Unfortunately, equation 7.3 has an infinite number of solutions for every m. Therefore, we have to make a presupposition for the periodic dielectric distribution of the multilayer structure. We impose that between two homogeneous layers, the intermixed regions of the concentration profile are described by error functions. The complex Fourier coefficients are now given by

$$c_m = [\xi_1(z, s_1, o_1, 2)]_{-\Lambda/2}^{-d} + [\xi_2(z)]_{-d}^{d} + [\xi_1(z, s_2, o_2, 1)]_{d}^{\Lambda/2} \tag{7.4}$$

with

$$\begin{aligned}
\xi_1(z, s_j, o_j, k) &= \int \frac{1}{2}\Delta\varepsilon(1 + (-1)^k \mathrm{erf}(s_j(z + o_j))) \exp\left(-\frac{i2\pi m z}{\Lambda}\right) \mathrm{dz} \\
&= (-1)^k \frac{\Delta\varepsilon\Lambda}{4\pi m} \exp\left(-\frac{i2\pi m z}{\Lambda}\right) \Bigg[i((-1)^k + \mathrm{erf}(s_j(z + o_j))) \\
&+ \mathrm{erfi}\left(\frac{\pi m - i\Lambda s_j^2(z + o_j)}{\Lambda s_j}\right) \exp\left(\frac{\pi m(-\pi m + 2i\Lambda s_j^2(z + o_j))}{\Lambda^2 s_j^2}\right) \Bigg] \\
\xi_2(z) &= \int \Delta\varepsilon \exp\left(-\frac{i2\pi m z}{\Lambda}\right) \mathrm{dz} = \frac{i\Delta\varepsilon\Lambda}{2\pi m} \exp\left(-\frac{i2\pi m z}{\Lambda}\right)
\end{aligned}$$

where $\Delta\varepsilon$ is the maximum optical contrast between the two layers, s_j determines the width of the interlayer, o_j the position of the interlayer, and $2d$ is the thickness of one of the layers (homogeneous concentration). The integration dz is over the multilayer period thickness. The period thickness Λ is calculated from the corrected Bragg equation

$$m\lambda = 2\Lambda \sin\theta_m \sqrt{1 - \frac{\bar{\delta}}{\sin^2\theta_m}} \tag{7.5}$$

with θ_m the position of the mth Bragg order of reflection and $\bar{\delta}$ the average refractive index decrement.

The described analysis method has one important advantage with regard to a fitting algorith using the recursive Rouard equation, namely no densities of the layers have to be assumed. The densities of the layers are related to $\Delta\varepsilon$. By taking the ratio of the intensities of two Bragg orders, $\Delta\varepsilon$ is factored out. Consequently, 4 parameters have to be determined using a least square fit with the model to the data, to calculate the period structure of the multilayer, namely σ_r, s_1, s_2 and d.

Table 7.1: *Binding energies of Si2p3/2 and C1s peaks for co-deposited Si-C layers with different Si/C ratio's. The labels refer to different configurations.*

ratio	E(Si) (eV)	E(Si_C) (eV)	E(C_C) (eV)	E(C_A) (eV)	E(C_D) (eV)
0.3	–	100.23	283.62	284.36	285.26
0.8	99.26	100.03	283.42	284.28	–
2.7	99.18	99.69	283.20	284.20	–

7.4 Results and Discussion

7.4.1 Interlayer formation during deposition

For the study of interdiffusion in Si/C layered structures, it is important to know the initial layer structure. That is, if the C layer is already fully intermixed with Si, no additional interdiffusion effects should be observed during annealing of the structures. To determine the thickness of Si-carbide interlayers, formed during deposition of Si/C layered structures, X-ray reflection measurements are analyzed with the extended Fourier analysis model.

From the X-ray reflectometry $\theta - 2\theta$ scan, $\bar{\delta}$ and Λ are calculated and found to amount to $\Lambda = 6.56 \pm 0.01$ nm and $\bar{\delta} = 1.0 \cdot 10^{-5} \pm 2 \cdot 10^{-6}$. The ratio's of the Fourier transformed Bragg peaks (I_i/I_j) were treated using the model discussed in the previous section. The least squares fit of the Fourier transformed data to the model (Fig.7.1a) results in the normalized concentration profile illustrated in Fig.7.1b. The error in $\bar{\delta}$ is too large to make a reliable estimation for the density of the C layer. Therefore, we optimize ρ_C directly from the integrated intensity of the Bragg peaks. For the calculation, we assumed the density of the Si layer to be 2.32 g/cm^3. The following characteristics of the C layer in the period structure are obtained: integrated C layer thickness is 1.1±0.06 nm, $\sigma_r = 0.17 \pm 0.02$ nm and $\rho_C = 2.50 \pm 0.01$ g/cm^3.

The roughness value is in good agreement with the AFM measurement of the surface of the multilayer structure. From this measurement we determined a value of $\sigma_r = 0.14 \pm 0.01$ nm. The calculated density of the C layer is in between the graphite and diamond phase (2.27 vs. 3.52 g/cm^3). Therefore, it is reasonable to assume that in Fig.7.1, the normalized value of 1 for the C concentration corresponds to a pure C layer. From this figure it is also apparant that one interlayer is larger than the other. One interlayer is very sharp ($\ll 0.1$ nm), whereas the other is a few tenths of a nanometer thick. From the Fourier analysis method, due to symmetry of the solution,

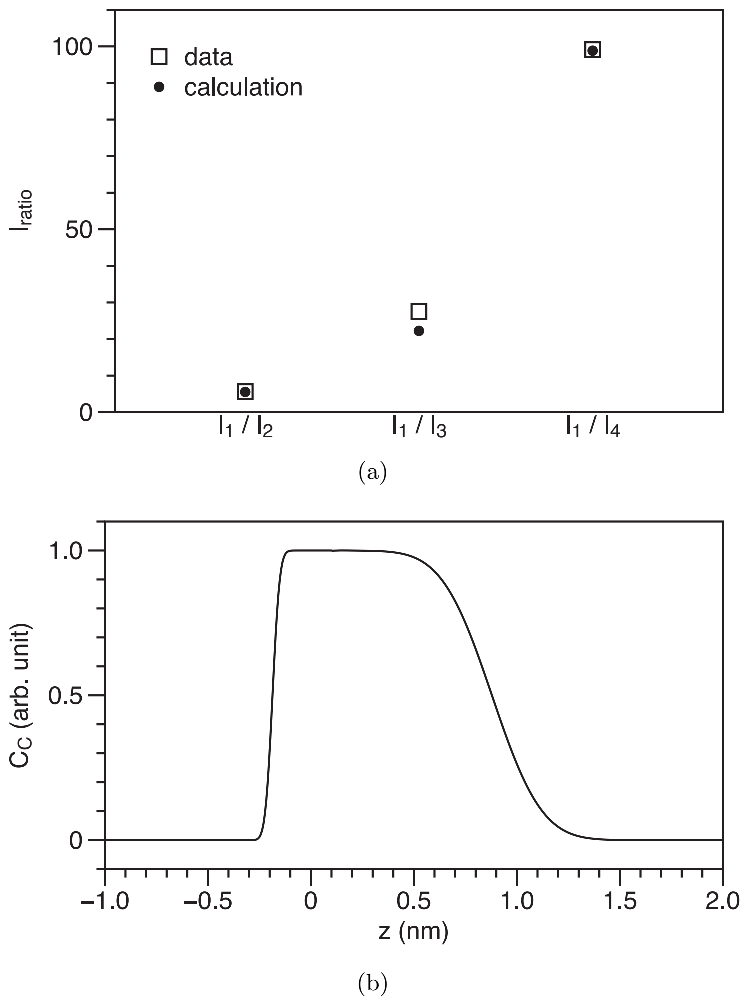

Figure 7.1: *Results of Fourier analysis of X-ray reflection data of the Si/C multilayer structure: (a) Calculated and measured intensity ratio's of the Fourier transformed Bragg peaks (I_i/I_j); (b) corresponding average, normalized C concentration profile at depth z within the multilayer period (figure shows the C concentration profile only around the C layer).*

we cannot say whether the Si-on-C interlayer is larger than the C-on-Si, or vice versa.

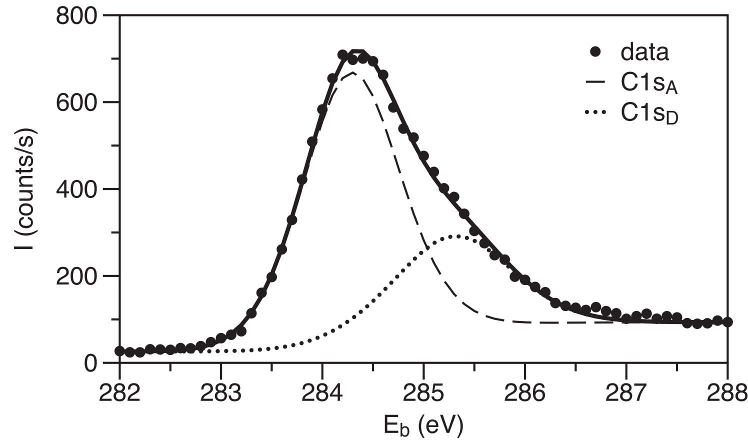

(a)

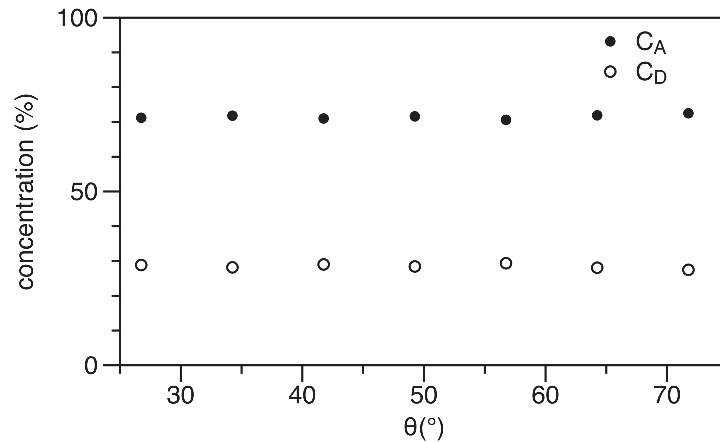

(b)

Figure 7.2: *XPS measurements of a deposited C layer (a) C1s XPS peak at 26.75°, the thick solid line through the data points is the added signal of the $C1s_A$ and $C1s_D$ peaks; (b) concentration of the $C1s_A$ and $C1s_D$ peak at different angles.*

To obtain chemical information of the SiC interlayers, ARXPS measurements were performed. The XPS data of the C reference layer is included in Fig.7.2a and b. The asymmetry of the C1s peak clearly shows that at least two peaks should be used to fit the data. Therefore, the C layer contains two different configurations. We will use the labels A and D to designate the

C1s peaks around 284.3 and 285.3 eV, respectively. The resulting concentrations of the A and D peaks at different angles shows that in depth both C configurations are homogeneously distributed (including the surface). Consequently, both XPS peaks refer to elementary C configurations.

The XPS results of the Si-C co-deposited reference systems with different Si/C ratio's are included in Fig.7.3a-c for C and Fig.7.4a-c for Si. The binding energies of the photoelectrons are listed in table 7.1. For the 0.3 Si/C ratio, 3 peaks are required to fit the C1s XPS peak: the $C1s_A$ and $C1s_D$ peaks of the pure C layer and a third peak which we will give the label $C1s_C$ to designate a carbide bond. For the Si/C ratio of 2.7, the Si2p peak has to be be decomposed into 2 doublets, one belonging to the elementary Si2p photoelectron binding energies and one belonging to the carbide. The Si2p carbide bonds will also be referred to with the 'C' label. As the Si/C ratio changes, both the $C1s_C$ and the $Si2p3/2_C$ (and the related $Si2p1/2_C$) photoelectrons shift by a few tenths of eV's in binding energy. To conclude, using XPS we can discriminate between C-rich and Si-rich carbide interlayer structures.

Using the obtained XPS information on the binding energies of the carbide layers, the Si/C(1nm) and C/Si(1nm) bilayer structures on a Si wafer are analyzed. In the structure with the 1nm C overlayer, the binding energy of the $C1s_C$ peak is given by 283.5 eV. Based on the results summarized in table 7.1, we suggest that the formed carbide is C-rich, having a Si/C ratio between 0.3 and 0.8. For the structure with the 1nm Si overlayer, the $Si2p3/2_C$ peak has a binding energy of 99.74 eV, suggesting a Si-rich carbide structure, having a Si/C ratio close to 2.7.

Apart from a suggested difference in Si/C ratio for the Si-on-C or the C-on-Si interlayer, another difference can be observed from ARXPS derived atomic fractions (Fig.7.5a and b). At every angle the relative C concentration of the C overlayer is higher than the Si concentration of the Si overlayer. Given that the attenuation length of C and Si are not too different (using the relation by Cumpson [7] we get attenuation lengths of 2.4 nm for C and 2.8 nm for Si), this suggests that the C-on-Si interlayer is thinner than the Si-on-C interlayer. In addition, for the C overlayer, the carbide fraction of the C signal is much lower than the carbide fraction of the Si signal in the Si overlayer. Both results confirm that the interlayers are asymmetric in width, confirming the Fourier analysis of the X-ray reflection measurement.

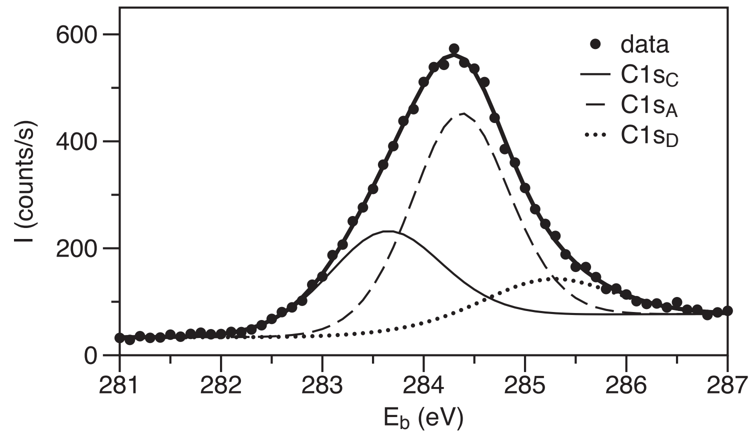

(a)

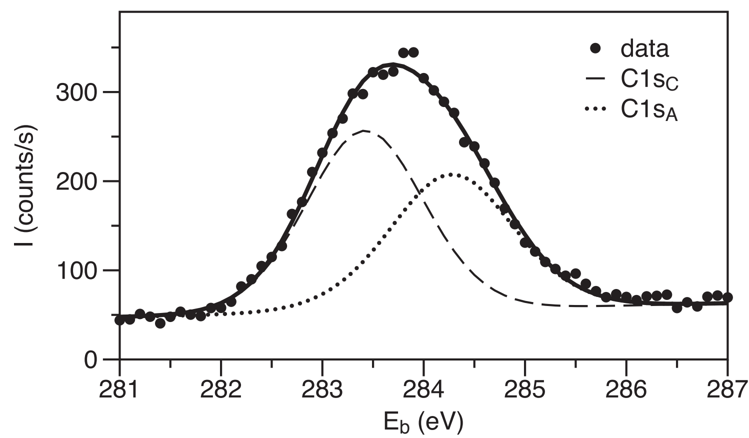

(b)

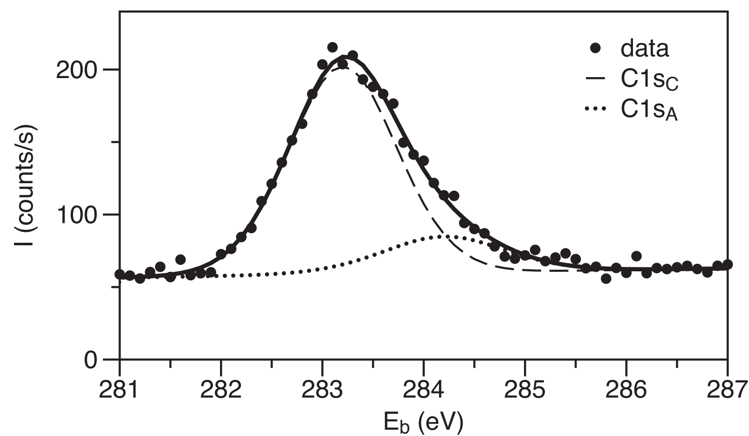

(c)

Figure 7.3: *XPS measurement of the C1s peak at 26.75° for a Si/C ratio of: (a) 0.3; (b) 0.8; (c) 2.7. The C1s peak can be decomposed into different, chemical compositions.*

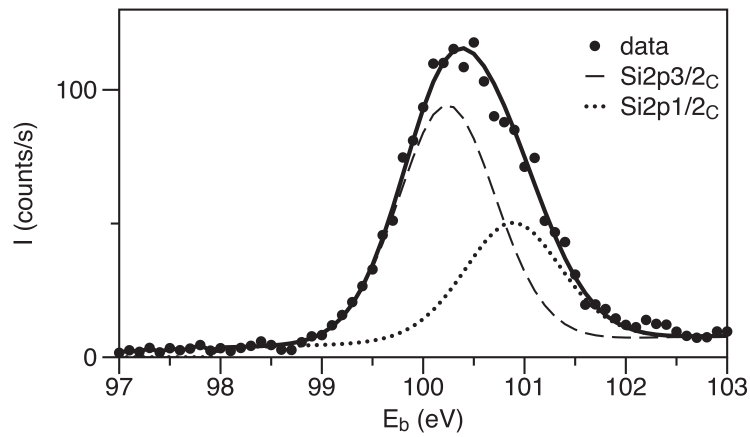

(a)

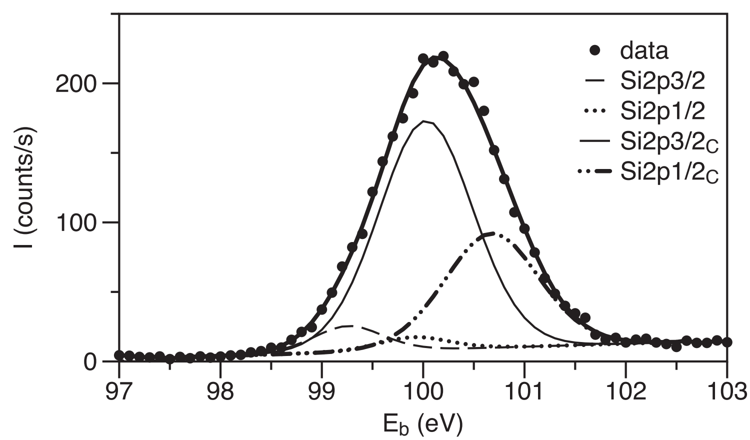

(b)

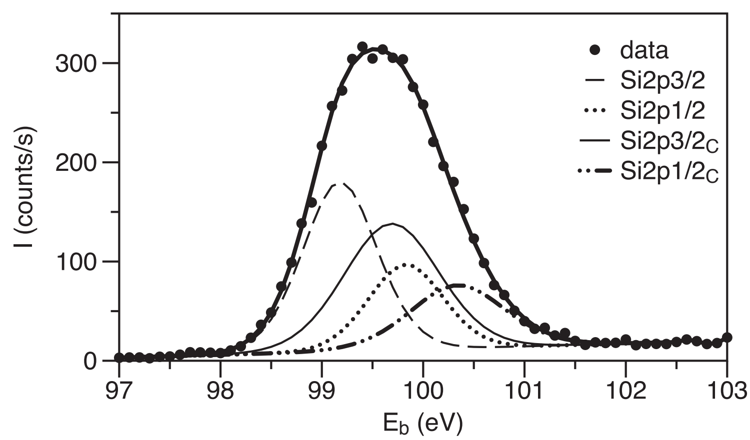

(c)

Figure 7.4: *XPS measurement of the Si2p peak at 26.75° for a Si/C ratio of: (a) 0.3; (b) 0.8; (c) 2.7. The Si2p peak can be decomposed into different, chemical compositions.*

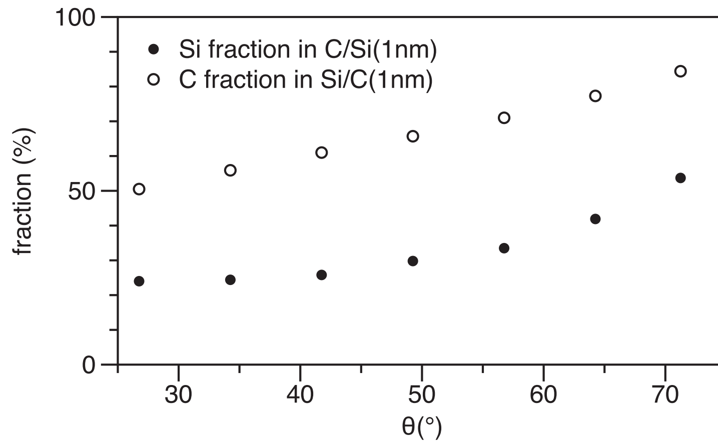

(a)

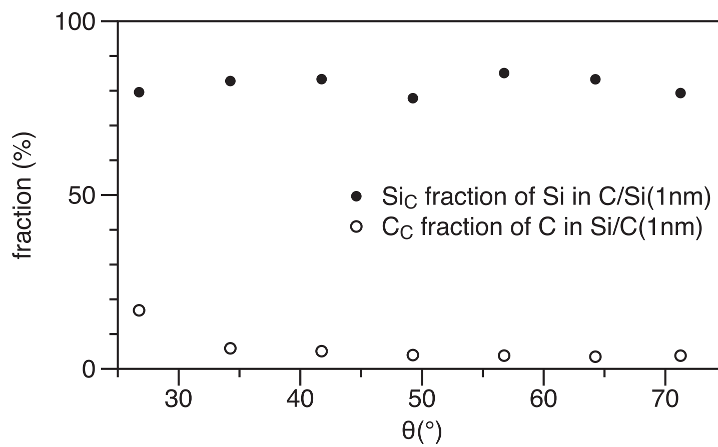

(b)

Figure 7.5: *The C fraction for several angles of the C overlayer and the Si fraction for several angles of Si overlayer are illustrated in (a). The corresponding percentage of the carbide signals relative to the total signal of the elementary peaks of the overlayers are included in (b).*

To conclude, in the initial C/Si multilayer structure, C and Si still exist as pure layers. Furthermore, no thick, homogeneous SiC interlayers are present at both Si-C interfaces to prevent or significantly slow down Si-C interdiffusion during annealing.

7.4.2 Interface dynamics during annealing

Annealing of a multilayer structure usually results in a change in period thickness. This is caused by a difference in atomic density of the growing interlayer compared to the densities of the individual consituents in their own lattice. The change in period thickness of the Si/C multilayer structure during annealing at 250°C was determined to be only 1 pm in 90 hours (graph not shown here). This means that either an interlayer is formed which has a comparable density with the Si and C layers, or there is almost no interdiffusion during the annealing. The latter would be consistent with the observation by Bosgra *et al* [3]. However, we see from Fig.7.6 a and b that the intensity of the Bragg peaks do increase and the full width half maximum (FWHM) of the first Bragg order also increases. Although changes are small, apparently there is some rearrangement of the atoms in the layered structure.

For a constant diffusion rate, it can be derived that $\ln(I(t)/I(t=0)) \propto -Dt$ [8]. Although this relation was derived for a symmetrical multilayer period, the result is similar when symmetry is not assumed. From Fig.7.6, it is concluded that the assumption of a constant diffusion rate during interlayer growth is violated. For nanoscopic systems, it has been shown by several authors that concentration dependent diffusion rates should be used for specific systems [9, 10, 11, 12]. Menon *et al* [9] observed that the logarithm of the intensities of the Bragg peaks in a Cu/Au multilayer structure do not exhibit a linear behaviour as a function of time. They provided a numerical analysis of diffusion in a layered structure using a concentration dependent diffusion rate. The diffusion rate was a quadratic function of the concentration. From the analysis they conclude that the mth order exhibits $(m-1)$ oscillations before decaying exponentially to zero. Although this could explain the increase in intensity of the second order Bragg peak, it clearly does not describe the behaviour of the first order Bragg peak.

In order to fully understand the increase in reflection, we have to look at the possible change in roughness of the Si-C interfaces upon annealing. We measured rocking curves (q_x direction) and detector scans ($q_x q_z$ direction) before and after 12 hours of annealing. From the rocking curves before and after annealing, it is concluded that the lateral correlation length of

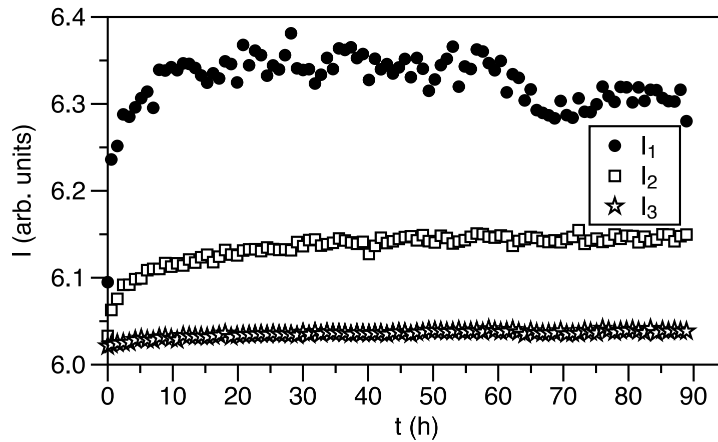

(a)

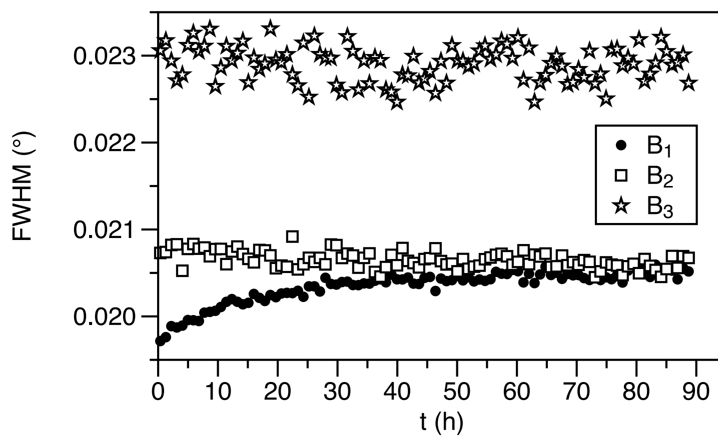

(b)

Figure 7.6: *Change in Bragg peaks during annealing: (a) integrated Fourier transform of the intensities of the first three Bragg orders, where I_2 and I_3 have been shifted in intensity for clarity on the differences; (b) full width half maximum (FWHM) of the first three Bragg orders.*

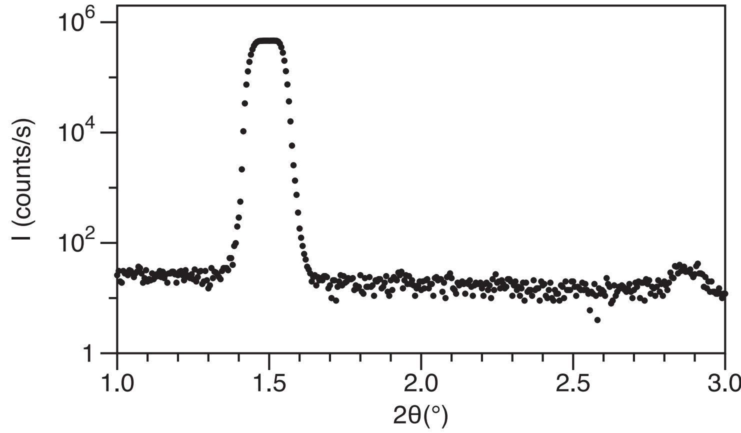

(a)

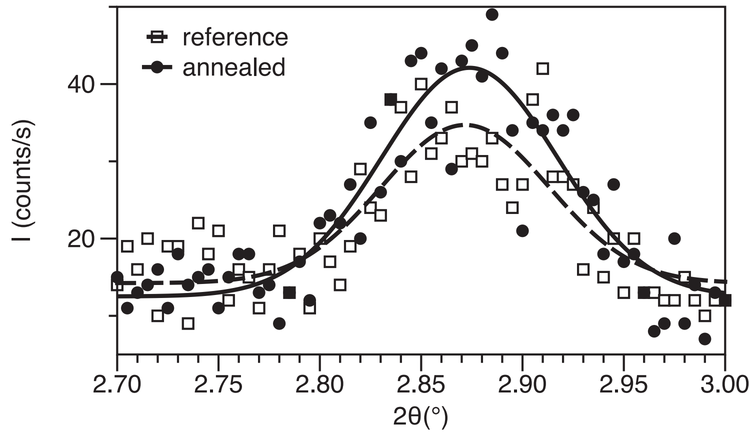

(b)

Figure 7.7: *Detector scan at $\theta = 0.75$ of (a) reference structure; (b) annealed and reference structure.*

the roughness did not change. However, when we look at the detector scan in Fig.7.7, we do see a subtle difference. It should be noted that the peak around 1.5° is wider than it should be. This is due to the opening of the detector slit, such that we can observe the low intensity peak around 2.8°. This latter peak suggests that there is some correlation between the roughness of the interfaces of the as-deposited structure. In figure 7.7b we see that the intensity of the peak at 2.8° slightly increased after annealing. The values in the Gaussian fit function $f(x) = a\exp(-(b-\theta)^2/\sigma^2)$: $a = 20.5 \pm 1.8$ vs $a = 29.6 \pm 1.8$ and $\sigma = 0.059 \pm 0.007$ vs $\sigma = 0.061 \pm 0.005$ for the as-deposited and annealed structure, respectively. This increase could in principle be ascribed to an increase in roughness amplitude or to an in-

crease in correlation length in the z-direction. The increase in roughness amplitude can be ruled out due to the fact that the reflectivity increased. Hence, it must be concluded that the correlation length in the z-direction increases during the annealing. In turn, the increased correlation may explain the increase in FWHM of the first order Bragg peak. As derived by Payne [13], when the correlation between interfaces increases, the off-specular peak under the specular peak increases in intensity and increases the width of the measured Bragg peak. This may increase the reflected intensity measured in the specular direction. In addition, since we did not see a change in lateral correlation length from the rocking curves, we speculate that the increased correlation length between interfaces, is a smoothening of the high frequency roughness of the interface profile, possibly at the atomic level.

These results confirm that indeed thin C layers can prevent Si diffusion towards the Mo_2C layer in the C/Mo_2C/C/Si multilayer structure [3]. Furthermore, it shows a potential to improve the reflection from multilayer structures during annealing for material combinations having a negative enthalpy of formation.

7.5 Conclusions

We extended the Fourier analysis of X-ray reflection measurements to include interlayer asymmetry in multilayer structures. Using the Fourier analysis method, we have observed that the C-on-Si interlayer is very sharp ($\ll 0.1$ nm), whereas the Si-on-C interlayer shows slightly more intermixing after deposition. In addition, using X-ray photoelectron spectroscopy, it was determined that the stoichiometry of the interlayers is also different: the Si-on-C interlayer has a Si-rich structure, whereas the C-on-Si interlayer has a C-rich interlayer structure.

Furthermore, we have shown that contrary to what can be expected based on the enthalpy of formation for SiC, Si/C multilayer structures under annealing at 250°C do not exhibit a significant, additional interlayer growth. Actually, the reflection of the multilayer structure increases during annealing. We argue that the increased reflection should be ascribed to a reduction of high frequency roughness and an increase in correlation of roughness between interfaces during annealing.

References

[1] W.A. Soer, P. Gawlitza, M.M.J.W. van Herpen, M.J.J. Jak, S. Braun, P. Muys, V.Y. Banine, Extreme ultraviolet multilayer mirror with near-zero IR reflectance, Optics Letters 34 (2009), 3680-3682

[2] H. Kleykamp, Gibbs energy of formation of SiC. A contribution to the thermodynamic stability of the modifications, Ber. Bunsenges. Phys. Chem 102 (1998), 1231-1234

[3] J. Bosgra, L.W. Veldhuizen, E. Zoethout, J. Verhoeven, R.A. Loch, A.E. Yakshin, F. Bijkerk, Interactions of C in layered Mo-Si structures, submitted to Thin Solid Films

[4] A.D. Akhsakhalyan, A.A. Fraerman, N.I. Polushkin,Yu.Ya. Platonov, N.N. Salashchenko, Determination of layered synthetic microstructure parameters, Thin Solid Films 203 (1991), 317-326

[5] R.S. Rosen, D.S.P. Vernon, G. Stearns, M.A. Viliardos, M.E. Kassner, Y. Cheng, Silicide layer growth rates in Mo/Si multilayers, Appl. Opt. 32 (1993), 6975-6980

[6] J. Bosgra, J. Verhoeven, R.W.E. van de Kruijs, A.E. Yakshin, F. Bijkerk, Non-constant diffusion characteristics of nanoscopic Mo-Si interlayer growth, Thin Solid Films 522 (2012), 228-232

[7] P.J.Cumpson, M.P.Seah, "Elastic scattering corrections in AES and XPS. II. Estimating attenuation lengths and conditions required for their valid use in overlayer/substrate experiments", Surface and Interface Analysis 25, 430-446 (1997)

[8] J.W. Cahn, Acta. Metall. 10 (1962), 179

[9] E.S.K. Menon, P. Huang, M. Kraitchman, J.J. Hoyt, P. Chow, D. de Fontaine, J. Appl. Phys. 73 (1993), 142

[10] Z. Erdélyi, M. Sladecek, L.-M. Stadler, I. Zizak, G.A. Langer, M. Kis-Varga, D.L. Beke, B. Sepiol, Science 306 (2004), 1913

[11] Z. Erdélyi, G.L. Katona, D.L. Beke, Phys. Rev. B 69 (2004), 113407

[12] J.-M. Roussel, P. Bellon, Phys. Rev. B 73 (2006), 085403

[13] A.P. Payne, B.M. Clemens, Phys. Rev. B 47 (1993), 2289

CHAPTER 8

VALORISATION

> *"We must not forget that when radium was discovered no one knew that it would prove useful in hospitals. The work was one of pure science. And this is a proof that scientific work must not be considered from the point of view of the direct usefulness of it. It must be done for itself, for the beauty of science, and then there is always the chance that a scientific discovery may become like the radium a benefit for mankind."*
> – Marie Curie

The first questions many people ask a scientist is something like: *"Why do you do it? And how do* **we** *benefit from your work/research?"* The first question is easy. The main motivation of doing scientific research is (at least for me) "the pleasure of finding things out".[1] In this respect, I also fully agree with the mathematician G.H. Hardy. In "A mathematicians apology" (essay published in 1940) he states on the motives to prosecute research: *"The first (without which the rest must come to nothing) is intellectual curiosity, desire to know the truth."* In his opinion, the most beautiful mathematics (the "real" mathematics) *"is almost wholly 'useless'."* For this reason, his most beloved field in mathematics was number theory. However, he also states: *"If the theory of numbers could be employed for any practical and obviously honourable purpose, if it could be turned directly to the furtherance of human happiness or the relief of human suffering, as physiology and even chemistry can, then surely neither Gauss nor any other mathematician would have been so foolish as to decry or regret such applications."*

In the past, when scientists were wealthy persons or had a wealthy benefactor, the answer to the first question might have been sufficient. However,

[1] title of a book written by Feynman.

similar to the history of Philips NatLab (from a large freedom in research under Casimir (1946-1972) towards research being more directly related to the production division of Philips), it is becoming increasingly important that research outcomes can be applied. The Dutch organization FOM (Stichting voor Fundamenteel Onderzoek der Materie) initiated a program to relate scientific research with industry. *"Born from the wish to contribute more visibly to the Dutch knowledge based economy without compromising the high scientific standards, the Industrial Partnership Programme started in 2004 (. . .)".*[2]. In an IPP, both the government and industry provide money for the research. Although it is clear that the existence of an IPP programme may increase the attention of scientists to more direct applicability of their research for the benefit of society, it also leads to an important question: does it give rise to a conflict of interest?

For industrial partners, it may sometimes be important not to publicly disclose all research findings. When the research is solely funded by a company itself (for example researchers working at Philips NatLab), there is no problem. However, in an IPP program, public money is involved. Therefore, from society point of view, the information should be made available to publicly funded research, since it was payed for by the general tax payer's money. Related to this, is a recent publication in Nature on nanotechnology and patents by J.M. Pearce.[3] For a company, it may be important to have many patents. However, Pearce states that *"Excessive patenting is increasing costs, slowing technological development and removing from the public domain fundamental knowledge about the understanding and control of matter on the atomic or molecular scale."* Regardless of whether the statement is completely true, obviously the scientific community should always keep this in mind and circumvent such a situation. Nonetheless, it should be noted that within the IPP program related to the research described in this thesis, I did not encounter such difficulties. Furthermore, there was complete freedom to define the research questions and I was allowed to publish all research findings.

An example of a field where industry and scientific research have worked together successfully for many years, is the field of multilayer optics for extreme ultraviolet (EUV) radiation. One of the important applications for the multlilayer mirrors is EUV lithography (fabrication of integrated circuits). The field of multilayer optics for EUV radiation is largely a field of research and development. The end product, the multilayer mirror, should reflect as much as possible and have a high thermal stability. To achieve these goals, sometimes apparently arbitrary choices are made. For example, much research to improve thermal stability has focussed on thin ((sub)nanometer) B_4C "barrier" layers between Mo and Si. However, not much research has

[2]P. de Witte; Nanotechnology Commercialization for Managers and Scientists

[3]J.M. Pearce, "Make nanotechnology research open-source", Nature 491 (2012), 519

actually been published on the reason why the B_4C layer actually works. For that matter, why should it work? When depositing a B_4C layer of sub nanometer thickness at room temperature (by e-beam evaporation or magnetron sputtering) it is highly unlikely that an “inert” compound of B_4C will form which also has a very low concentration of vacancies. Furthermore, C has a higher melt temperature than B_4C. Therefore, C would be a more logical choice to use as a barrier layer. Consequently, more research should focus on thin C layers, and not on thin B_4C layers to improve thermal stability of Mo/Si based multilayer structures.

Another approach in literature to improve thermal stability, was deposition of the Mo_2C/Si multilayer structure.[4] However, this structure also suffers from the same problem as the previous structure with the B_4C layers, namely upon deposition at room temperature of the Mo_2C layer, no “perfect” or stable compound layer will form. Whereas the Mo-silicides are more favorable to form than the Mo-carbides, this structure is still inherently unstable.

In this thesis, a further developed multilayer structure was demonstrated to be stable up to a temperature of 600°C, where the other structures already degraded. The multilayer consists of a C/Mo_2C/C/Si periodical structure. Due to the high activation energy for Si-C interdiffusion, the C layers in the C/Mo_2C/C/Si multilayer structure prevented Mo-silicide formation. Upon annealing, the Mo-carbide layer can further relax/reorganize to improve the quality of the layer by conversion to a stable compound. It is subsequently much harder to form Mo-silicides. The research on this modified multilayer structure resulted in a patent.

Apart from improving the thermal stability of the multilayer structures, we also improved the reflection of the EUV mirrors. For this we introduced a sub nanometer thick layer of Y on top of the Mo layers. This material was selected for the reason that metal-silicides are expected to form at the interfaces between the materials. The Y-silicide has better optical properties than the Mo-silicide in Mo/Si multilayer mirror structures for 13.5 nm radiation. Hence, the reflection for multilayer mirror structures with thin Y layers is shown to be higher than the Mo/Si multilayer structure. With this work we have demonstrated that imperfections, like in this case silicide formations, can be used to develop a better product.

In the development and improvement of nanoscopic systems, information of the structure is required on a (sub) nanometer scale. A novel method was introduced, based on extended X-ray absorption fine structure (EXAFS) measurements. In EXAFS measurements the local environment of a specific atomic species is probed, averaged over the entire sample. In our method, described in this thesis, we made the EXAFS measurements sensitive to a specific location of a layer in the structure. To achieve this, the material

[4] S. Braun, H. Mai, M. Moss, R. Scholz, A. Leson, Jpn. J. Appl. Phys 41 (2002) 4074

under study is replaced by another material, except at the location where information on the structure of that specific material was required. For this method to work, both materials are required to have the same crystallographic structure and the same lattice dimension. The thickness of the layer, consisting of the material under study, can be of sub nanometer thickness. In order to have a large enough signal (i.e. to improve the signal-to-noise ratio), the structure is repeated in the form of a periodic multilayer stack. Compared to the alternative method of using waveguides, our method does not have the intrinsic limitation on the achievable resolution.

To summarize, stimulated by fundamental interest in solid state physics at the nanoscale, this work has been aimed to contributed to improvement of multilayer structures, applicable for reflection of EUV radiation. The reflection of the Mo/Si based multilayer was increased by introduction of thin interlayers. Furhtermore, the thermal stability of the multliayer structure was improved up to 600°C. It still remains to optimize the thermally stable structure for reflection. For instance, the C layer thickness has to be optimized such that the layer thickness has a minimum width and still prevents Si interdiffusion with the Mo-carbide layer. In addition, an optimum temperature should be found such that the Mo-carbide layer relaxes to a more stable structure, thereby ensuring a long lifetime of the optic. Besides improving the characteristics of the multilayer structure, we introduced a new method, based on EXAFS, to obtain information on the local morphology of layers at the nanoscale.

CHAPTER 9

SUMMARY

The research described in this thesis is on Mo/Si based multilayer mirror structures. Two important topics in this field are increase of reflection and improvement of thermal stability. The “standard” Mo/Si multilayer structure in theory can reflect about 75% of the incoming 13.5 nm radiation. However, interlayer formation during deposition and roughness of the interfaces reduce the reflection of deposited multilayer structures. To further improve the multilayer structures, a better understanding of interdiffusion effects at the interfaces is required.

Using density functional theory calculations, the atomic adsorption and clustering energy were calculated for Mo atoms on a Si (100) surface and Si atoms on a Mo (100) surface. It was found that the local energy gain in both cases (Si-on-Mo and Mo-on-Si) is approximately 8 eV per adsorbed atom. Locally, this should lead to a short and substantial increase in temperature, stimulating interdiffusion around the adsorbed atom. In addition to the energy gain due to adsorption and cluster formation, we also calculated the energy required to move an atom from the substrate towards the formed cluster at the surface. It was found that the trapping probability for Si substrate atoms during growth of Mo clusters on a Si surface should be much higher than for the reverse case. The difference in trapping probability of substrate atoms by the growing clusters is likely an important reason that the Mo-on-Si interlayer is thicker than the Si-on-Mo interlayer.

Apart from an asymmetry in Mo-Si interlayer thickness after deposition, there is also an asymmetry in interlayer growth of the two interface types during annealing. Although the interdiffusion rate in Mo-Si multilayer structures has been considered to be constant (i.e. diffusion limited Mo-Si interlayer growth is assumed), various values for the activation energy for interdiffusion are reported in literature, ranging from 0.5 to 2.4 eV. In this

thesis, it is demonstrated using X-ray reflection during annealing of Mo-Si based multilayer structures, that the (inter)diffusion rate cannot be considered as a constant during the interlayer growth. A method is introduced to treat the non-constant diffusion rate data. It is determined that the activation energy for interdiffusion at the Si-on-Mo interface changes during the interlayer growth from 1.7 to 2.5 eV with increasing interlayer thickness (where 1.7 eV is an upper boundary for the initial activation energy for interdiffusion). For the Mo-on-Si interlayer growth, a nearly constant value of 2.6 eV for the activation energy for interdiffusion was determined. Combining the reflectometry data with X-ray diffraction measurements of the Mo layers, it is shown that the interlayers grow in a different stoichiometry.

To inhibit interdiffusion in Mo/Si multilayer structures, the chemical potential as a driving force for interdiffusion was reduced by fabricating a modified periodical structure: C/Mo_2C/C/Si. The C layers prevent Mo-Si bonds from being formed in the initial, “metastable” deposited Mo-carbide layer. After deposition, no complete crystalline Mo_2C layer structure is formed yet. Given the negative enthalpy of formation, it can be expected that Si and C will interdiffuse into each other during annealing at 600°C. Therefore, the C layers should be sufficiently thick to provide sufficient time for the Mo-carbide layer to crystallize into a stable structure. However, surprisingly, even at 600°C, Si and C showed no interdiffusion. Therefore, the structure is stable up to this temperature.

Annealing of a Si/C multilayer structure showed no significant interdiffusion. However, the first order Bragg peak of X-ray reflection increased during annealing. This phenomenon cannot be described by interdiffusion, neither with a constant diffusion rate nor with a concentration dependent diffusion rate. It was shown that during annealing, the correlation of the roughness between the interfaces increases, thereby increasing the reflection.

A more direct approach to increase the reflection of the Mo/Si multilayer structure is to introduce a sub-quarter wavelength thick layer of Y into the multilayer stack. This material was chosen, based on the assumption that interlayers of a few tenths of a nanometer will anyhow form during deposition. A material has to be selected for which the silicide has better optical properties than Mo-silicide. The B_4C/Mo/Y(0.2 nm)/Si multilayer structure increased the reflection from 70.0% (for a B_4C/Mo/B_4C/Si multilayer structure; or 69.1% for a Mo/Si multilayer structure) to 70.3%. Although this is a relatively small gain for only one mirror, it is significant for EUV lithography machines where several (8 to 10) mirrors are used.

This result demonstrates that doping at interfaces can possibly increase multilayer mirror reflection for structures designed for wavelengths smaller than 13.5 nm. This could be investigated for example for La/B_4C multilayer structures designed for 6.8 nm radiation.

CHAPTER 10

SAMENVATTING

In dit proefschrift worden twee belangrijke problemen in het onderzoek naar Mo/Si multilaagspiegels voor extreem ultraviolette straling behandeld: verbetering van thermische stabiliteit en verbetering van reflectie van de multilaagspiegels. Een Mo/Si multilaagspiegel kan in theorie ongeveer 75% van het inkomende licht met een golflengte van 13.5 nm reflecteren. Echter, interlaagformatie tijdens depositie van de multilaagstructuren en ruwheid op het grensvlak van Mo en Si, reduceren de reflectie van de spiegels. Om de eigenschappen van deze multilaagspiegels te verbeteren, is er een beter begrip nodig over de interdiffusie van materiaal rond de grenslagen.

Met behulp van dichtheidsfunctionaaltheorie zijn de energieën berekend voor adsorptie van Mo atomen op een Si (100) oppervlak en voor adsorptie van Si atomen op een Mo (100) oppervlak. Tevens is de energie berekend die gepaard gaat met diffusie van atomen uit het substraat naar klusters op het oppervlak. Tijdens adsorptie van zowel Mo atomen op het Si oppervlak als Si atomen op het Mo oppervlak, neemt lokaal de energie toe met ongeveer 8 eV per geadsorbeerd atoom. Plaatselijk leidt dit tijdelijk tot een verhoging van de temperatuur, met als gevolg een verhoogde interdiffusie rond het geadsorbeerde atoom. Er is tevens berekend dat de waarschijnlijkheid om een Si atoom te vangen in een groeiend Mo kluster op het Si oppervlak veel groter is dan de waarschijnlijkheid om een Mo atoom te vangen in een groeiend Si kluster op het Mo oppervlak. Het verschil in waarschijnlijkheid wordt verantwoordelijk geacht voor het verschil in interlaagdikte na depositie van Mo/Si multilaagstructuren.

Naast een verschil in initiële interlaagdikte in Mo/Si multilagen, is er ook een verschil in interlaaggroei van de twee verschillende interlaagtypes (Mo-op-Si en Si-op-Mo) tijdens verwarmen van de structuren. Hoewel de interdiffusiesnelheid in Mo-Si multilaagstructuren tot dusver als constant veronder-

steld was (diffusie-beperkte interlaaggroei), zijn er sterk variërende waarden voor de activeringsenergie voor interdiffusie gerapporteerd, namelijk variërend van 0.5 tot 2.4 eV. Door middel van metingen met röntgenstraling aan Mo/Si multilaagstructuren tijdens verwarming, wordt in dit proefschrift getoond dat de interdiffusiesnelheid niet constant verondersteld mag worden tijdens de interlaaggroei. Er is een methode geïntroduceerd om de data met de niet constante diffusiesnelheid te behandelen. De activatie energie voor de interdiffusie op het Si-op-Mo grensvlak blijkt te veranderen tijdens de interlaaggroei, en loopt op van 1.7 naar 2.5 eV met toenemende laagdikte (de waarde van 1.7 eV is de bovengrens voor de aanvankelijke activeringsenergie op dit grensvlak). Daarentegen, voor de Mo-op-Si interlaaggroei is een bijna constante waarde van 2.6 eV bepaald. Door de reflectiemetingen te combineren met diffractiemetingen aan de Mo lagen, is tevens aangetoond dat de beide interlagen met een verschillende stoichiometrie groeien.

Om de interdiffusie in Mo/Si multilagen te beperken, is de chemische potentiaal, die de interdiffusie veroorzaakt, gereduceerd door het maken van een gemodificeerde structuur: C/Mo_2C/C/Si. De C lagen voorkomen dat Mo-Si bindingen kunnen vormen tijdens de depositie van de metastabiele Mo_2C laag (tijdens depositie wordt namelijk niet een perfect kristallijne Mo_2C structuur gevormd). Gezien de negatieve vormingsenthalpie mag het verwacht worden dat Si en C in elkaar zullen diffunderen tijdens verwarming op 600°C. Daarom moeten de C lagen voldoende dik zijn, zodat interdiffusie van Si in de Mo-carbide laag voldoende vertraagd wordt, en de Mo-carbide laag voldoende tijd heeft om een stabielere structuur te vormen. Echter, zelfs op 600°C is er geen interdiffusie tussen Si en C waargenomen. Daardoor is de gemaakte multilaagstructuur tenminste stabiel tot deze temperatuur.

Het verwarmen van de Si/C multilaag toonde geen significante interdiffusie. Echter, de eerste orde Bragg-reflectie van de röntgenstraling nam toe tijdens het verwarmen. Dit effect kan niet verklaard worden aan de hand van interdiffusie met een constante diffusiesnelheid, echter ook niet met behulp van een diffusiesnelheid die van de lokale concentratie afhangt. Het is aangetoond dat de correlatie tussen de ruwheid van de grensvlakken tijdens het verwarmen toeneemt. Dientengevolge neemt tijdens het verwarmen de reflectie van de eerste Bragg-orde ook toe.

Een meer directe manier om de reflectie van de multilaagspiegels te verhogen, is door middel van het toevoegen van een dunne lagen in de Mo/Si multilaagstructuur. Gebaseerd op de aanname dat zich altijd een interlaag van een paar tienden van een nanometer zal vormen tussen twee materialen, moeten silicides meegenomen worden in het onderzoek naar verbetering van reflectie. In theorie leiden zowel een Y laag als een Y-silicide laag tot een hogere reflectie dan een Mo-silicide laag op Mo in een Mo/Si multilaagspiegel (voor 13.5 nm straling). Ook in praktijk heeft de toevoeging van een dunne Y laag op Mo geleid tot een verhoogde reflectie. De B_4C/Mo/Y(0.2 nm)/Si multilaagstructuur verhoogde de reflectie van 70%

(voor de B_4C/Mo/B_4C/Si multilaagstructuur; of 69.1% voor de Mo/Si multilaagstructuur) naar 70.3%. Hoewel dit maar een kleine verhoging is voor een enkele spiegel, is dit een significante verhoging voor EUV lithografiemachines waar meerdere (8 tot 10) spiegels gebruikt worden.

Dit resultaat toont aan dat het doteren van grensvlakken mogelijk ook de reflectie zou kunnen verhogen van multilaagspiegels die ontworpen zijn voor golflengtes kleiner dan 13.5 nm. Dit zou bijvoorbeeld onderzocht kunnen worden voor La/B_4C multilaagspiegels die voor 6.8 nm golflengte ontworpen zijn.

ACKNOWLEDGEMENTS